Learning from biology to design stimuli-responsive capsules

NATASHA SUZANNE RIGBY

Learning from biology to design stimuli-responsive capsules

Natasha Rigby

Thesis submitted in partial fulfilment of the requirements for the degree of Doctor of Philosophy

Supervisor: Dr. Margarita Staykova

Department of Physics

Durham University

October 2021

Abstract

As well as being model cell membranes, lipid vesicles are widely used as an encapsulation technology due to their impermeable membrane. Hydrogels are similarly useful due to their biocompatibility, mechanical strength, and potential for stimulus-responsive behaviour. By combining these two structures, the benefits of both can be reaped, giving a structure with both mechanical strength and the possibility to encapsulate actives within an impermeable membrane. However, the interactions between the gel and membrane, and their implications, are not well understood. This thesis considers two different composite structures of lipid vesicles and hydrogels as potential systems for encapsulation and controlled release. These structures are hydrogel-embedded vesicles, and Gel-Filled Vesicles (GFVs). The hydrogel-embedded vesicles are subjected to different types of mechanical stresses. Osmotic shocks are used to apply a uniform pressure on the lipid bilayer, and compression of the hydrogel by a micromanipulator is used to cause a uni-directional force.

Agarose-embedded vesicles are shown to experience an adhesive interaction between the membrane and the gel, causing vesicle behaviours to be altered in comparison to free-floating vesicles. Of particular note is the formation of a buckled morphology for embedded vesicles subjected to hyperosmotic shocks.

Additionally, the formation of GFVs demonstrating the poration mechanism of controlled release is attempted. A suitable gel core of poly(acrylamide-*co*-acrylic acid) is synthesised and characterised for Upper Critical Solution Temperature behaviour.

In summary, this thesis demonstrates that interactions between the lipid bilayer and a hydrogel can strongly affect membrane behaviours, and therefore their uses for either encapsulation systems or for biophysical models.

Declaration

The work presented in this thesis was conducted under the supervision of Dr. Margarita Staykova in the Physics Department of Durham University. The results, analysis, figures, and text are all my own unless otherwise stated. None of the work in this thesis has been submitted for any other degree or qualification.

Acknowledgements

Firstly, I would like to thank my supervisor, Dr. Margarita Staykova, for all of her advice throughout my studies. I have really enjoyed being part of the research group, and am really grateful for all the opportunities this has presented me with.
My thanks also go to my supervisors at Mondelēz International, Beth Green and Alison Branch, for their insight and support throughout my PhD, and especially during my placement.

I am grateful to all the members of the Staykova Biophysics research group, past and present, with whom I have thoroughly enjoyed sharing the labs and office.
Thank you to Cohort 3 of the SOFI CDT for always being there for me, despite actually being all over the world.

I would also like to thank the Rigby family for all their pep talks, proofreading, and for their unique interpretations of what my research entails!
Finally, my thanks go to Dan Day, who has supported and inspired me every day of our PhD journeys.

List of Abbreviations

- **AA** Acrylic acid
- **AM** Acrylamide
- **DEAP** 2,2-diethoxyacetophenone
- **DOPC** 1,2-dioleoyl-sn-glycero-3-phosphocholine
- **EPT** Emulsion Phase Transfer
- **FRAP** Fluorescence Recovery After Photobleaching
- **GFV** Gel-Filled Vesicle
- **GUV** Giant Unilamellar Vesicle
- **ITO** Indium tin oxide
- **LCST** Lower Critical Solution Temperature
- **NIPAM** *N*-isopropylacrylamide
- **O/W** Oil-in-Water
- **p(AM-*co*-AA)** poly(acrylamide-*co*-acrylic acid)
- **p(NIPAM)** poly(*N*-isopropylacrylamide)
- **Rh-DPPE** 1,2-dipalmitoyl-sn-glycero-3-phosphoethanolamine-N-(lissamine rhodamine B sulfonyl) (ammonium salt)

- **ROI** Region of Interest
- **SLB** Supported Lipid Bilayer
- **SUV** Small Unilamellar Vesicle
- **TFA** Thermal Fluctuation Analysis
- **UCST** Upper Critical Solution Temperature
- **W/O** Water-in-Oil

Contents

Chapter 1

Introduction

This thesis concerns the design of encapsulation systems, capable of controlled release, inspired by structures found within the natural world. These structures are hydrogel-embedded vesicles and Gel-Filled Vesicles (GFVs), both of which relate closely to the structure of cell membranes and their surroundings.

Lipid vesicles are already used for encapsulation purposes with wide-ranging applications such as food preparation and drug delivery. However, although their combination with hydrogels, either externally or internally, is known to provide mechanical strength and altered release properties to the vesicle, these are not yet so widely used.

The aim of this thesis is to learn from biological lipid membranes to design encapsulation and controlled release technologies, with an emphasis on encapsulation in food systems, and particularly confectionery.

This chapter will introduce the key structures, their uses and applicability to encapsulation, and the physics underpinning the processes that make the lipid bilayer capable of encapsulation and release of actives.

1.1 Vesicle - Hydrogel Composite Structures

The lipid bilayer is a structure essential to life. It contains within the cell all the required nutrients and components, and simultaneously acts as a barrier to the extracellular environment [1]. Spherical bilayers, known as vesicles, can be formed from any of a range of amphiphilic molecules, including phospholipids, block copolymers, nonionic surfactants, etc. [2]. Liposomes, i.e. vesicles where the bilayer is formed by phospholipid molecules, are a model of the cell membrane and have been utilised for various purposes, such as: preparation of model cells and biophysical studies; encapsulation and drug delivery; and as microreactors [3–6]. The formation of lipid bilayers in aqueous solution is driven by the hydrophobic effect, due to the amphiphilic nature of the constituent phospholipids: the hydrophilic headgroups are oriented towards the internal and external aqueous solutions, while the hydrophobic lipid tails are prevented from coming into contact with water molecules [7]. Figure 1.1a shows a diagram of a lipid vesicle.

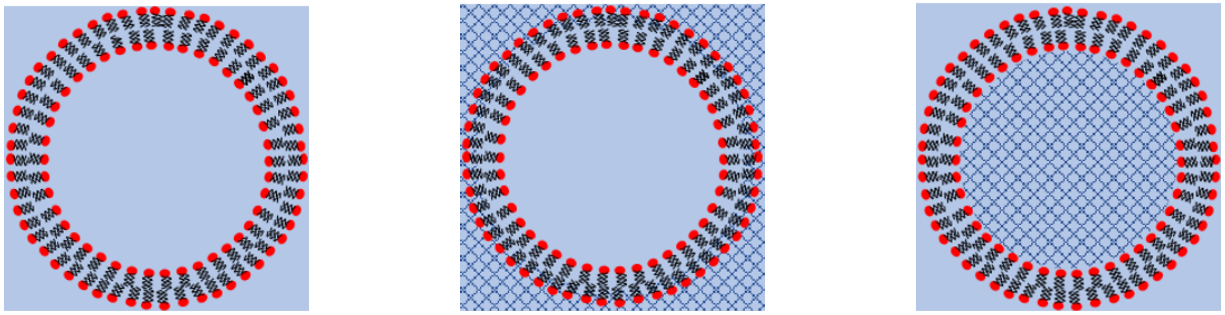

(a) Lipid Vesicle

(b) Hydrogel-Embedded Vesicle

(c) Gel-Filled Vesicle

Figure 1.1: Diagrams showing the structures of lipid vesicles, hydrogel-embedded vesicles, and Gel-Filled Vesicles (GFVs). The blue regions denote aqueous solution, and the crosshatching denotes a gelled structure.

1.1.1 Biological Coupling

In nature, the cell membrane is not free-floating but is anchored by the presence of an extracellular matrix (ECM) [8]. In animal cells, the ECM consists of proteins and

proteoglycans [9] and has many functions, including the adhesion of cells into tissues, and the signalling of external stimuli to the cell [10]. In plants and yeasts, the ECM is a rigid cell wall, which is typically composed of a network of polysaccharides [11–13]. The plant cell wall ensures that upon changes in turgor and osmotic pressure across the cell membrane, tissue integrity is preserved [14].

Despite their different chemical compositions, the animal ECM and cell walls are structurally similar, both consisting of a filamentous network of polymers [11]. The porosity of these structures allows for the diffusion of small molecules necessary for signalling, but can also act as a filtration mechanism against pathogens [15].

An important feature of both ECM and cell walls is that they can support the cell membrane in various non-spherical shapes in order to allow for different cell functions [16, 17].

Additionally, cellular contents are not entirely fluid, but rather there are cytoskeleton elements comprising actin filaments, microtubules, and intermediate filaments [18]. As well as imparting mechanical strength, the cytoskeleton acts as a scaffold for cells, allowing them to adopt non-spherical shapes with significant excess membrane area which can act as a resevoir of membrane material [19]. The difference in spreading dynamics between cells and vesicles has been shown to be related to the deformability of the cytoskeleton and its ability to rearrange [20, 21].

The cytoskeleton and ECM are typically bound to the cell membrane via focal adhesions, which are networks of trans-membrane and cytoplasmic proteins [22] which are also responsible for signalling environmental information to the cell [23, 24].

These extra- and inter-cellular structures can be mimicked for model lipid membranes by using a hydrogel support for the membrane [25, 26]. Hydrogels are crosslinked networks of polymers which are highly swollen in water [27] and contain over 20% water by mass, and in some cases over 99% water [28, 29].

Hydrogels are widely used for biomedical applications due to their similarity to biological tissues and in fact the cell cytoplasm is very similar to a hydrogel in many of its characteristics, including its ability to absorb large volumes of water and to respond to its environment [30, 31]. They are also used in drug delivery systems [32, 33], although due to their hydrophilic structure they are limited mainly to encapsulating hydrophilic actives [34].

The crosslinks between polymers that cause a hydrogel network to form can be either physical interactions or covalent bonds [35]. Many biopolymers, such as agarose or gelatin, show physical crosslinking [36]. The cause of the physical crosslinks can be chain entanglements, physical interactions between chains such as hydrogen bonds or van der Waals interactions, or entropic effects [37]. Covalently crosslinked hydrogels can, in some cases, be cytotoxic due to either the leaching of unreacted monomers and initiators, or due to their degradation products. For this reason, physically crosslinked hydrogels (and particularly biopolymers) are often preferred for encapsulation purposes [38].

As well as better mimicking cellular structures, combining lipid vesicles with hydrogels can yield a composite structure that possesses the benefits associated with each structure - namely, the impermeability of the lipid membrane with the mechanical stability of the hydrogel [39].

There are a range of different vesicle-hydrogel composite structures that have been reported in the literature. This thesis considers both gel-filled vesicles (GFVs) and vesicles embedded in hydrogels, both shown in Fig. 1.1. There are also many other composite structures of vesicles and hydrogels, such as liposome-coated microgels [40–42], microgel-coated liposomes [43], and hydrogel-coated liposomes [44, 45].

1.1.2 Vesicles Embedded in Hydrogels

Hydrogel-embedded vesicles have many uses in biophysical studies and controlled release applications. The preparation of these systems is very simple - a suspension of vesicles is

mixed into a gelling solution while it is still fluid and then allowed to gel. This has been demonstrated for a range of hydrogels, including biopolymer gels such as agarose, alginate or gelatin, or synthetic gels including poly(vinyl alcohol), poloxamers, or poly(acrylamide) [46–52]. The size distribution of vesicles is not affected by gelation, but not all vesicles added might survive the gelation process intact, depending on how the vesicles are mixed into the gelling solution and the strength of the gel [46, 53].

Many cell studies involve culturing cells in a hydrogel as a 3D scaffold in order to mimic their in vivo conditions [54, 55]. For this reason, embedding vesicles in a hydrogel matrix can be used as a model of the extracellular matrix and its effect on the cell membrane [56].
Embedding liposomes into a hydrogel matrix is also used as a step towards model tissues. The hydrogel support can be used to control the relative positions of vesicles to create a patterned structure as is required for tissues [57]. Similarly, hydrogels containing magnetically oriented microgels can be used as matrices for cell growth to promote the desired cell alignment, which has been proposed as a wound healing system [58].

Vesicles embedded into hydrogels are immobilised which can allow for high definition imaging, for example of phase-separated lipid domains, or for the process of membrane collapse due to the addition of surfactants or enzymes [53]. For GUVs embedded into agarose hydrogels, some properties of the membrane (such as lateral mobility of membrane lipids) were previously found to be unaffected by the presence of the hydrogel, whilst others, including the electroporation lifetime, were affected. Further, agarose-embedded vesicles were also compared to agarose-filled vesicles, and the electroporation behaviour was again significantly different, with the pores formed in GFVs never re-sealing [46]. As yet, it is unclear why only certain membrane behaviours should be affected by the presence of agarose, which adds complexity to the seemingly simple system of hydrogel-embedded vesicles. In order to utilise hydrogel-embedded vesicles for controlled release purposes, it

will be of particular importance to understand how membrane poration is affected by the hydrogel.

1.1.3 Gel-Filled Vesicles

The preparation of GFVs is not as simple as that of hydrogel-embedded vesicles. There are two broad classes of methods for preparing GFVs. The first class involves using a liposome as a reactor for the gelation step. Vesicles are prepared to encapsulate a fluid, pre-gel solution, which is then caused to gel by e.g. temperature changes or exposure to UV illumination [59–61].

Secondly, GFVs can be prepared by fusing a lipid bilayer around a pre-existing microgel, typically by the adsorption of lipids (usually in the form of small unilamellar vesicles, SUVs) on to the gel surface [62], followed by their rupture to form a continuous bilayer. There are many methods that exist to promote lipid adsorption on the gel surface, such as hydrophobic modification of the gel, electrostatic attraction, etc. [59, 63–65].

Finally, water-in-oil (W/O) emulsions can be used to prepare microgels coated with a phospholipid monolayer, which is later converted to a bilayer by transferring the lipid-coated microgel through a planar lipid monolayer [66].

GFVs are often reported as a step towards a bottom-up synthetic model cell [67–71], due to the fact that cell contents are not entirely fluid but gel-like [31]. Of particular biological relevance are GFVs where the gel core is formed from actin filaments which make up the cytoskeleton [72, 73]. These have been used to model how the presence of the cytoskeleton influences cell behaviours, such as their response to cell indentation [74], or the water permeability of the membrane [72].

Outside of the area of biological gels, GFVs with a poly(*N*-isopropylacrylamide) (p(NIPAM)) core are perhaps the most widely studied. The p(NIPAM) gel core demonstrates Lower Critical Solution Temperature (LCST) behaviour; i.e. above a critical

temperature T_c, the hydrogel expels water and shrinks, becoming more hydrophobic [75]. However, different responses of the lipid bilayer to gel shrinkage have been observed. For GFVs formed by gelation of an internal pre-gel solution, the lipid bilayer is strongly adhered to the gel surface due to penetration of p(NIPAM) chains into the hydrophobic region of the bilayer, preventing delamination of the membrane from the gel surface [71, 76–78]. Conversely, GFVs formed by the fusion of a bilayer onto a pre-existing p(NIPAM) microgel did display membrane delamination [62], suggesting that the difference in formation method resulted in a much weaker gel-membrane interaction, which in turn affects the membrane behaviour in response to changes in the gel structure. This highlights how the nature of the interaction between the gel and the membrane may alter membrane properties.

1.2 Encapsulation and Controlled Release

Both hydrogel-embedded vesicles and GFVs, as well as other composite structures, have been suggested as encapsulation systems. Encapsulation is the process of containing an active material (or "cargo") within a coating of a differing material in order to protect the active from its surroundings, to prevent degradation, to mask unpleasant aromas or tastes in foods, or to control its release rate [79, 80].

According to Huynh and Lee, controlled release is defined as "the tailorable delivery of compounds at an effective level in response to time and stimuli" [81]. Conventional release from encapsulates is of a "burst"-type release where all or a large amount of the cargo is rapidly released in a single event. In a conventional (non-controlled release) dosage form, there can be significant fluctuations in the available concentration of the active ingredient, with the possibility in drug delivery systems of exceeding the threshold for toxicity or being below the minimum effective concentration. The aim of controlled release systems is to maintain the available concentration within the effective and safe levels without these

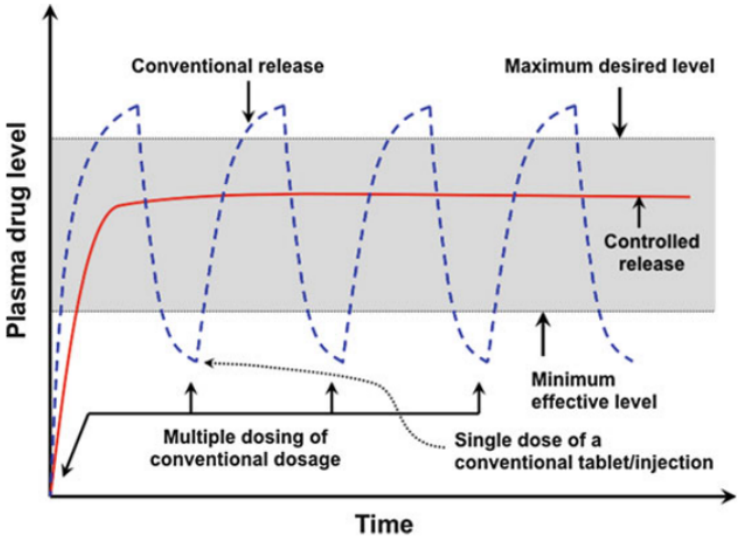

Figure 1.2: Examples of conventional vs. controlled release profiles. Reprinted by permission from **Springer Nature Customer Service Centre GmbH**: **Springer Nature, Encyclopedia of Polymeric Nanomaterials** by **Huynh and Lee** © (2014) [81].

fluctuations and without the need for multiple dosing. Figure 1.2 shows the difference between these release systems.

There are different classes of controlled release systems. Firstly, delayed release systems are those which either introduce a lag time before the active is released [82], or which significantly slow the rate of release (also termed sustained release) [83]. In contrast, triggered release systems only release their contents in response to a particular stimulus. A large variety of different stimuli have been demonstrated, such as temperature [84], osmotic stress [85], magnetic fields [57], pH [86], etc.

1.2.1 Release from Vesicles

A benefit of lipid vesicles as an encapsulation technology is that they are intrinsically able to encapsulate both hydrophilic and lipophilic actives: hydrophilic actives are located in the aqueous core of the vesicle and lipophilic actives can be incorporated into the hydrophobic tails region of the bilayer [87].

Controlled release properties can be added to vesicles in an assortment of ways. One method of controlling release is to manipulate the phase behaviour of lipid bilayers via changing the temperature. Depending on the temperature, vesicles can exist in different phases: above the melting temperature of the membrane T_m, membranes are in the fluid phase and the phospholipids are able to flow within the membrane. Below T_m, the membrane is in the gel phase, where phospholipids adopt a regular arrangement and have no fluidity. The permeability of bilayers is known to increase in the vicinity of the phase transition temperature [88]. This has been suggested to be due to the co-existence of two different phases: the boundaries between the co-existing phases form defects which increase the permeability [89]. As a result, increasing the temperature of gel-phase vesicles to near the transition temperature has been used to trigger the release of encapsulated ions which can then cause an in situ alginate gelation [90].
Vesicles can be made to be stimulus-responsive by incorporating responsive lipids or proteins into the membrane. For example, vesicles of synthetic pH-responsive lipids have been demonstrated to release their contents due to either acidification of the external medium or due to internal acidification on reaction with encapsulated salts [91, 92]. The Mechanosensitive channel of large conductance, a protein found in bacterial cell walls, can open a channel or pore in the membrane in response to large osmotic shocks. It can be reconstituted into lipid vesicles and therefore utilise osmotic pressure as a trigger for releasing encapsulated materials from the vesicle [93].

Generally, vesicles can open membrane pores in response to varying stimuli, including hypoosmotic shock (swelling due to a change osmotic pressure), electroporation (membrane disruption due to the application of an electric field), or addition of porogens (species which insert into or adsorb onto the membrane and cause poration). Encapsulated actives can then be released from the vesicle while the membrane pore remains open. The release rate depends on the hydrodynamic radius of the cargo in relation to the size of

the opened pore [94]. In the case of hypoosmotic shock, the pores re-seal after releasing some of their encapsulated contents [95], whereas in other cases the pores may remain open for the duration of the stimulus [96].

Currently, lipid vesicles are widely used for encapsulation of a range of actives in both the pharmaceutical and food industries [97]. For example, in cheese production, enzymes are encapsulated within liposomes which are then used to target delivery of the enzymes to the curd, giving a better flavour profile [98]. Within drug delivery applications, many different liposome-encapsulated drugs have been clinically approved and are now in the market. These vesicles are typically nanometre-sized, depending on the target location within the body, and often make use of the thermal phase transition to induce drug release [99, 100].

1.2.2 Release from Hydrogels

Hydrogels are useful for encapsulation purposes due to their tuneable porosity, which allows for loading and release of cargoes depending on their size, and their high water content which promotes biocompatibility [101]. Their hydrophilicity allows for hydrophilic actives to be easily encapsulated, whereas hydrophobic actives must be incorporated within oil droplets or other hydrophobic structures [32, 102]. Although chemical crosslinking opens up a wider range of hydrogels as potential encapsulation systems, physically crosslinked hydrogels are preferred for many biomedical applications, due to the avoidance of potentially toxic or harmful crosslinkers [27, 103].

In general, hydrogels display a burst-release profile for encapsulated actives, with the timescale controlled by factors such as the ratio of the active size to the mesh size, and interactions between the active and the polymer [32, 33].
Responsive polymer hydrogels, particularly poly(*N*-isopropylacrylamide) (p(NIPAM)), are widely used for encapsulation. Responsive (or "smart") polymers are those which change

their properties in response to an applied stimulus, such as temperature, solvent, or ionic strength [104].

P(NIPAM) is an example of a thermoresponsive polymer: its solubility in aqueous solution changes in response to temperature [105]. The release profile depends strongly on whether the polymer is in its soluble state or collapsed: below the critical temperature (T_c), the gel is fully water soluble and shows a slow release profile, but above T_c, expulsion of water from the gel structure causes a faster release of the encapsulated active molecule [106]. This mechanism can be exploited to "switch on" the release when the temperature is raised above T_c [107].

1.2.3 Release from Vesicle - Hydrogel Composite Structures

Hydrogel-embedded vesicles are used to improve on the drug delivery properties of free-floating vesicles. By embedding vesicles into a hydrogel matrix, the vesicles are retained at the desired location rather than being washed away, due to the higher viscosity of the hydrogel [83, 108]. In general, actives encapsulated within the embedded vesicle show a sustained release profile compared to hydrogels, which show a burst-release profile [52, 109, 110]. Triggered release behaviour has been shown for liposomes embedded in a thermoresponsive p(NIPAM) hydrogel: above its transition temperature, as the hydrogel becomes more hydrophobic, it causes the formation of defects on the membrane which release encapsulated actives more quickly than in the fully hydrated state. However, the released actives are then trapped within the hydrophobic environment which slows their release. Additionally, the shrinkage of the gel can cause liposomes to be expelled from the matrix along with water. Overall, the release profile shows a very slow, linear release above T_c, and a fast burst release when the hydrogel is below T_c [111].

In general, GFVs have been shown to exhibit sustained release behaviour, with release of actives occurring over a longer timescale than either liposomes or microgels alone [66, 67, 112–115]. This is a consequence of combining the two structures. In comparison to

microgels, GFVs have a sustained release due to the presence of the lipid bilayer coating the gel surface and preventing significant release of actives from the gel surface. In comparison to (fluid-filled) liposomes, GFVs display sustained release as the encapsulated actives must first diffuse through the porous gel core before being released through the bilayer [113].

Interactions of the active molecule with the gel structure can also affect the release: electrostatic attraction between the gel and the active increases the encapsulation of the active [73, 114, 116], and adhesive interactions between the gel and the active effectively slow down the release [32].

The coupling of the lipid bilayer to an internal hydrogel allows for new mechanisms of controlled release which are specific to GFVs [39]. These are:

- The "sponge-like" release, where shrinking of the gel core away from the membrane causes release of the active into the interstitial space, followed by diffusion through the bilayer, on a timescale of hours;
- The poration mechanism, where expansion of the internal gel core imposes a strain on the bilayer, which opens membrane pores and release actives on a timescale of minutes; and
- The burst mechanism, where degradation of the internal gel increases the swelling pressure within the vesicle, leading to complete membrane rupture and release of actives on a timescale of seconds.

These mechanisms of controlled release are specific to GFVs since they rely on properties of both the lipid bilayer and the encapsulated hydrogel. The burst-type mechanism has been demonstrated for GFVs with a core of Dextran-hydroxyethyl methacrylate (Dex-HEMA) which degraded on incubation with either basic solutions or at increased temperature [64].

In another case, GFVs with a pH-sensitive methacrylic acid core were shown to exhibit

triggered release of encapsulated actives. However, although this was related to the swelling of the gel core, it was in fact caused by electroporation of the membrane [68, 117]. Therefore, since the triggered release behaviour is technically a property of the lipid bilayer and is not dependent on the gel core [118], it is not an example of the poration mechanism.

Otherwise, it appears that despite the range of responsive hydrogels reported, very few have been utilised as the trigger for release of encapsulated actives from GFVs, and the sponge-like and poration mechanisms are yet to be demonstrated. One of the aims of this thesis is to develop GFVs which exhibit the poration mechanism as a potential triggered release system.

Supported Lipid Bilayers (SLBs) coupled to an elastic substrate have been shown to form membrane pores upon expansion of the substrate. These pores were found to be stable as long as the substrate stretch was maintained [119]. Therefore, deforming or stretching the gel core of a GFV would be a suitable route to demonstrating the poration mechanism.

1.3 Vesicle Deformation and Volume Loss

This thesis will investigate how lipid membranes respond to different mechanical perturbations if coupled to a hydrogel, either internally or externally. One of the main effects studied will be the deformation of vesicles to non-spherical shapes or non-equilibrium volumes as a response to mechanical perturbations, and whether these can be used as the trigger for controlled release.

1.3.1 Methods of Vesicle Deformation

In the Area-Difference Elasticity (ADE) model, the shape of a vesicle is parametrised by two geometric factors: the reduced volume, v, describes the volume within the vesicle relative to a sphere of the same membrane area [120], and can be considered as a measure of the volume-surface area ratio. $v = 1$ for spherical vesicles, and decreases to zero as the

volume reduces. The second parameter is the area difference between membrane leaflets, Δa, which is affected by the fusion of extra lipid material into one leaflet [121] or due to asymmetry in the leaflet composition [122].

Figure 1.3 shows a phase diagram of possible vesicle shapes for a range of v and Δa values according to ADE theory. Many of these vesicles have been observed experimentally under a range of conditions [123].

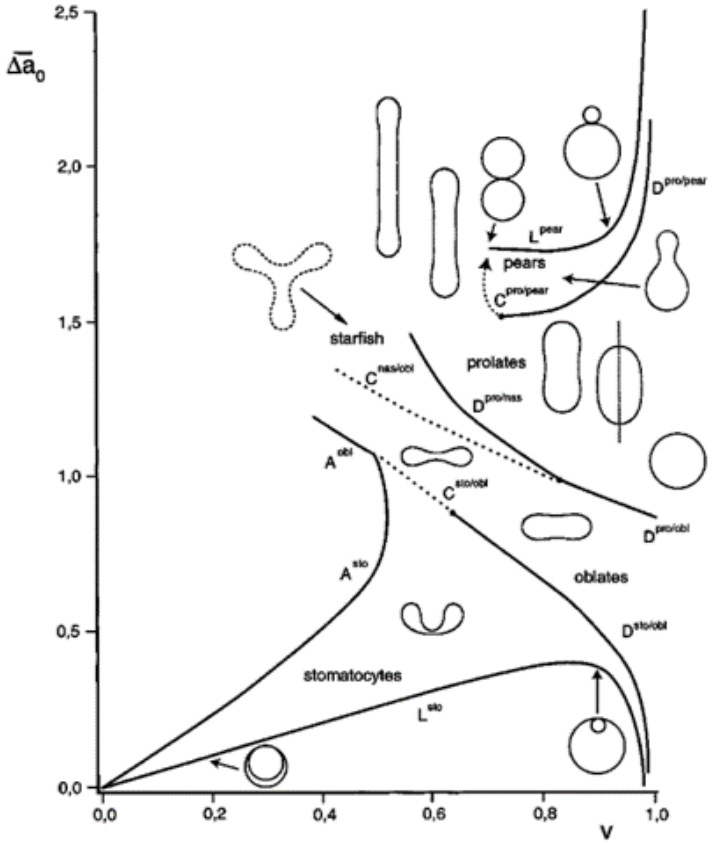

Figure 1.3: Phase diagram of vesicle morphologies according to ADE theory. Reprinted from Current Opinion in Colloid & Interface Science, 5, Hans-Günther Döbereiner, Properties of giant vesicles, Pages 256-263, Copyright 2000, with permission from Elsevier.

Imposing a uniform pressure on the lipid bilayer, such as osmotic pressure or hydrostatic pressure, has been shown to cause water efflux through the bilayer and hence a reduction in v [124, 125]. This results in shape transformations to non-spherical shapes including prolates, oblates, starfish, etc., as shown in Fig. 1.3, with a strong sensitivity to

the "history" of the system, including for example the method of increasing the osmotic pressure [126, 127].

Rather than applying a uniform, environmental pressure to cause vesicle deformation, a local force can be utilised to effect a shape change, for example by using a microfluidic stamp or tipless AFM cantilever [74, 128], by the deformation of a responsive hydrogel in which the vesicles are deposited [129], or by vesicle stretching with optical tweezers [130].

1.3.2 Vesicle Buckling

One of the most significant vesicle shape changes studied in this thesis is vesicle buckling. Buckling is a large shape change in response to a small change in the applied pressure [131], and buckling of solid thin shells has been studied extensively within the last century. The theory of buckling of spherical thin shells was developed by Zoelly in 1915 [132, 133]. Extensions to this theory have included considerations for imperfections or defects in the shell [131] and for post-buckling behaviour [134].

Elastic thin shells buckle in response to pressure changes (and hence volume deflation). At first, as the volume is reduced, the spherical shape is the equilibrium morphology. When the volume passes a critical buckling point, the spherical morphology becomes unstable and the buckled morphology becomes the equilibrium shape [135].
Buckling has been observed for macroscopic structures such as tubes [131, 136] and spherical shells [137–139]. But more recently, a variety of soft matter and nanoscale examples of buckling have also been demonstrated in the literature. Under application of a point force, polymer microcapsules were shown to exhibit the same buckling behaviour as table tennis balls [140].
Osmotic shocks, which can be used to apply a uniform pressure onto a spherical shell, cause buckling of elastic shells. Polyelectrolyte capsules of a well-defined radius and thickness were shown to buckle in response to osmotic pressure. The critical buckling

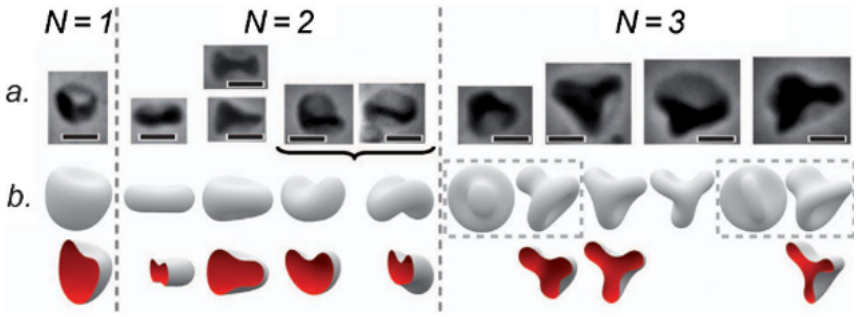

Figure 1.4: Experimental (a) and computational (b) results showing buckled gel-phase vesicles under hyperosmotic shock, displaying differing numbers of buckled regions. Scale bar = 5 µm. Reprinted figure with permission from Quemeneur et al., Physical Review Letters, 108, 1-5, 2012. Copyright 2021 by the American Physical Society [142].

pressure, P_c, was found to rely on the shell thickness and radius in very good agreement with Zoelly theory [141].

In some specific cases, lipid vesicles may also buckle in response to hyperosmotic shocks. Quemeneur et al. studied the buckling of gel-phase lipids with a DPPC membrane below its melting transition temperature. Experiments showed that in response to hyperosmotic shock, the gel-phase membrane buckled into one of a defined series of morphologies. These were classified by the number of depressions, N, which was found to depend on the vesicle size, and membrane parameters including the bending rigidity k_C and Young's modulus as in classical Zoelly theory [142]. Figure 1.4 shows the series of vesicle morphologies observed.

Fluid-phase vesicles do not have the shear rigidity required to form buckled morphologies; however, this shear rigidity can be imparted by the presence of a hydrogel coating. Kusters et al. demonstrated that covalently binding an actin gel shell to the exterior of the vesicle membrane allowed buckling in response to hyperosmotic shock. As shown in Figure 1.5, the gel-coated vesicles either buckled or wrinkled depending on the thickness of the actin shell [143]. Due to the strong covalent interaction between the membrane and its surrounding gel shell, the actin buckled along with the membrane rather

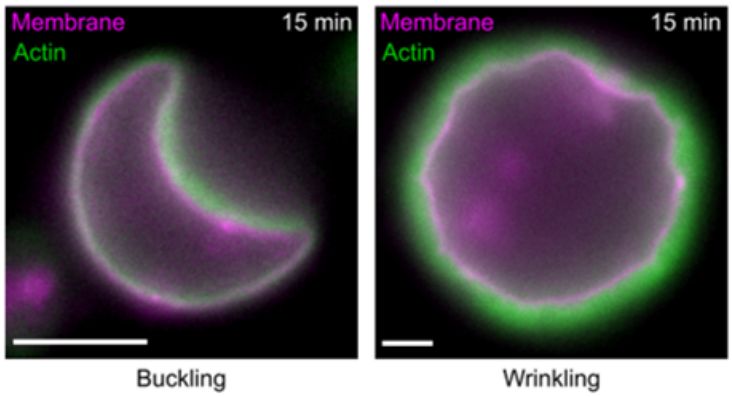

Figure 1.5: Actin-coated lipid vesicles exhibiting buckling or wrinkling depending on the thickness of the actin shell. Scale bar = 5 µm. Reproduced from Ref. [143] with permission from the Royal Society of Chemistry.

than detaching and remaining spherical. Previously, actin-coated lipid vesicles were shown to buckle in response to the application of a local force perpendicular to the membrane with optical tweezers, whereas uncoated vesicles did not buckle [144]. In general, however, fluid-phase vesicles do not form buckled shapes, as they lack the requisite shear rigidity. As described above, vesicle shape changes including buckling may occur due to a reduction of the internal volume. This may occur either by permeation through the lipid bilayer, or by the formation of membrane pores. The mechanisms of volume loss and shape change can be studied using fluorescence microscopy.

1.3.3 Fluorescence Techniques for Studying Volume Changes

The fluorophore calcein (shown in Figure 1.6a) is frequently used to study information about volume changes in both vesicles and cells [4, 128, 145–149]. It can be encapsulated within vesicles as a hydrophilic model active, and its low diffusion coefficent through the hydrophobic region of the membrane means that it does not cross the bilayer over experimental timescales [150]. However, it is easily released from the vesicle if membrane pores are formed [4, 151, 152]. Therefore, it is particularly useful as a hydrophilic model active molecule to be encapsulated within GUVs, as it can show whether or not membrane pores have been formed. If a vesicle loses some of its encapsulated volume

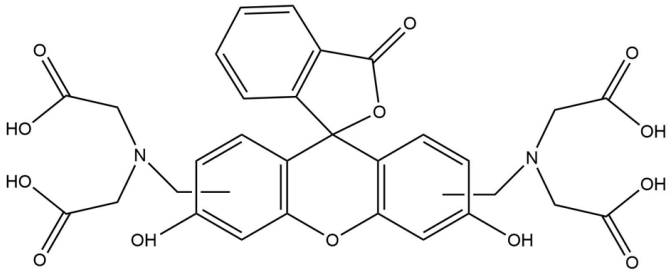

(a) Calcein, a hydrophilic fluorophore, can be encapsulated in the vesicle cores as a model active.

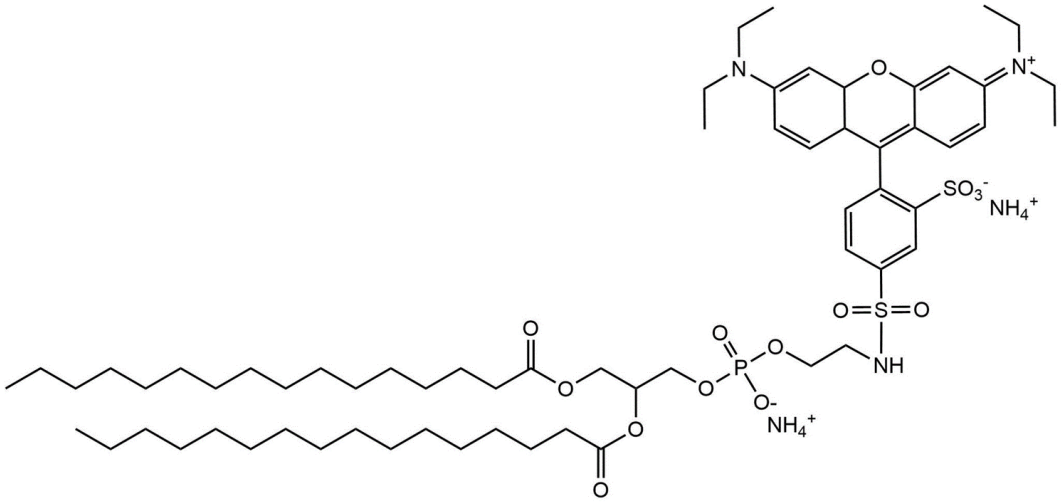

(b) Rh-DPPE is a headgroup-labelled fluorescent lipid, which is incorporated in the membrane.

Figure 1.6: Structures of the two fluorophores used in this work, calcein and Rh-DPPE.

by the formation of membrane pores, this is observed as a loss of fluorescence signal from within the vesicle. However, water can cross the lipid membrane on a much faster timescale than calcein, which can be observed as an increase in the concentration and hence mean fluorescence intensity of calcein.

Rhodamine-labelled 1,2-dipalmitoyl-sn-glycero-3-phosphoethanolamine (Rh-DPPE, shown in Fig. 1.6b) is a headgroup-labelled fluorescent phospholipid which can be incorporated into lipid membranes along with other membrane components, which allows

visualisation of the membrane shape via fluorescence microscopy. However, it cannot be ruled out that the inclusion of a fluorophore might perturb the membrane properties [153, 154] and so inclusion levels are often in the region of 0.1 - 1.0 %mol in order to minimise this effect. Another significant limitation of fluorescence microscopy is that only the the fluorophores are detected: it is possible that any changes to the rest of the membrane may be undetected. However, fluorescence microscopy has a higher depth of field than other microscopy techniques (such as phase contrast) [155], and so is useful for studying the relatively thick samples of hydrogel-embedded vesicles imaged in this work.

1.4 Membrane Energetics

Since the vesicle shape is determined by the membrane energetics, this section will consider the various contributions to membrane free energy. The preferred vesicle shape is that with the lowest membrane free energy, subject to the constraints of fixed volume and membrane area [156, 157].

The membrane free energy E is the sum of bending (E_{bend}), stretching ($E_{stretch}$), and adhesion energies (W), as described by Equation 1.1:

$$E = E_{bend}+E_{stretch}+W = \int dA[(\frac{k_C}{2}(C_1+C_2-C_0)^2+\bar{k}_C C_1 C_2)+(\frac{k_A}{2}\frac{(a-a_0)^2}{a_0})]+W \quad (1.1)$$

The following sections will consider each of the contributions to the free energy in turn.

Bending Energy

Equation 1.1 shows that the first term, bending energy E_{bend}, depends strongly on three membrane curvatures (C_0, C_1, C_2). C_1 and C_2 are the two principal curvatures of the membrane for a given shape, and C_0 is the spontaneous curvature of the membrane [158]. For vesicles of a fixed topology, the term $\bar{k}_C C_1 C_2$ is constant and can be neglected [159].

The bending energy of a membrane is closely linked to its chemical composition: different membrane components can have differing molecular shapes, which are approximated as being either cylindrical, conical, or inverted-conical [160]. These molecular shapes each have a preferred shape that they can pack into: for cylindrical-shaped membrane components, such as the phospholipid 1,2-dioleoyl-sn-glycero-3-phosphocholine (DOPC), this bending energy is minimised in planar membrane configurations with no curvature [161].

The spontaneous curvature, C_0, is the "preferred" curvature of the membrane [123]. It can arise from either a difference in membrane composition between leaflets, or from asymmetry in the aqueous environment on each side of the bilayer [162]. For example, lipid GUVs are often prepared encapsulating sucrose but dispersed in glucose in order to give good sedimentation and refractive index difference; however this results in a spontaneous curvature which favours membrane bending towards the external (glucose) phase [163].

Bending a bilayer membrane requires simultaneous expansion of one monolayer and compression of the other [161]. The energy required to bend a membrane in this way depends strongly on the membrane thickness d [161]. As lipid membranes are typically very thin ($\sim$4 nm) in relation to their lateral size (up to $\sim$100s µm), this makes them highly flexible [164].

The bending modulus k_C can be measured by a range of techniques including fluctuation microscopy, mechanical deformation (e.g. by micropipette aspiration), or scattering methods. k_C depends on the phase state of the membrane: gel phase vesicles have much higher values of k_C than fluid phase vesicles, even with the same composition. The presence of other molecules in the membrane, such as charged lipids, cholesterol, surfactants, etc., can all affect the value of k_C [165].

In general, the bending moduli of lipid membranes are relatively low, on the order of $k_C \approx 10^{-20} - 10^{-19}$ J [7, 165, 166]. This means that for DOPC membranes, thermal

energy at room temperature is sufficient to cause some membrane fluctuations, which can be experimentally observed with high magnification microscopy. These fluctuations have typical amplitudes of tens to hundreds of nanometres, depending on the vesicle radius and osmotic conditions [167, 168]. The fluctuation wavelengths vary from just a few nanometres to up to lengths comparable to the vesicle size, where the shorter wavelength fluctuations are controlled by the bending rigidity and longer wavelength fluctuations are controlled by the membrane tension [167, 169].

Stretching Energy

The stretching energy contribution to the total membrane area is a consequence of the bilayer structure: stretching the membrane beyond its equilibrium area per lipid a_0 would lead to exposure of the hydrophobic tail groups in the membrane core to the aqueous environment which has an entropic penalty [160].

The energy $E_{stretch}$ required to change the area per lipid, a, of a membrane from its equilibrium value a_0 is given by Equation 1.2 [161]:

$$E_{stretch} = 2\gamma a_0 + \frac{\gamma}{a}(a - a_0)^2 \tag{1.2}$$

where γ is the surface tension of the water and lipid interface, which generally has values of around 0.02 - 0.05 J/m^2 [161]. The first term describes the repulsive energy between over-crowded lipid molecules, and the second term describes the extra energy required to expose the hydrocarbon lipid tails to the water interface. Near to the equilibrium point a_0, Equation 1.2 can be re-written in terms of an area compression modulus, k_A:

$$E_{stretch} = \frac{k_A}{2}\frac{(a - a_0)^2}{a_0} \tag{1.3}$$

which is the form used in Equation 1.1.

For DOPC membranes, k_A has been estimated to be around 0.24 J/m^2 by micropipette pressurisation [170].

From Equation 1.3, the stretching energy is minimised by maintaining the area per lipid a at its equilibrium value a_0. However, when the membrane is forced to stretch (for example by water influx into a vesicle by hypoosmotic shock, or by mechanically stretching a Supported Lipid Bilayer (SLB)), a must increase. This induces a lateral stress to the membrane, which is known as the membrane tension, σ, and depends strongly on the amount of stretch or compression applied to the membrane.

When the membrane tension exceeds a critical lysis tension, the membrane ruptures, opening a membrane pore and allowing lipid molecules to rearrange in order to regain the optimal lipid packing at a_0 and minimise the free energy.

The formation of a membrane pore results in the addition of a line tension term to the free energy of the membrane, given by Equation 1.4[171]:

$$E(r) = 2\pi\lambda r - \sigma\pi r^2 \tag{1.4}$$

where r is the pore radius and λ is the line tension, which is the energy required to create a unit length of membrane edge. The first term is the work required to create a circular pore of perimeter given by $2\pi r$, and the second term corresponds to the work done by external forces including the membrane tension. This second term is a function of the pore area, πr^2.

The line tension, λ, depends on the composition of the membrane: both the tail length and degree of saturation affect the line tension for a given lipid [130]. For a pure DOPC membrane, the line tension λ has been reported to be in the range 6 - 300 pN [130, 171, 172]. The inclusion of other membrane molecules can alter the line tension, depending on their molecular shape. Inverted-cone shaped molecules, such as cholesterol which is used in many GUV systems, increase the line tension, whereas cone shaped molecules such as detergents significantly decrease the line tension. This relationship between line

tension and molecular shape is related to the fact that, at the pore edge, molecules need to rearrange such that the hydrophilic headgroups orient towards the centre of the pore, rather than leaving the hydrophobic tails exposed [172].

Adhesion Energy

Finally, interactions between the membrane and its substrate can have an effect on the membrane energetics and hence its shape. In some cases, membranes are covalently tethered to the substrate, such as by lipopolymers or biotin-avidin linkages [26, 74, 173, 174].

More generally, three different physical forces can contribute to the adhesion of a membrane to a substrate. These are van der Waals forces, electrostatic interactions, and entropic effects. In general, physical forces act over a longer range than chemical (covalent) forces [175].

Van der Waals forces arise from the instantaneous fluctuations in the dipole moment of an atom or molecule which induce dipoles in neighbouring atoms or molecules. These dipoles can interact which gives rise to an instantaneous attractive force between the atoms/molecules. Van der Waals forces are typically much weaker than electrostatic and hydrophobic forces.

Electrostatic interactions only apply to atoms or molecules with a permanent electrostatic charge. This interaction is described by Coulomb's Law, and the strength of the interaction between ions can be as strong as covalent bonds [175]. Hydrogen bonds are a specific type of electrostatic interaction that occur between hydrogen atoms that are covalently bound to an electronegative atom (such as oxygen or nitrogen), and a second electronegative atom [176]. Hydrogen bonds therefore form between lipid headgroups, water molecules, and any sugar molecules in the aqueous phase [177, 178] and this hydrogen-bonded structure has been suggested to have an influence on membrane properties such as the bending rigidity [179].

Entropic forces may also contribute to the adhesion between a membrane and its substrate. Generally, the membrane will fluctuate about its minimum energy conformation due to thermal energy, but as the membrane approaches a substrate, its fluctuations are suppressed. As a result, the membrane-substrate adhesion needs to be sufficient to account for this drop in entropy [180].

As discussed earlier, the hydrophobic effect is a driver of vesicle formation for phospholipids in aqueous solutions [181]. However, it can also be harnessed as a method for tethering lipid membranes to hydrophobically-modified substrates: hydrophobic alkyl chains on the substrate penetrate the bilayer in order to minimise their exposure to the aqueous environment [182]. In the case of p(NIPAM), this has been shown to give rise to an adhesion energy on the order of $W \sim 10^{-4}$ J, which is significantly higher than the adhesion strength between the membrane and cytoskeleton of red blood cells [76]. This opens up the possibility that although the nature of interaction differs from biological systems, by adjusting the amount of alkyl chains present at the surface, the adhesion energy might be tuned to biological values.

In summary, the vesicle shape is determined by a balance of bending, stretching, and adhesion energetics, subject to area and volume constraints. In particular, a reduction in the encapsulated volume of the vesicle can allow for a range of non-spherical shapes to be adopted. This thesis will study volume changes in both hydrogel-embedded vesicles and GFVs, and how the coupling of a hydrogel to the membrane affects the membrane's response to the volume change.

1.5 Thesis Overview

To conclude, composite structures combining lipid vesicles with hydrogels can combine the impermeability of the lipid bilayer with the mechanical strength of the hydrogel.

This has been harnessed in encapsulation systems, model systems for various cells, etc. However, in biology, the presence of the extracellular matrix or internal cytoskeleton supports the cell membrane in various non-spherical morphologies. Hence, this might alter the behaviours of the lipid membrane of either hydrogel-embedded vesicles or GFVs, and processes that usually allow for the release of vesicle contents may not apply to the composite structures.

At the outset of this work, the aim was to develop GFVs capable of exhibiting the same poration behaviour that has been shown for Supported Lipid Bilayers (SLBs) on elastic substrates. This would, hopefully, lead towards the design of a food-grade encapsulation system able to demonstrate controlled release of flavour molecules in confectionery. As the experimental work progressed, many barriers to this were found: mainly, the identification of a suitable trigger for poration and the corresponding gel chemistry, combined with finding a method of GFV preparation suitable for both the membrane and the gel.

Consequently, the focus of this work changed to the inverse structure, hydrogel-embedded vesicles, which are experimentally much easier to prepare but still allow for possible interactions between the gel and the membrane to be studied. This system also has the benefit of being somewhat more applicable to confectionery systems which often consist of a gel matrix.

Although ultimately different gel chemistries were used for each system studied here, the work on hydrogel-embedded vesicles is still informative for the preparation of GFVs; the findings on the interaction between the hydrogel and embedded lipid bilayers and how this affects vesicle behaviour will be useful for future work on membrane poration in GFVs.

The underlying aim of this work is to investigate how the coupling of a hydrogel to the lipid membrane affects its shape deformation in response to mechanical perturbations, and for the purposes of encapsulation and controlled release, whether the deformation is

accompanied by release of the vesicle contents. In particular, encapsulation and release in the context of food systems will be considered.

Chapter 2 will describe the materials and methods used throughout this work.

Chapter 3 investigates how the behaviours of lipid vesicles under osmotic shock are affected when embedded into an agarose hydrogel, and how the membrane properties are affected by the presence of agarose. Particular focus will be given to the similarities between hydrogel-embedded vesicles and plant cells.

Chapter 4 studies mechanical compression of agarose-embedded vesicles in comparison to other methods of deforming lipid vesicles. Again, the effect of interactions with the agarose hydrogel is discussed.

Chapter 5 will study the formation of thermoresponsive Gel-Filled Vesicles with the specific aim of demonstrating membrane poration in response to an environmental stimulus, related to the ability of planar SLBs to open stable membrane pores in response to substrate expansion.

Finally, Chapter 6 will conclude the thesis by drawing together the main themes of Chapters 3 - 5 and discussing the future outlook of this work.

Chapter 2

Materials and Methods

This chapter will describe the experimental methods employed in this work for both sample preparation and measurements. In particular, two different methods of GUV formation (electroformation and emulsion phase transfer) were utilised in the work, due to their suitability for different systems.

GUVs are particularly suited to measurements by optical microscopy-based methods, due to their typical diameters on the order of tens of micrometres. The different types of microscopy used, and the analysis of their images, is also discussed.

2.1 Materials

1,2-dioleoyl-sn-glycero-3-phosphocholine (DOPC; purity >99%; product code 850375), and 1,2-dipalmitoyl-sn-glycero-3-phosphoethanolamine-N-(lissamine rhodamine B sulfonyl) (ammonium salt) (Rh-DPPE; purity >99%; 810158) were purchased as solutions in chloroform from Avanti Polar Lipids.

Lecithin from egg yolk (Egg Lecithin; min. 60% phosphatidyl choline; product code 27608) was purchased from Universal Biologicals.

Sucrose (purity $\geq$ 99.5%; product code S7903), glucose (purity $\geq$ 99.5%; G7528), NaCl (purity $\geq$ 99%; 746398), hydrophilic fluorophore calcein (C0875), acrylamide

(purity $\geq$ 98%; 01700), *N,N'*-Methylenebisacrylamide (bisacrylamide; purity = 99%; 146072), acrylic acid (purity = 99%; 147230), light mineral oil (non-sterile; M8410), surfactant sodium dodecyl sulfate (SDS;), low melting agarose ($\leq$ 0.10% anion traces as sulfate; A9414), and fluorescent blue (amine-modified) and green (carboxylate-modified) polystyrene latex tracer particles (aqueous suspension, 2.5% solids; product codes L0280 and L4530) were purchased from Sigma Aldrich.

UV initiator 2,2-diethoxyacetophenone (DEAP; purity = 96%; product code 10743401) was purchased from Fisher Scientific.

All aqueous solutions were prepared using ultra-pure water (18.2 MΩ, 0.5 ppm organics) from Merck Millipore.

2.2 Preparation of Vesicles

From their discovery by Bangham et al. in the 1960s, GUVs were formed via a method of gentle hydration, in which a dried lipid film is hydrated in aqueous solution which allows lipids to self-assemble into GUVs. However, gentle hydration is slow and typically leads to a suspension of giant vesicles of mixed lamellarities [183]. For studying the biophysical properties of lipid membranes, unilamellar vesicles are strongly preferred, since Multi-Lamellar Vesicles (MLVs) can display altered properties such as the bending rigidity, permeability, etc. [184].

2.2.1 Giant Unilamellar Vesicles by Electroformation

The electroformation method (shown in Figure 2.1), developed by Angelova and Dimitrov in the 1980s [185], overcomes these limitations by applying an alternating electric field to the vesicle suspension during its formation. During hydration, the dried lipid bilayers are separated, overcoming the van der Waals interactions between them, to form unilamellar vesicles. The addition of an electric field aids this step by imposing an electrosomotic flow of the surrounding fluid as well as of the phospholipids themselves [186].

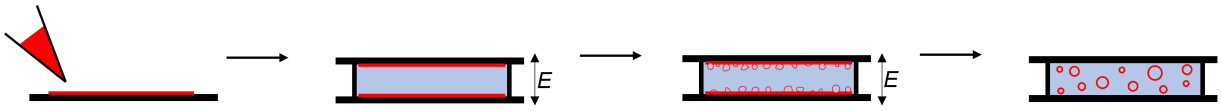

Figure 2.1: Schematic showing the formation of GUVs via electroformation. ITO-coated slides (black) are coated with the lipid mixture (red) and then hydrated in an aqueous solution (blue), aided by an alternating electric field *E*.

In Chapters 3 and 4, GUVs were prepared following a standard electroformation procedure [185]. Lipid mixtures were prepared and stored at 2.5 mg/mL in chloroform. The standard lipid mixture was DOPC including 0.5% mol Rh-DPPE as a fluorescent tag. 10 µL of this lipid mixture was applied onto each of two indium tin oxide (ITO)-coated glass slides which were then desiccated for >1 h to remove residual chloroform. The slides were then separated by a PDMS spacer and filled with the hydration solution, typically 300 mM sucrose, sometimes containing 0.02 mg/mL calcein. The slides were connected to a function generator and an alternating current (3 Hz, 1.5 V_{pp}) was applied for >6 h or usually overnight.

During electroformation, the chamber was contained in an oven at 60 °C and protected from light to prevent photobleaching. Protection from photobleaching was particularly important for GUVs containing the fluorophore calcein.

These parameters and setup were found to give a good yield of suitably sized (>20 µm) GUVs.

Although electroformation can lead to high yields of unilamellar vesicles, it is only applicable to limited systems. Firstly, electroformation cannot be used in cases where the vesicle mixture contains more than a small proportion of charged lipids. Similarly, salts and other ionic solutes cannot be included in the hydrating solution, as these charged species can accumulate at the electrodes [187]. Further, membrane proteins are also unsuited to electroformation [188].

Finally, electroformation is not suited to preparing vesicles with well-defined asymmetry

in either the aqueous solutions (i.e. different solutions internal and external to the bilayer) or the membrane (i.e. different membrane composition in each membrane leaflet). In fact, because different membrane components respond to electric fields differently, electroformation does not have inherent control over the membrane composition and as such there can be differences in the composition of different vesicles [187].

2.2.2 Giant Unilamellar Vesicles by Emulsion Phase Transfer

The Emulsion Phase Transfer (EPT) method of GUV formation is shown in Figure 2.2. This method, developed by Pautot et al. in the early 2000s, exploits the amphiphilic nature of phospholipids to design vesicles which can have both membrane asymmetry and solution asymmetry [189]. Phospholipids are firstly used to stabilise a water-in-oil (W/O) emulsion, effectively forming the inner leaflet of the vesicle membrane. The emulsion droplets are then transferred through a second, planar lipid monolayer assembled at an oil-water interface, which forms the outer membrane leaflet.

EPT was developed as a simple method for preparing GUVs with membrane asymmetry, but it has since been shown that, due to differing interfacial activities and solubilities, different membrane components may incorporate into the membrane in differing ratios to their proportions in the lipid mixture [4]. Also, the yield following the transfer step is closely linked to the density difference between the internal and external aqueous phases [147].

This method is employed in Chapter 5 to form GUVs as well as to attempt to form GFVs, by incorporating a pre-gel solution as the internal aqueous phase. EPT was chosen for GFVs because, firstly, it allows the use of salts and charged monomers in the internal aqueous phase, which are required for the chosen gel chemistry but would not be suitable for electroformation. Secondly, the solution asymmetry of this method is beneficial as in a symmetric system, if the internal phase can gel, so can the external phase. The asymmetry therefore removes the need for an extra step in the method to prevent external

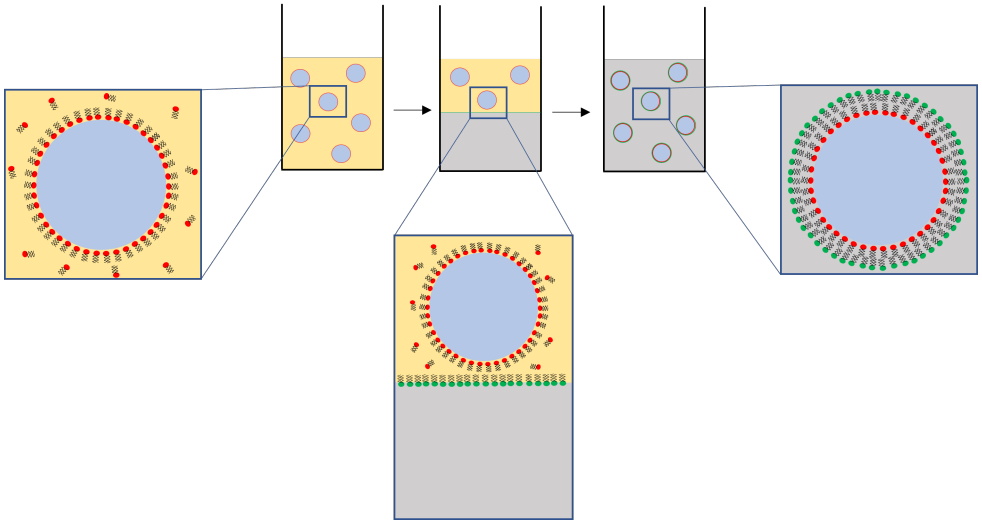

Figure 2.2: Schematic showing how GUVs can be formed from a phospholipid-stabilised W/O emulsion, giving both membrane asymmetry and solution asymmetry. Aqueous solutions are shown in blue or grey, oil solution is shown in yellow, and different phoshpholipids are shown in red and green.

gel formation [39].

Firstly, 150 µL of the external aqueous phase (typically 300 mM glucose solution) was added to a 1.5 mL polypropylene centrifuge tube. 150 µL of mineral oil containing 2 mg/mL egg lecithin lipids was added on top and the tube was left for >1 hour for the oil-water interface to become fully packed with lipids. Egg lecithin was used for these GUVs as DOPC is ineffective at preparing stable emulsions [190].

To form the emulsion, 50 µL of the internal aqueous phase was then emulsified by pipetting with 500 µL of a solution of mineral oil containing 2 mg/mL egg lecithin. The emulsion was carefully layered on top of the packed interface and the tube was centrifuged at 9,000 $\times g$ for 30 minutes. The oil phase was removed without disturbing the lower aqueous phase, and 150 µL more external aqueous phase was added. Finally, the vesicle suspension was re-centrifuged at 6,000 $\times g$ for 10 minutes. To form GFVs, the internal aqueous phase contained the pre-gel solution.

All GUVs were stored at 4 °C until required and used within one week of preparation.

2.3 Preparation of Hydrogels

As described in Chapter 1, hydrogels can be either physically or chemically crosslinked. In this work, the physically crosslinked biopolymer agarose is used for hydrogel-embedded vesicles, and the chemically crosslinked synthetic polymer poly(acrylamide-*co*-acrylic acid) is used to prepare GFVs with a temperature responsive core.

2.3.1 Agarose

Agarose can display significant variability in its chain length, degree of sulfation, etc., leading to variability in macroscopic parameters such as the gel stiffness [191, 192].
Many derivatives of agarose with different chemical structures have been developed and are used for various different applications, such as chromatography, enzyme immobilisation, etc. [193, 194]. In this work, 2-hydroxyethyl agarose (low melting agarose) is used as this particular derivative has previously been shown to stably embed lipid vesicles during gelation [46].

Low melting agarose was dissolved in either water, sucrose, or glucose solutions at 2% w/v. The solution was mixed with magnetic stirring in a water bath at 80 °C until fully mixed and homogeneous.
Agarose solutions were stored at 4 °C until required, as storing the solutions at temperatures above the melting point would cause a gradual degradation of the polymer which both increases the osmolarity and decreases the gel strength [195]. Before experiments, agarose solutions were heated with stirring to 80 °C for >1 hour to melt and homogenise and then the temperature was reduced to 50 °C for sample preparation. For agarose containing embedded vesicles, this temperature was found to give a good balance of keeping the agarose fluid above its gelation temperature, whilst not losing encapsulated calcein from the vesicles due to increased membrane permeability.
Agarose solutions were diluted to the required concentration and allowed to gel (covered)

at room temperature for 15 minutes before beginning experiments. Although the rate of cooling has been previously shown not to affect mechanical properties of agarose such as the compressive modulus, the elastic modulus does depend on the temperature at which the gel is cured [196, 197].

2.3.2 Poly(acrylamide-*co*-acrylic acid)

In Chapter 5, poly(acrylamide-*co*-acrylic acid) (p(AM-*co*-AA)) is identified as a potentially suitable gel core for GFVs which can display the poration mechanism of controlled release, due to its Upper Critical Solution Temperature (UCST) behaviour. However, it has previously been shown for LCST materials that the degree of temperature-dependent shrinking and swelling depends strongly on the preparation method, particularly the choice of initiation used: thermal initiation and photoinitation have been shown to result in different gel microstructures and hence different abilities to shrink [198].

Since p(AM-*co*-AA) is thermoresponsive [199], thermal polymerisation would be inappropriate as it could affect the solubility of the growing polymer chains during polymerisation. Therefore, photopolymerisation was chosen as a suitable method. In this method, a UV initiator 2,2-diethoxyacetophenone (DEAP) is included in the solution of monomers and, upon exposure to UV light, breaks down to form free radicals which initiate the reaction between monomers to form polymers.

2.4 Imaging

Since GUVs are of similar size to many types of cells, they are well suited to observations with optical microscopy. In particular, in this thesis the aim is to study how the hydrogel-coupled lipid membrane responds to mechanical perturbations, which includes possible shape changes. The below sections detail the experimental parameters used in each setup.

2.4.1 Brightfield Imaging

Brightfield images were collected using an inverted Nikon Ti-E microscope. The light source was a CoolLED pE-100 lamp and the camera was an ANDOR Neo sCMOS.

2.4.2 Fluorescence Imaging

The Nikon Ti-E microscope was also used for fluorescence imaging. The fluorophores used in this work and their relevant fluorescence parameters are:

- Rh-DPPE, a fluorescent headgroup-labelled lipid used to stain the lipid membrane by mixing with other lipids before vesicle formation. λ_{ex} =560 nm, λ_{em} =600 nm
- Calcein, a hydrophilic fluorophore encapsulated within vesicles by incorporating in the hydrating solution. λ_{ex} =470 nm, λ_{em} =510 nm

In all the figures of this thesis, any fluorescence signal arising from Rh-DPPE is coloured red, and any signal from calcein is coloured green.

2.4.3 Confocal Fluorescence Imaging

Confocal imaging uses a pinhole in the optical path to collect only emitted light arising from a particular focal plane and to remove background or out-of-plane fluorescence. This is useful both for imaging a cross-section of a sample, or for collecting a Z-stack of images which can be later used to form a 3D projection.

A Zeiss 880 inverted confocal microscope was used to collect 3D images, and a Leica SP5 inverted confocal microscope was used for FRAP experiments.

2.5 Analysis

2.5.1 Image Analysis

Image analysis was carried out in FIJI [200]. The lipid membrane contour was detected by auto-thresholding the image using the standard Minimum algorithm. For each frame, the membrane contour was saved as a Region of Interest (ROI). The background calcein intensity was subtracted (rolling ball radius = 200 px) in order to remove any fluorescence from either unencapsulated calcein or from out-of-focus vesicles. The mean and integrated intensities within each ROI were then measured.

2.5.2 Error Analysis

Many of the measurements in this work are related to changes in the membrane shape or area, and hence rely on image thresholding to detect the position of the membrane. Since the membrane itself is thinner than the resolution of optical microscopy, its position cannot be precisely known and so the thresholding step introduces an error to the measured values.

Figure 2.3 shows how the error on the membrane position was calculated. The membrane intensity profile (representative example shown in Fig. 2.3a) was first transformed into a radial profile (black line in Fig. 2.3b). This step averages the membrane intensity around the entire projected image of the vesicle to reduce the effects of any defects or other out-of-focus fluorescence. This profile was then fitted to a Gaussian (red line in Fig. 2.3b), and the half-width of the Gaussian is then taken as the error on the membrane position.

The membrane position is then assumed to lie within a ring of pixels either side of the detected contour, as shown in Figure 2.4, with the width of the ring given by the half-width of the fitted Gaussian. The area of the ring, which gives the error on the membrane area, was then calculated using the measured perimeter and the width of the

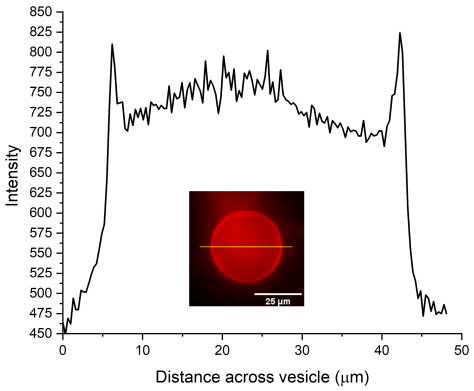

(a) Membrane intensity across a single equatorial line, shown in inset.

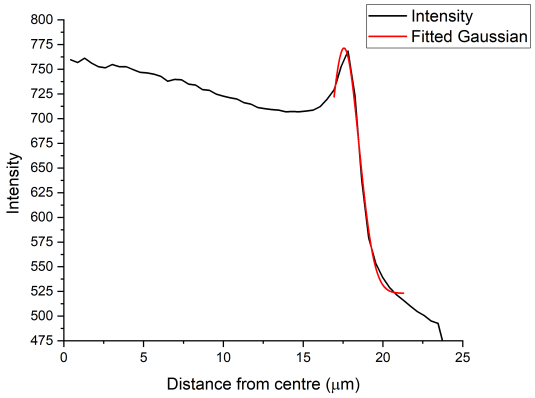

(b) Radial plot of membrane intensity in black, with the fitted Gaussian shown in red.

Figure 2.3: Representative membrane intensity profile, and the associated radial plot and fitted Gaussian used to find the error on the membrane position.

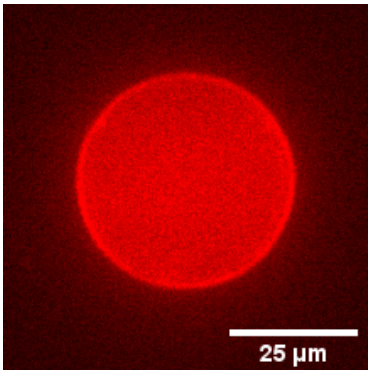

(a) Original Image

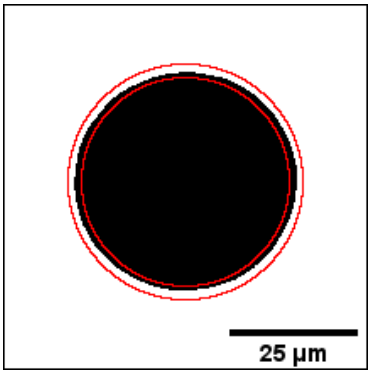

(b) Masked Image

Figure 2.4: Original and masked images of a representative vesicle. The black region is the measured area and the red lines show the region of error on detecting the membrane position.

ring. The perimeter measurement was carried out on smoothed images which was found to give a more accurate measurement of the perimeter. Errors on measurements such as the integrated intensity, which depend on the measured area, were then calculated by error propagation.

2.5.3 Statistical Analysis

A single factor Analysis of Variance (ANOVA) test was used to measure the statistical significance of measured trends. The analysis was carried out in Microsoft Excel. Additionally, Welch's t-test for unequal variances was carried out to test pairwise comparisons for statistical significance. This test is comparable to Student's t-test, but is modified for the case where the sample populations do not have equal variances. In each analysis, the significance level was chosen as $\alpha = 0.05$, i.e. 95% confidence.

Chapter 3

Osmotic Shocks on Hydrogel-Embedded Vesicles

3.1 Introduction

Maintaining the correct osmolarity within a cell despite environmental changes is vital for cellular survival [201]. An increase in the concentration of osmotically active (membrane-impermeable) substances external to the cell is termed a hyperosmotic shock, and can be caused by either external water loss or by the addition of concentrated sugar solutions. Cellular responses to these osmotic shocks consist of both an active process (involving synthesis of solutes within the cell and modification of the membrane permeability), and a passive process of water flux through the lipid membrane. Typically the passive process occurs first on a very fast timescale of seconds, with the active processes occurring over minutes or hours [202].

In plants, cell membranes are supported by an external cell wall which ensures that, upon changes in turgor and osmotic pressure across the cell membrane, the plant tissue integrity is preserved [12, 14]. In this chapter, lipid vesicles are embedded into an agarose hydrogel in order to mimic the plant cell wall, and to investigate how this system responds to osmotic perturbations.

During shrinking, the plant cell membrane can detach from its cell wall and form structures known as Hechtian strands. These are strands of the plasma membrane, adhering the membrane to its original position against the cell wall. They are suggested to play a substantial role in allowing the cell to return to its original state on being returned to its initial osmolarity; the shrinking behaviour of plant cells is reversible [203, 204].
Similarly, free-floating lipid vesicles can be deflated by hyperosmotic shocks, adopting non-spherical shapes, and re-inflated to a spherical shape by hypoosmotic shocks [205]. This chapter studies whether the presence of a hydrogel external to the lipid membrane may disrupt this reversibility.

Hydrogel-embedded vesicles have also been used as controlled release systems [86, 109, 206]. Under hypoosmotic shocks, free-floating lipid vesicles have previously been shown to cyclically open and re-seal membrane pores, releasing a small portion of their contents each time [207]. Therefore, the use of hypoosmotic shocks on embedded vesicles is studied as a potential trigger for the release of encapsulated actives.

In this chapter, agarose hydrogels were chosen to embed the GUVs, as these have a particularly simple preparation and have been shown to allow GUVs to be stably embedded over suitable timescales without affecting the size distribution of vesicles [46, 53, 208]. The presence of agarose was previously shown to alter some membrane properties and not others: lipid diffusion was not significantly affected, but the lifetime of membrane pores after electroporation was much longer than for free-floating vesicles. As a result, this chapter will investigate how two membrane properties (membrane pinning and membrane fluctuations) are related to the osmotic behaviour.

The aim of this chapter is to study how the coupling of a lipid membrane to an agarose hydrogel affects its response to osmotic shocks. Particular focus is given to the

formation of a buckled morphology, which has not been previously reported for fluid-phase vesicles. Also, the effect of the external agarose hydrogel on membrane fluctuations and lipid diffusion are examined.

3.2 Experimental

3.2.1 Sample Preparation

Giant Unilamellar Vesicles (GUVs) of DOPC with 0.5% mol Rh-DPPE were formed by electroformation as described in Chapter 2. The GUVs were formed in 300 mM sucrose containing 0.02 mg/mL calcein.

Low melting agarose was dissolved at 2% w/v in 300 mM sucrose and homogenised at 80 °C for >1 h. The agarose solution and GUV suspension were then kept at 40 °C for sample preparation. Agarose solutions were stored at 4 °C until needed, to prevent degradation of the polymers which decreases the gel strength [195].

The GUVs were then mixed with agarose (approximately 5% v/v GUVs) and more sucrose to give the desired final concentration. 30 µL of the fluid GUV-in-agarose solution was then pipetted onto a clean glass slide, covered with a glass cover slip, and allowed to gel at room temperature for 15 minutes.

The gel concentration was varied between 0.25% and 1.0% during osmotic shock experiments. This range covers the range of gel concentrations previously demonstrated to successfully immobilise GUVs without rupturing them during gelation [46].

For particle tracking experiments, green-fluorescent tracer particles (average diameter 2 µm) were included in the hot agarose solution at 5 µL/mL. These relatively large particles were chosen as they are significantly larger than the pore size of agarose and therefore are immobilised into the gel structure, rather than being free-floating in the aqueous phase. This means that if the tracer particles are observed to move, then this implies that the

gel structure is also changing.

3.2.2 Application of Osmotic Shocks

Samples were prepared in an enclosed chamber during gelation to prevent any osmotic shock due to evaporation. After being uncovered, they were then subjected to a change in osmolarity by pipetting a glucose shock solution directly onto the gel surface. The range of shock values Δc varied from 100 mM to 1M. A schematic of this setup is shown in Figure 3.1.

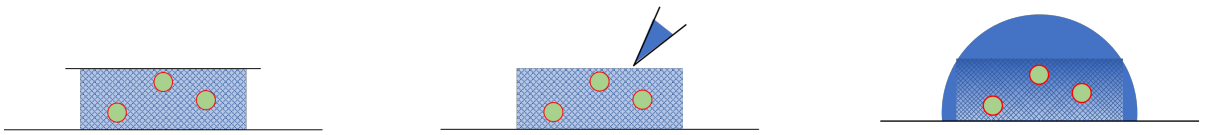

(a) The sample is gelled in a closed chamber.

(b) The lid of the chamber is removed and a shock solution is pipetted on top of the gel sample.

(c) The shock solution covers the whole gel sample and diffuses inwards.

Figure 3.1: Experimental setup for osmotic shocks on embedded vesicles.

3.2.3 Imaging

Epifluorescence Imaging

Most images were collected on an inverted Nikon Ti-E widefield epifluorescence microscope. The objective used had 40X magnification, Numerical Aperture (NA) = 0.6, working distance = 2.8 mm. An ANDOR Neo sCMOS camera was used to acquire images. 2x2 pixel binning was used to further increase the signal to noise ratio.

Generally, a single vesicle or a small number of vesicles in the same field of view were imaged for 1 h after the application of an osmotic shock to capture the response dynamics. Following this, a Z-stack of images was collected every 1 µm through the height of the sample at the same field of view. This captured a large number of vesicles (typically in the range of 30 - 60 vesicles per experiment) which were used to quantify the variety of

shapes for the given experimental parameters.

The shape descriptors, area, and intensity (both rhodamine and calcein) of the detected vesicles were quantified using ImageJ.

Shape Descriptors for GUVs

There are many shape descriptors that can be used to analyse vesicle shape changes. Two shape descriptors that will be used in this work are the solidity S and the roundness R. These are calculated according to Equations 3.1 and 3.2:

$$S = \frac{A}{A_{CH}} \tag{3.1}$$

$$R = \frac{4A}{\pi d_1^2} \tag{3.2}$$

where d_1 is the major diameter, A is the projected area of the vesicle and A_{CH} is the area of its convex hull, i.e. the smallest entirely convex shape that includes all the pixels within A.

Both the roundness R and solidity S can discriminate between a different set of vesicle shapes. For example, Figure 3.2 shows three vesicles after hyperosmotic shocks. The vesicle shown in Fig. 3.2b has high solidity but low roundness ($S = 0.970$; $R = 0.809$), whereas the vesicle shown in Fig. 3.2c has low solidity as well as low roundness ($S = 0.621$; $R = 0.655$). Solidity can be used to distinguish between different buckled shapes: although they both have low values of R, the values of S are very different. However, for buckled shapes with high solidity (such as Fig. 3.2b), roundness can still change significantly over the course of shrinking despite there being little change in solidity values. In this case, roundness is a more useful measure.

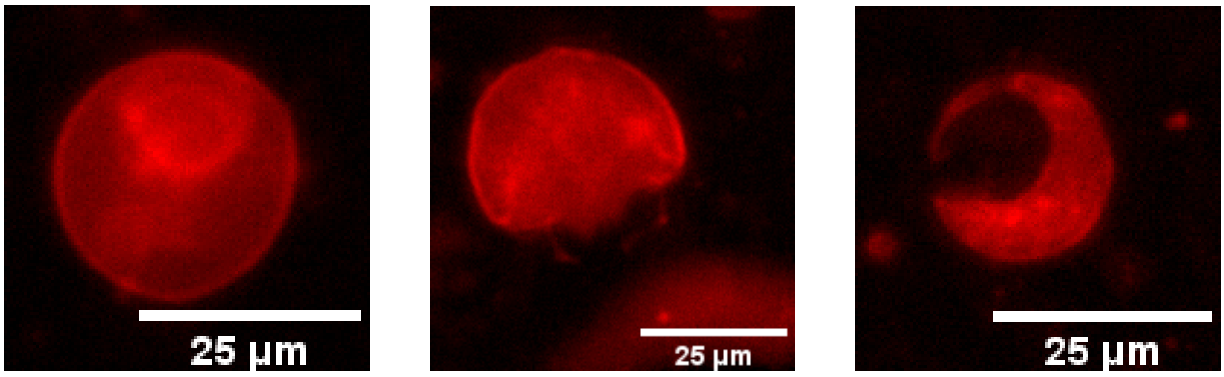

(a) High solidity and high roundness.
$S = 0.978; R = 0.968$
Gel concentration = 0.25%,
shock strength = +200 mM.

(b) High solidity and low roundness.
$S = 0.970; R = 0.809$
Gel concentration = 1.0%,
shock strength = +200 mM.

(c) Low solidity and low roundness.
$S = 0.655; R = 0.621$.
Gel concentration = 1.0%,
shock strength = +1000 mM.

Figure 3.2: Representative vesicle shapes with high or low roundness R and solidity S.

3D Images

Z-stacks were collected using a Zeiss 880 inverted confocal microscope with a 63X oil immersion objective. The objective had NA = 1.4, working distance = 0.14 mm. The pinhole size was set to 1 Airy Unit. Z-stacks were collected with <1 µm separation between slices.

Thermal Fluctuation Analysis

Thermal fluctuations of the lipid membrane were analysed for vesicles embedded in different concentration agarose gels. Samples were prepared as described in Section 3.2.1 but then uncovered and left at room temperature for 15 minutes to allow for a slight evaporation of the aqueous solution at the surface of the hydrogel. This results in a small degree of hyperosmotic shock without the application of a shock solution. This technique is used to relax the membrane tension slightly, which allows for more thermal fluctuations than if the membrane is under tension [209].

Embedded vesicles were then imaged using a 60X oil immersion objective (NA = 1.49, working distance = 0.16 - 0.07 mm) on an epifluorescence Nikon Ti-E microscope as described above. The vesicle was imaged for a minimum of 300 frames with the minimum

time step, which for this setup was 100 ms. At least 8 vesicles were imaged for each gel concentration studied.

The membrane contours were detected in ImageJ and the standard deviation of the membrane roundness over time was calculated.

Measurement of Lipid Diffusion

Fluorescence Recovery After Photobleaching (FRAP) was used to measure the effect of gel concentration on the lipid diffusion within the membrane.

A Leica SP5 confocal microscope with 63X oil immersion objective was used for FRAP imaging. A chosen vesicle was imaged for 10 frames pre-bleaching. The laser power was then increased to maximum and the membrane was bleached for 20 frames, inside a defined region of interest (ROI) of a known size. The entire vesicle was then imaged again post-bleaching for 300 frames.

The collected image series was then analysed using ImageJ. The intensity pre- and post-bleach was normalised to the average pre-bleach intensity and plotted against time. The post-bleach section was then fitted to a single exponential using OriginPro.

Each measurement was carried out ≥ 3 times in total. The plotted values are given as the average for each experiment and the error bars are the standard error between measurements.

3.3 Results

3.3.1 Encapsulation and Long-Term Stability of the System

Firstly, the agarose-embedded vesicles were observed over a timescale much longer than the typical experiment in order to measure any background instabilities or leakage of calcein. The vesicle membrane and encapsulated calcein were imaged every hour over 15 h. The samples were contained within a closed chamber to protect them from evaporation

throughout the experiment, which would lead to an osmotic shock on the vesicle.

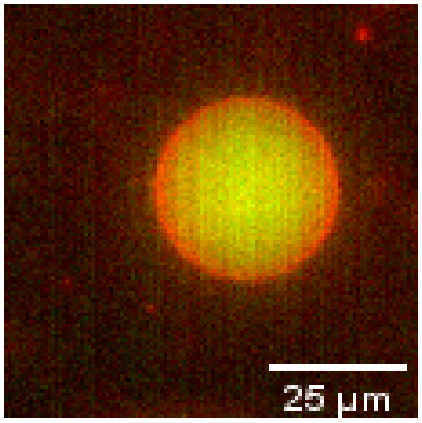

(a) Vesicle at time = 0 h

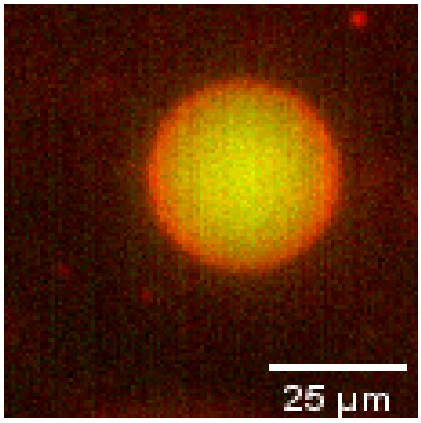

(b) Vesicle at time = 15 h

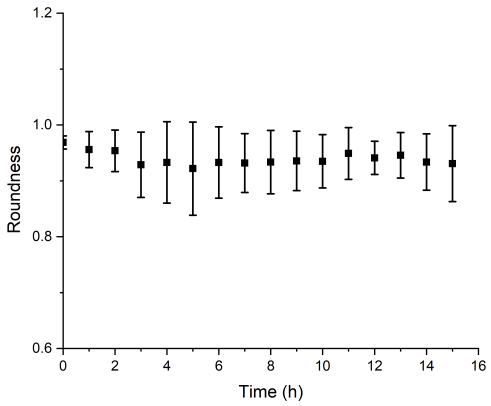

(c) Roundness over time

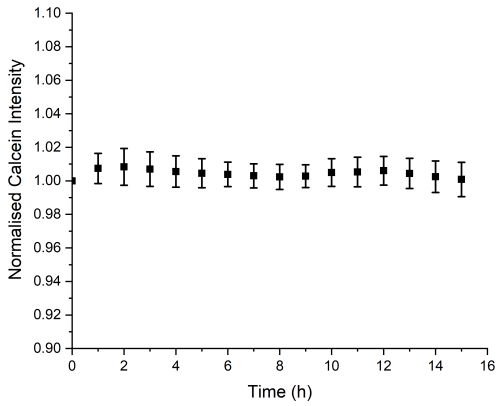

(d) Encapsulation over time

Figure 3.3: Long term stability of DOPC vesicles embedded in a 1% agarose hydrogel. (a) and (b) show a representative vesicle at the beginning and end of the experiment, respectively. Roundness (c) and calcein intensity (d) plots are prepared from 5 vesicles. Error bars are the standard deviation between vesicles.

Figure 3.3 shows a typical vesicle at the beginning and end of the long timescale experiment. It appears by eye to remain roughly spherical, and Fig. 3.3c confirms that R stays constant at slightly below 1.0 throughout the entire experimental time. This means that over long timescales there are no vesicle shape changes observed due to any effect of embedding the GUVs into an agarose matrix.

The normalised integrated calcein intensity, shown in Fig. 3.3d, remains at 100% (within experimental error) throughout the course of the experiment which suggests that no calcein

is lost from the vesicle over many hours. Therefore in further experiments, any calcein loss or membrane shape changes can be attributed to an applied stimulus rather than the effect of embedding the vesicles into the gel matrix.

3.3.2 Hyperosmotic Shocks

Osmolarity is a measure of the number of solute particles in a unit volume of solution. Equation 3.3 gives the definition of osmolarity O on the concentration c of each species i present in the solution [210]:

$$O = \sum \phi_i n_i c_i \tag{3.3}$$

where ϕ_i is the ideality of the solute, n_i is the number of particles it dissociates into in aqueous solution (i.e. $n_{sucrose} = 1, n_{NaCl} = 2$), and c_i is its concentration. For the ideal solutions of simple sugars used here, the value of O in units of Osm/L is equal to the sugar concentration in units of M, so throughout this chapter solutions are referred to by their concentrations rather than osmolarities.

For ideal solutions ($\phi = 1$), the osmotic pressure Δp_{osm} is related to the concentration difference across the membrane by the van't Hoff equation (Equation 3.4 [211]):

$$\Delta p_{osm} = k_b T N_A \Delta c \tag{3.4}$$

This osmotic pressure Δp_{osm} results in the flow of water across the membrane until the osmolarity is equilibrated, according to Equation 3.5 [212]:

$$J = -P_{water} \Delta c \tag{3.5}$$

for P_{water} the permeability of the lipid membrane to water. For fluid lipid membranes, P_{water} is typically on the order of 10^{-3} cm/s. Polar molecules such as sugars have much lower permeability constants, of the order $P_{glucose} \sim 10^{-11}$ cm/s [213].

Hyperosmotic shocks occur when the concentration of osmotic agents is greater outside the vesicle outside than inside the vesicle. This can be caused by the addition of a more concentrated solution to a sample of vesicles, or by allowing the external solution to concentrate by evaporation. In both cases, this causes an efflux of water from the vesicle interior which reduces the vesicle volume.

Since no sugar (or calcein) molecules cross the bilayer during an osmotic shock, the equilibrium volume V_f after water loss from the vesicle can be calculated according to Equation 3.6:

$$\frac{V_f}{V_0} = \frac{c_0}{c_f} = \frac{c_0}{c_0 + \Delta c} \tag{3.6}$$

where V_f is the vesicle volume after water efflux, V_0 is its volume before osmotic shock, and c_f and c_0 are corresponding solute concentrations. $\Delta c = c_f - c_0$ is the strength of the osmotic shock.

V_f depends on both the initial internal osmolarity c_0 and the imposed external osmotic shock Δc. Figure 3.4 shows the calculated vesicle volume for a range of shock strengths Δc and initial concentration within the vesicle, c_0.

The final volume of the vesicle as a proportion of its initial volume ($\frac{V_f}{V_0}$) is shown in Fig. 3.4b for a range of different initial internal concentrations c_0 and applied shocks Δc. The larger the applied shock Δc, the more water is lost from the vesicle so the smaller its final volume, V_f. Also, for a fixed value of the applied shock Δc, the larger the initial internal concentration c_0, the larger the final volume V_f.

The curves in Figure 3.4b fall onto a master curve, shown in Fig. 3.4c. The volume $\frac{V_f}{V_0}$ is shown to depend on the ratio of the applied shock to the initial internal concentration, $k = \frac{\Delta c}{c_0}$.

Equation 3.6 is based purely on the conservation of the amount of each solute on either side of the bilayer. In reality, particularly at higher values of k, there are likely to be more factors at play. Firstly, the solutes take up a finite amount of space within the

(a) Schematic showing the concentrations c and volumes V of an embedded vesicle before and after the application of osmotic shock

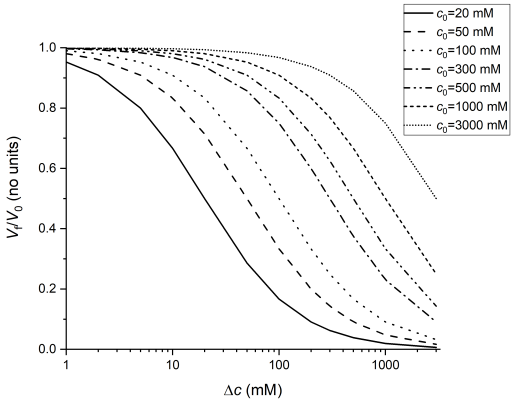

(b) Varying the initial concentration or the shock concentration affect the final volume

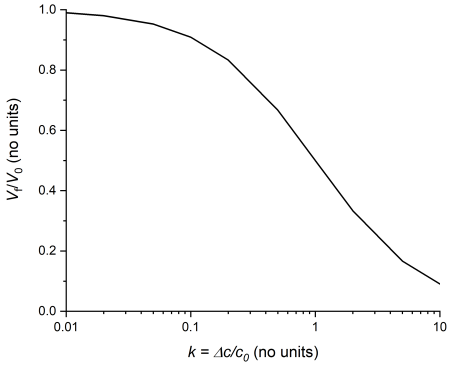

(c) Master curve for all initial concentrations and shock concentrations

Figure 3.4: Effect of initial internal concentration and applied shock concentration on the final volume of a deflated vesicle, according to Eq. 3.6.

vesicle, and so practically the enclosed volume of the vesicle will not ever go to zero even in the case of extremely high shocks. Secondly, previous experiments have shown that as Δc increases, vesicles are more likely to open a membrane pore due to the high pressure difference Δp_{osm}, and this frequently results in the complete rupture and disappearance of the vesicle [214]. Instead, it is likely that Equation 3.6 only holds for moderate values of k where the only mechanism of water efflux is via membrane permeation.

Effect of Hyperosmotic Shocks on the Lipid Bilayer

Osmotic shocks of varying strength were applied to GUVs embedded into agarose hydrogels. Figure 3.5 shows a time series of a representative embedded GUV in response to a hyperosmotic shock. The vesicle appears to detach from the gel matrix and form a

non-spherical, buckled shape. This is shown by the value of the roundness, R, (shown in Fig. 3.5e) which decreases significantly from a value of $R = 0.98$ to $R = 0.80$ over the course of the experiment.

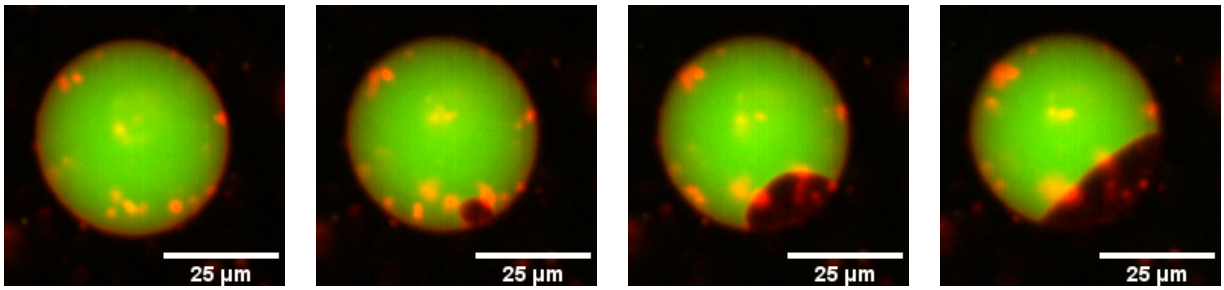

(a) t = 0 min (b) t = 34 min (c) t = 47 min (d) t = 75 min

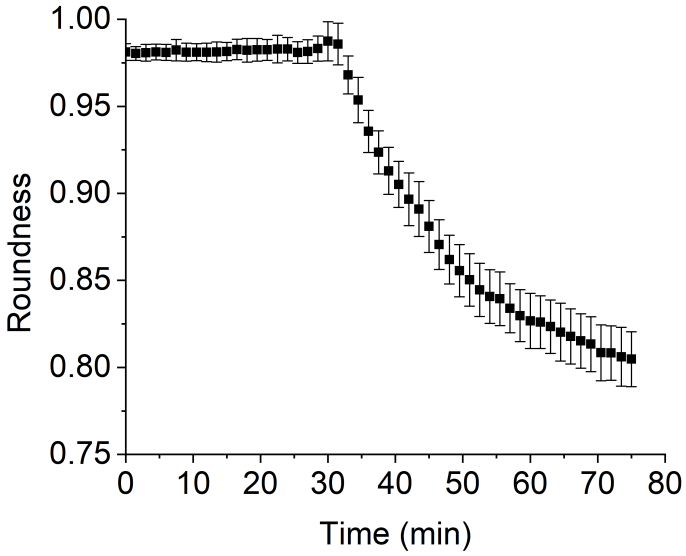

(e) Roundness of the embedded vesicle over time. Error bars are calculated by propagating the error from the projected area.

Figure 3.5: Change in roundness of an embedded vesicle over time due to hyperosmotic shock. Gel concentration = 1.0%.

Buckling of rigid spherical capsules upon deflation and of lipid vesicles in the gel phase have been discussed already in the literature and ascribed to the finite shear rigidity of the capsule wall, which is able to support these deformed shapes [215, 216]. However, the vesicles used in this study are composed of 99.5% mol DOPC and 0.5% of a rhodamine-labelled phospholipid. At room temperature, these vesicles are in the fluid

phase (as confirmed by FRAP experiments, Section 3.3.5) and as such their buckling behaviour is very unexpected. The buckling behaviour is hypothesised to be related to either an adhesive interaction between the gel and the membrane, or the effect of confinement on the vesicle.

This chapter will discuss buckling of fluid vesicles embedded in hydrogels, explore the mechanisms of buckling, and relate the observation on vesicle model systems to the more complex behaviour of plant and yeast cells under plasmolysis.

High magnification confocal Z-stack imaging was used to construct a 3D image of a similarly buckled vesicle, shown in Figure 3.6. The vesicle has buckled from the gel matrix and formed internal membrane structures in the hemisphere that remains. Where the vesicle has buckled, there are membrane strands that remain adhered to the gel, forming a cage-like structure of membrane tubes. This indicates that an adhesive interaction between the gel and the membrane could be causing the buckling behaviour.

Another noteworthy feature of Fig. 3.6 is the presence sharp corners of the membrane at the edge of the buckled region. This will be discussed later in this chapter.

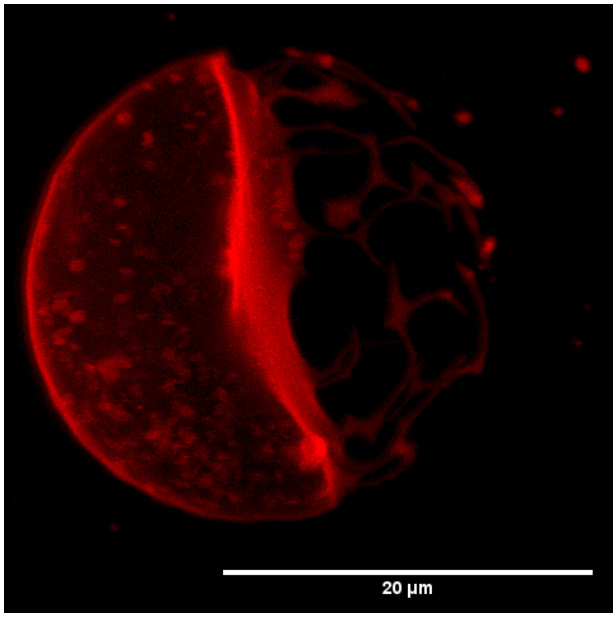

Figure 3.6: High magnification 3D image of a deflated embedded vesicle. Gel concentration = 1.0%, shock strength = +240 mM.

Dynamics of Shrinking

The formation of the buckled shape was investigated by imaging embedded vesicles over the course of shrinking.

Generally, shrinking commences with a reduction in the projected area whilst maintaining an externally spherical shape, as shown in Figs. 3.7a and 3.7b. This pre-buckling shrinkage is accompanied by the formation of internal membrane structures such as daughter vesicles and membrane tubes, which can be seen as bright regions within the vesicle.

The buckling step occurs very rapidly in comparison to pre-buckling shrinkage, as shown by the plot in Figure 3.7e. This particular vesicle exhibited a decrease in the projected area of approximately 10% over just 30 seconds.

The buckled morphology differs from the expected behaviour for free-floating, fluid-phase GUVs. Generally, as the volume of a vesicle is reduced, it quickly adopts a prolate or oblate shape. This may then spontaneously transform, with constant volume, into one of a number of different morphologies, depending on the volume reduction v and the area difference between membrane leaflets, Δa, as described in Section 1.3.1 [123, 124]. For vesicles with $\Delta a < 1.0$, the equilibrium morphology is a stomatocyte or "cup-like" shape. This shape can evolve from a spherical vesicle via the process: sphere $\rightarrow$ prolate $\rightarrow$ "cigar" $\rightarrow$ discocyte $\rightarrow$ stomatocyte [124].

The buckled morphology of the deflated hydrogel-embedded vesicle is similar to the stomatocyte morphology in that it contains an invagination in a spherical exterior shape. However, Figure 3.7 shows that the vesicle transforms directly from spherical $\rightarrow$ buckled rather than following the same shape trajectory as free-floating vesicles. Another notable difference is that stomatocytes (and other morphologies of free-floating vesicles) are smooth, rounded shapes, that do not contain any sharp edges, unlike the buckled vesicles shown in Figures 3.5 - 3.6.

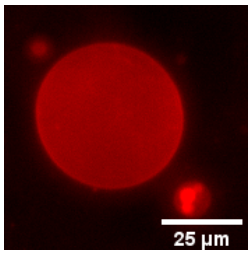

(a) t = 0.5 min

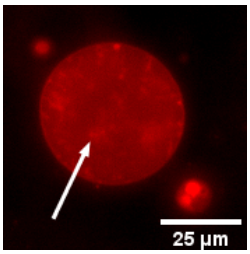

(b) t = 28.0 min

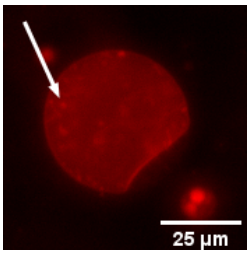

(c) t = 28.5 min

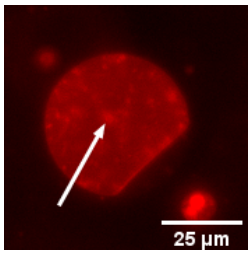

(d) t = 41 min

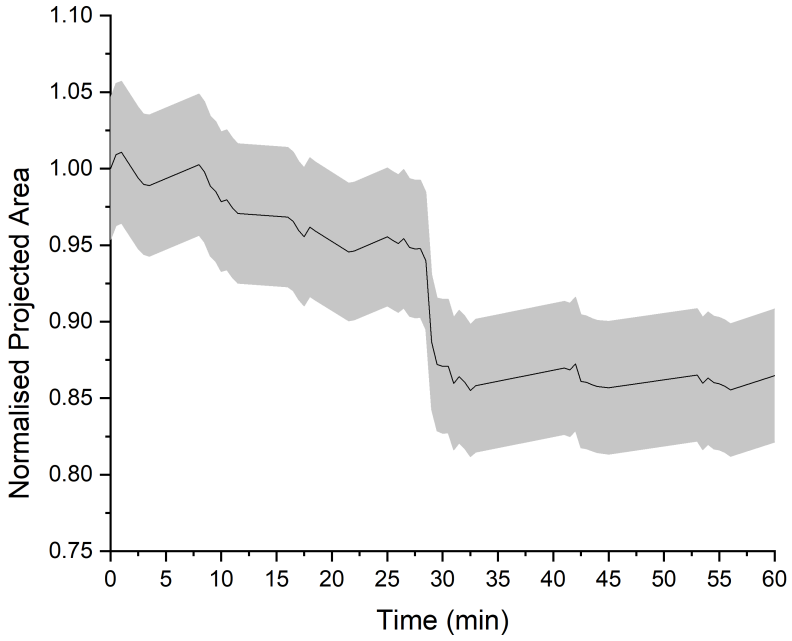

(e) Change in projected area of an embedded vesicle over the course of a hyperosmotic shock experiment. The projected area is normalised to its value before addition of the shock solution. The grey region denotes the error on the area measurement.

Figure 3.7: Shrinking dynamics of buckling of an embedded vesicle. Gel concentration = 0.5%, shock strength = +160 mM. red
White arrows in (a)-(d) refer to internal daughter vesicles which were detached from the external vesicle membrane.

The shape of a vesicle after deflation also depends on the spontaneous curvature, C_0 [123]. Spontaneous curvature is the "preferred" curvature of the membrane which arises from asymmetry - such as membrane asymmetry or asymmetry in the solutions on either side of the bilayer [217]. The spontaneous curvature arising from different solutes

generally favours membrane "bulging" towards the smaller solute, or the compartment with the smaller concentration of solutes. This is due to the depletion layer formed by the sugar molecules at the membrane surface, and the resulting membrane curvature depends linearly on the solute concentration [163]. The sign convention used is that spontaneous curvature is positive if the membrane bends towards the exterior compartment, and negative if it bends towards the interior compartment [217].
In the case of external glucose and internal sucrose, as used here, the spontaneous curvature should result in the formation of external membrane tubes or blebs [218]. However, for embedded vesicles, most experiments showed instead the formation of internal membrane structures (see for example Figs. 3.7 - 3.9). This could possibly be due to a contribution to the spontaneous curvature arising from the agarose hydrogel. Alternatively, it could be that membrane tubes and blebs preferentially form towards the inside of the vesicle due to the steric hindrance imposed by the external hydrogel. This effect will be considered further in Section 3.4.1.

In this system, the dynamics at play are a combination of the diffusion of the shock solution through the gel matrix and the permeation of water through the lipid membrane. As described earlier, the permeability of water through the membrane (P_{water}) is on the order of 10^{-3} cm/s [213]. Since lipid membranes have a thickness of only around 4 nm [161], the permeation of a molecule of water through the membrane takes only around 0.4 ms. These values will however depend on the membrane composition, with the value of P_{water} decreasing as the membrane thickness increases, for example due to the incorporation of cholesterol in the membrane, or by using phospholipids with longer or more saturated alkyl tails [150, 219, 220].
Diffusion through the agarose matrix has been studied for a range of solutes. Lira et al. found that any water-soluble molecules or particles with sizes up to 5 nm can diffuse through a hydrogel of 0.5% low-melting agarose to reach the GUVs. This was shown by FRAP and autocorrelation for two different fluorescent dyes, sulforhodamine B and

carboxyfluorescein. The authors also found that micelles of the detergent Triton X-100 were free to diffuse throughout the gel [46]. Similarly, Weng et al. studied the diffusion of glucose through agarose hydrogels of various concentrations using changes in the refractive index. The data for glucose was found to fit well with a diffusion coefficient of $D = 6.26 \times 10^{-10}$ m^2/s for 0.5% agarose and $D = 5.73 \times 10^{-10}$ m^2/s for 1.5% agarose. Generally, D was found to decrease as the concentration of agarose increased, due to increased obstruction from the gel increasing the path length the glucose must take [221]. However, these values are for unmodified agarose, rather than the low-melting agarose used in this work, so the values of D may not relate to the present work. Nevertheless, the authors conclude that glucose can freely penetrate the agarose hydrogel.

So, we assume that when the shock solution reaches the embedded GUVs, they are able to very quickly equilibrate the osmotic pressure by the permeation of water across the membrane. In further experiments concerning the shapes of the deflated vesicles, the shocked gels were left to equilibrate for 1 h before analysis of the vesicle shape, in order to allow the glucose to fully permeate the gel sample and shock all vesicles.

Pinning and De-pinning

During vesicle deflation, membrane pinning is frequently observed. Substrates can pin lipid membranes, preventing motion of the membrane due to a strong attractive interaction at discrete positions [222]. This occurs in cells, where the cell membrane is pinned to the cytoskeleton, and is related to the membrane composition and the mesh size of the cytoskeleton [222, 223].

During shrinking, agarose-embedded vesicles were observed to be pinned to the surrounding gel at distinct locations. An example of this is shown in Fig. 3.8d: rather than having a smooth, rounded shape, the membrane displays sharp corners with high curvature.

To understand how pinning affects the dynamics of vesicle shrinking, the projected

vesicle area of a vesicle displaying membrane pinning was studied over the course of shrinking. Figure 3.8 shows a time series of an example of this. The vesicle originally shrinks quickly within the first five minutes, adopting a buckled shape with membrane remnants adhered to the gel surface. Between Figs. 3.8b and 3.8c (t = 5.30 min and t = 5.63 min respectively), the membrane quickly recedes from the pinning point indicated by the white arrow to the pinning point indicated by the green arrow. The membrane remains pinned at this location for a relatively long timescale, up to around t = 30 min, shown in Fig. 3.8d. During this time, the membrane recedes slightly further in the "free", unpinned, region and this shrinking is accompanied by formation of more internalised structures. Subsequently, there is another de-pinning event between t = 30.97 min and t = 31.30 min (Fig. 3.8e). At each de-pinning, some membrane material remains adhered to the gel due to the strong pinning between agarose and the membrane.
Figure 3.8f shows the area change for the de-pinning event between Figs. 3.8b and 3.8c. Although the relative change in area is very small compared to the experimental error, the de-pinning exhibits a fast reduction in area similar to the buckling shown in Fig. 3.7e.

From these results, we can conclude that the interaction between the lipid membrane and the agarose gel is not spatially homogeneous but instead there are pinning points which are regions of strong attraction holding the membrane in a fixed position. Membrane pinning affects the dynamics of shrinking as shown in Figures 3.7 and 3.8: rather than exhibiting a smooth, gradual decrease in size as free-floating vesicles do [212], the embedded vesicles have step-like decreases in the projected area corresponding to membrane de-pinning from the agarose hydrogel.

However, it is unclear what the origin of this membrane pinning might be. Firstly, pinning may arise due to an attractive interaction between the gel and the membrane. Although DOPC, the major component of the membrane, does not have a net charge, the fluorophore Rh-DPPE contains a positively charged headgroup (as shown in Figure

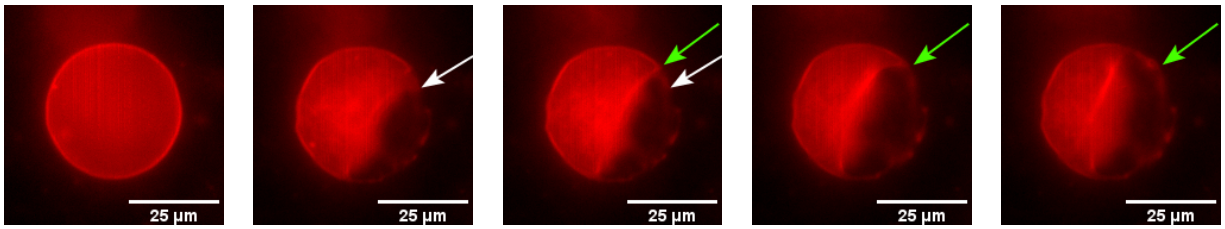

(a) t = 0 min (b) t = 5.30 min (c) t = 5.63 min (d) t = 30.97 min (e) t = 31.30 min

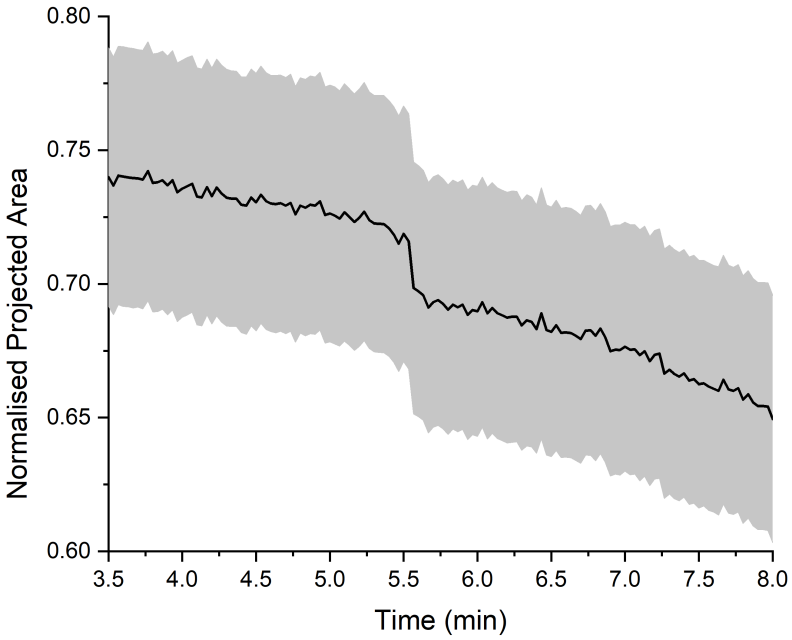

(f) Normalised projected area for the de-pinning event observed between Figs. 3.8b and 3.8c. The grey region denotes the experimental error on the area.

Figure 3.8: Shape evolution of a shrinking GUV exhibiting pinning points. The white and green arrows show points where the membrane appears to be pinned to the gel. Gel concentration = 1.0%, shock strength = +500 mM.

1.6b). Similarly, although the structure of agarose as a polysaccharide would suggest that it is uncharged, the grade of agarose used in this study can contain up to 0.1% of negatively charged sulfate groups. So, we hypothesise that the small amount of sulfate present in the agarose chain experiences an electrostatic attraction to the Rh-DPPE within the membrane, causing spatially heterogeneous points of stronger interaction between the gel and the membrane.

This hypothesis could be investigated by varying the amount of Rh-DPPE included in the membrane and by changing the degree of sulfation of agarose via chemical modification [224] to observe how this affects the amount of membrane pinning.

Alternatively, it is possible that the adhesion is due to hydrogen bonding between all components of the system (phospholipids, agarose, sugar, and water), and that the specific pinning sites are due to regions within the gel of higher density, since the structure is not completely spatially homogeneous [197, 225]. To test this hypothesis, the heterogeneity of the gels could be inhibited via faster gel cooling [226], although this might require the addition of more GUVs to the gel, since faster cooling rates can reduce the proportion of vesicles that remain intact after gelation.

Shape analysis of deflated vesicles

Next, the morphologies of the deflated vesicles are described, studied for a range of gel concentrations and shock strengths. The gel concentration was varied from 0.25% to 1.0% agarose, which spans the range of gel concentrations in which GUVs are successfully immobilised but are not ruptured during gelation. The shock strength was also varied over a large range of values, from +200 mM to +1000 mM. A large number of vesicles in each condition (>65 GUVs per condition) were imaged 1 h after the application of osmotic shock. Figure 3.9 shows representative images for shrunken vesicles sorted by shock strength and gel concentration.

In contrast to the high concentration gels, many vesicles in low concentration gels

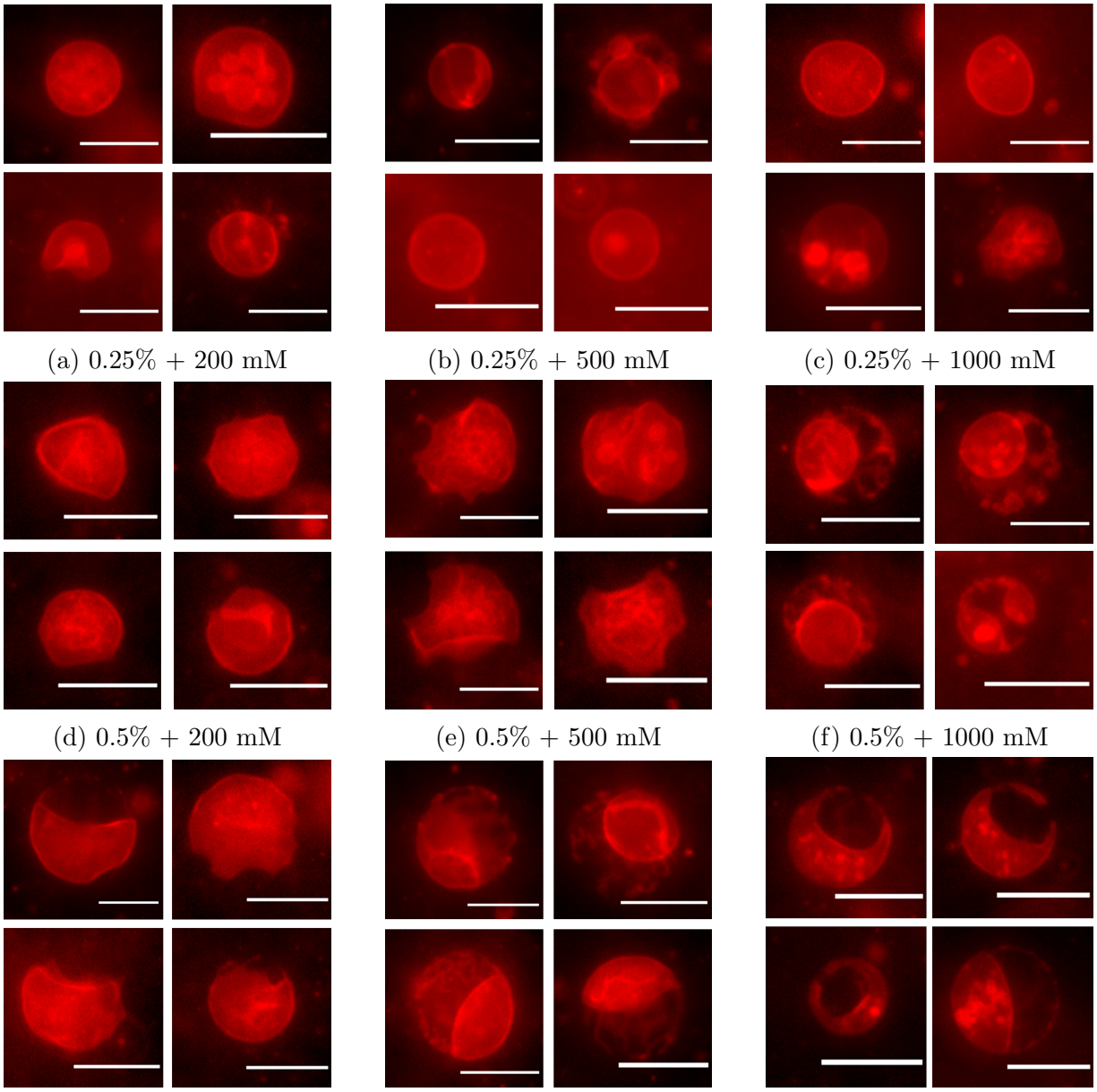

(a) 0.25% + 200 mM (b) 0.25% + 500 mM (c) 0.25% + 1000 mM

(d) 0.5% + 200 mM (e) 0.5% + 500 mM (f) 0.5% + 1000 mM

(g) 1.0% + 200 mM (h) 1.0% + 500 mM (i) 1.0% + 1000 mM

Figure 3.9: Gallery of representative vesicle shapes for differing gel concentrations and shock strengths, at t = 1 h after application of the shock solution. All scale bars are 25 µm.

appear to have a spherical shape (Figs. 3.9a-3.9c). To confirm that these spherical vesicles have responded to the hyperosmotic shock, single GUVs were imaged over the course of shrinking. Figure 3.10 shows a typical vesicle before and 1 h after the application of a +500 mM hyperosmotic shock. The vesicle has clearly decreased in projected area whilst maintaining its approximately spherical external shape and forming internal membrane structures (visible as regions of higher intensity fluorescence within the vesicle). From this it can be concluded that the observed spherical vesicles have deflated spherically, and therefore that they have a significantly different response to hyperosmotic shocks than vesicles in higher concentration gels.

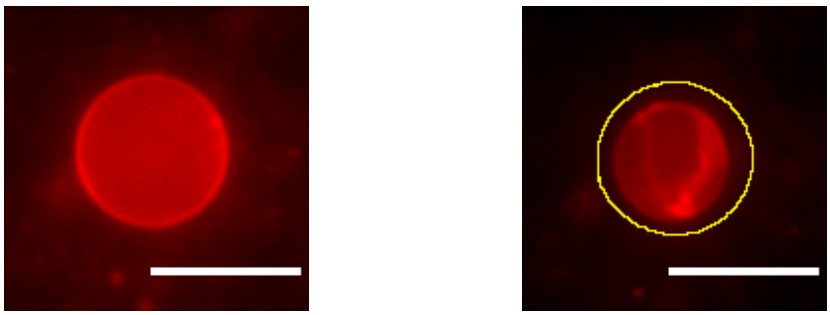

(a) Before shock (b) t = 1 h after shock

Figure 3.10: Confirmation that a representative spherical vesicle after hyperosmotic shock has deflated. Gel concentration = 0.25%, shock strength = +500 mM. The yellow overlay shows the original size and shape of the vesicle. Scale bar = 25 µm.

In higher concentration gels (Figs. 3.9g-3.9i), the predominant vesicle shape is no longer spherical, but the buckled morphology. In some cases (e.g. Fig. 3.9e), vesicles exhibit multiple buckling regions rather than the single buckle which is more predominant. Many of the deflated vesicles also display membrane strands which are attached to the agarose gel.

To further understand the trends in vesicle morphology, the vesicle shape descriptors were analysed for a large number of vesicles in each condition. Figure 3.11 shows the calculated values of solidity, S, and roundness, R, for each gel concentration and

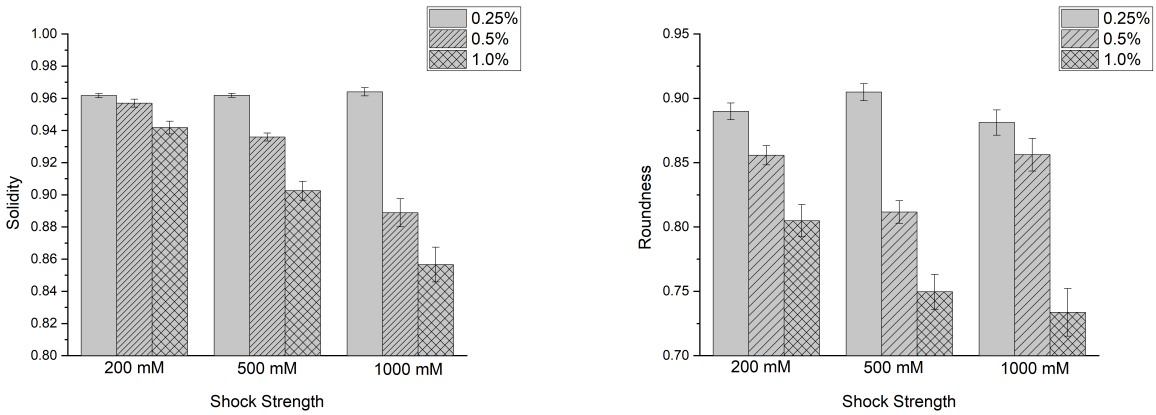

(a) Solidity (b) Roundness

Figure 3.11: Shape descriptors measured for vesicles in different gel concentrations and shock strengths.
$n > 65$ vesicles for each condition. Error bars are the standard error for each condition.

shock strength ($n > 65$ vesicles per condition). It is clear that increasing either the gel concentration or the shock strength causes a reduction in the average solidity and roundness of the embedded vesicles.

Firstly, increasing the gel concentration causes a decrease in the values of both S and R. As seen in Figure 3.9, at low gel concentrations embedded GUVs are likely to retain a roughly spherical shape during shrinking, which is characterised by high solidity and high roundness ($S = 0.962 \pm 0.001$ and $R = 0.894 \pm 0.004$, measured across all shock strengths).
As the gel concentration is increased to 1.0%, more buckled vesicles are observed, and these are characterised by S values in the range of 0.86 - 0.94 and R values of 0.73 - 0.80, depending on the shock strength.

For small shocks, across all gel concentrations (Figs. 3.9a, d, g), R decreases due to osmotic shock while S maintains a high value. From Figure 3.9, it can be seen that this is because although the vesicles adopt a non-circular shape with lower roundness, in general there are no significant membrane protrusions that would decrease the solidity value. In

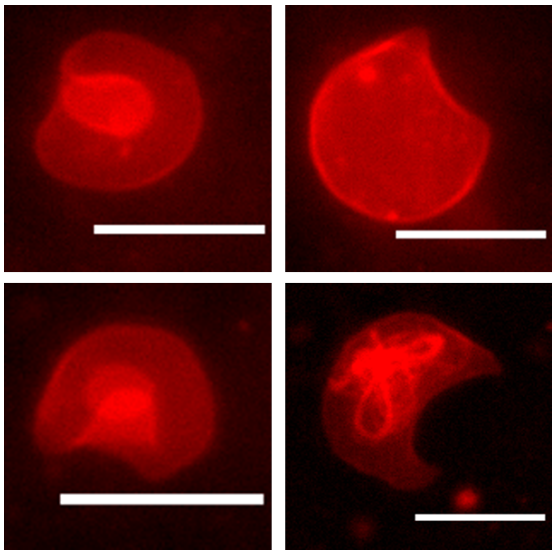

(a) Gel concentration = 0.25%

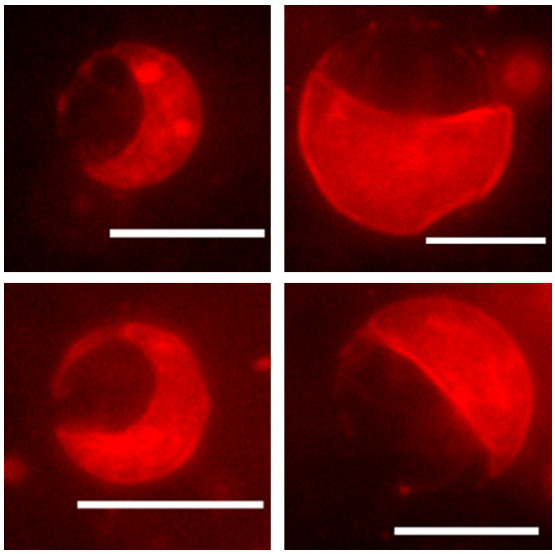

(b) Gel concentration = 1.0%

Figure 3.12: Representative images of vesicles embedded in different concentration agarose gels after hyperosmotic shocks.

comparison, many of the vesicles at high shocks (Figs. 3.9f, i) show a highly internalised membrane invagination which gives a much lower value of S in addition to low values of R.

Additionally, the gel concentration was found to affect the membrane curvature, particularly at the buckled edge. In low concentration gels, the vesicles exhibit generally rounder shapes: either the vesicle maintains a circular shape while deflating, or the buckled region of the membrane is smoother (Fig. 3.12a). In high concentration gels, the vesicles display regions of high membrane curvature and sharp membrane corners which are not observed for lower gel concentrations (Fig. 3.12b).

The shock strength controls the final volume of the vesicle, as shown in Figure 3.4. At low gel concentrations, many embedded vesicles remain spherical, as shown by the high values of both S and R (Fig. 3.11). In order for these vesicles to lose volume and maintain a spherical shape, they must detach from the agarose gel. Therefore the larger shock strengths lead to more detachment from the gel.

At high shock strengths and high gel concentrations, many of the vesicles exhibit membrane regions of high negative curvature. The vesicle shapes (Fig. 3.9i) and the energetic factors that produce them will be discussed in more detail later in this chapter.

Effect of Hyperosmotic Shocks on Encapsulated Calcein

In order to test the integrity of the membrane during the formation of buckled vesicle shapes, the intensity of encapsulated calcein was measured throughout shrinking.

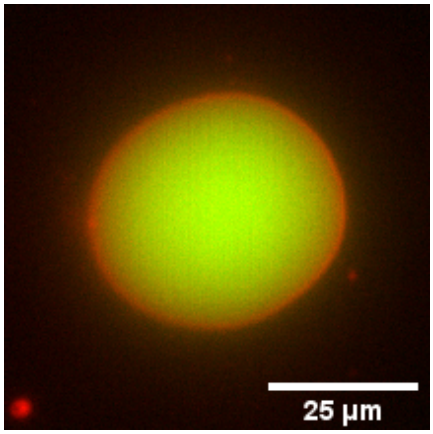

(a) Before Shock

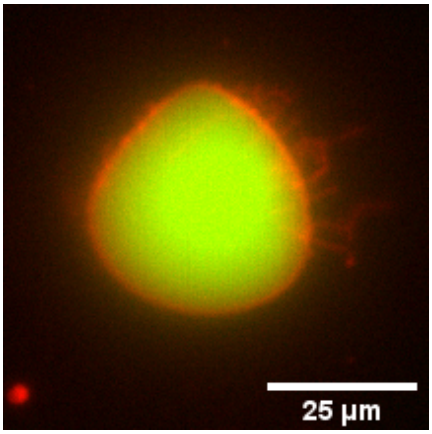

(b) t= 75 min after shock

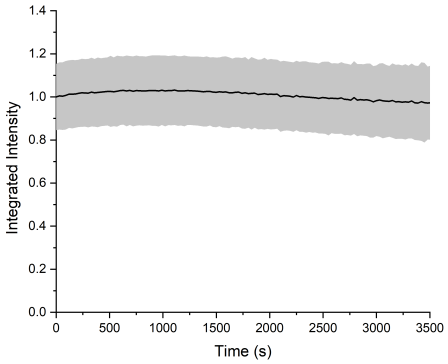

(c) Normalised integrated intensity of encapsulated calcein. The shaded grey region shows the error on the intensity measurement.

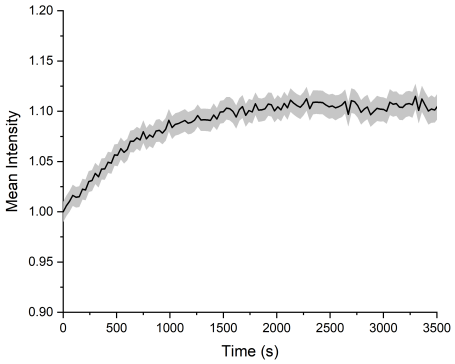

(d) Normalised mean intensity of encapsulated calcein. The shaded grey region shows the error on the intensity measurement.

Figure 3.13: Calcein intensity during a hyperosmotic shock. DOPC GUV embedded in 1% agarose, subjected to a shock of $\Delta c = +200$ mM.

The intensity of the encapsulated calcein can be measured either as the integrated intensity, which is the sum of all pixel intensities within the vesicle, or the mean pixel

intensity. Figure 3.13c shows the integrated intensity over the whole experiment remains constant within experimental error, which confirms that the calcein content within the vesicle does not change during shrinking. In addition, the mean intensity (Fig. 3.13d) increases during shrinking, confirming that as the water is lost from the vesicle, the average concentration of calcein increases.

These confirm that the buckled morphology observed is formed by an intact lipid bilayer with no significant defects or pores which would allow the release of calcein, and that the water loss and volume decrease lead to an increase in calcein concentration within the embedded vesicle.

3.3.3 Reversibility

Vesicles have been described as ideal osmometers - that they are permeable to water and impermeable to solutes, and they respond predictably and reversibly to the osmolarity of their surroundings [213, 227]. The reversibility of agarose-embedded vesicles was investigated in order to understand if the interaction of the agarose and the lipid membrane has any effect on the ideal osmometer behaviour.

Also, the presence of the external agarose surrounding the lipid membrane resembles the structure of plant cells and yeast cells, both of which have a cell wall surrounding the cell membrane. So, the reversibility response of the embedded vesicles is studied in order to know whether this is also similar to that of plant or yeast cells.

The reversibility of the response was tested by first applying a hyperosmotic shock to embedded vesicles and allowing them to shrink, followed by applying a hypoosmotic shock of equal magnitude to the same sample to reswell the shrunken vesicles to its original osmolarity.

Figure 3.14 shows a time series for a representative vesicle and the plots of the normalised projected vesicle area, roundness, and mean calcein intensity over time. The gel concentration was 1% and the shock strengths were ± 200 mM. For these conditions,

Figure 3.11 shows that hyperosmotic shock is likely to reduce the roundness but not the solidity, so roundness is the most appropriate shape descriptor to show shape changes in this case.

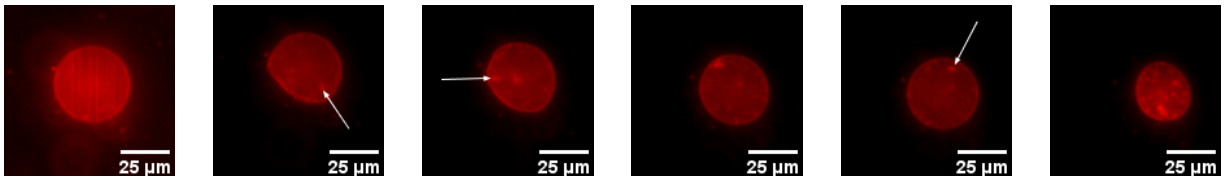

(a) t= 0 min (b) t= 6 min (c) t= 12 min (d) t= 16 min. (e) t= 19 min (f) t= 24 min

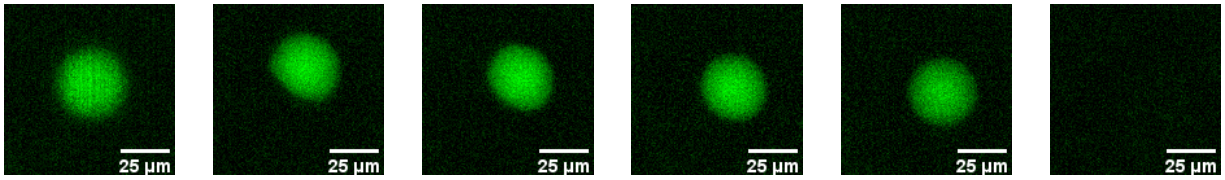

(g) t= 0 min (h) t= 6 min (i) t= 12 min (j) t= 16 min. (k) t= 19 min (l) t= 24 min

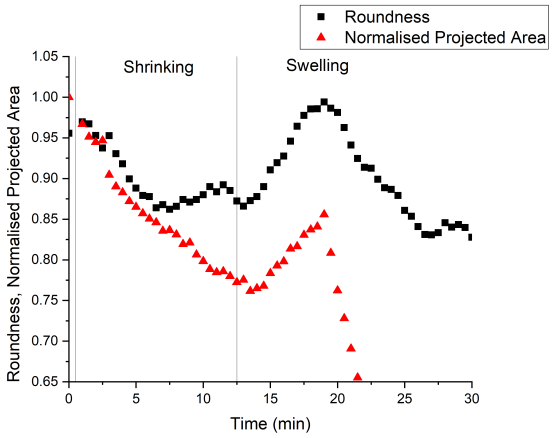

(m) Projected Area and Roundness plots for the vesicle shown above.

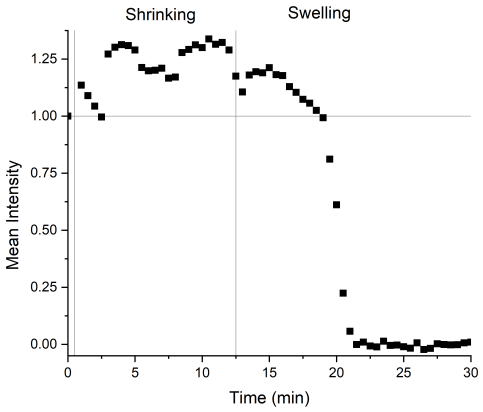

(n) Mean Calcein Intensity plot for the above vesicle.

Figure 3.14: Sequential hyper- and hypoosmotic shocks on the same embedded vesicle. A DOPC GUV embedded in agarose gel of 1% subjected to hyperosmotic shock of Δc = +200 mM at t = 0.5 min followed by hypoosmotic shock of Δc = -200 mM at t = 12.5 min. White arrows denote the locations of some representative daughter vesicles within the shocked vesicle.

Figs. 3.14a - 3.14f show that the vesicle, which is initially spherical, buckles at roughly t = 6 min and shrinks further. After the hypoosmotic shock is added at t = 12.5 min, the vesicle regains its spherical shape by t = 19 min.

However, the projected area of the vesicle does not show the same reversible behaviour

that is suggested by the roundness. The projected vesicle area returns to $< 90\%$ of its original value at t = 19 min. At t = 19.5 min, the vesicle ruptures which is seen as a sudden decrease in both the roundness and the projected area.

Figures 3.14g - 3.14l show the fluorescence signal of the encapsulated calcein throughout the experiment, and the mean intensity is shown in Fig 3.14n. The mean intensity increases significantly during shrinking (as also shown in Fig. 3.13d) and during reswelling, returns to its initial value by t = 19 min. From t = 19.5 min onwards, the calcein is quickly lost from the vesicle, which confirms that the vesicle has ruptured.

Understanding why the vesicle does not return to its original size and osmolarity without rupturing requires a consideration of the membrane dynamics. The lipid membrane and the surrounding fluids exhibit viscous relaxation with a characteristic time τ. For DOPC vesicles stretched by optical tweezers, the relaxation time was measured by flicker spectroscopy to be on the order of $\tau = 1$ s [228]. Any vesicle shape perturbations that occur faster than the relaxation time of the system are likely to cause irreversible changes in the membrane shape. For example, rapid fusion of adhered SUVs to a GUV, or fast temperature changes around the phase transition temperature, have been demonstrated to lead to budding of the membrane and the formation of daughter vesicles and/or lipid aggregates [229, 230]. These daughter vesicles or aggregates are inaccessible to the GUV membrane for any further shape changes.

As a result, when a large hyperosmotic shock is applied to the embedded vesicles, the fast water efflux causes the membrane to bud daughter vesicles into the internal compartment, as can be seen located by the white arrows in Figure 3.14. These daughter vesicles were observed to be freely floating within the vesicle's encapsulated fluid core, rather than fixed in position relative to the external membrane, from which it seems they have detached from the vesicle membrane. Such membrane invaginations are seen in almost all vesicles after hyperosmotic shock (Figure 3.9). On the application of a hypoosmotic shock, the

daughter vesicles are inaccessible to the swelling GUV, and hence it does not have sufficient membrane material to regain its original size. Consequently, as the osmolarity is returned to its original value, the influx of water causes the vesicle to rupture.

3.3.4 Hypoosmotic Shocks

Following the results of the reversibility experiments, hypoosmotic shocks were applied to embedded GUVs directly, without a preceding hyperosmotic shock, in order to understand how this affects the vesicle response to swelling.

Hypoosmotic shocks occur when the external solution to a vesicle is less concentrated than the internal solution. In order to equalise the osmotic pressure, there is an influx of water to the vesicle. The vesicle can accommodate some of this extra volume by membrane stretching, but beyond an area increase of around 3% [19], the membrane forms pores or ruptures. The formation of membrane pores does have an energy penalty due to line tension of the pore edge, but this allows the lipids to regain their optimal area per lipid, preventing exposure of the hydrophobic tail region to the aqueous solution. Simulations of pore formation in lipid bilayers have revealed that, when the tense membrane ruptures, it first forms a "hydrophobic defect" (Fig. 3.15a) where lipid tails are now exposed to the aqueous environment. Since this is entropically unfavourable, the hydrophobic defect form is short-lived and the membrane instead quickly rearranges into a "hydrophilic pore" (Fig. 3.15b) so that headgroups are oriented towards the aqueous environment and alkyl tails are shielded from it [164, 171].

For free-floating vesicles, the release of the internal solution can theoretically be either quasi-steady or pulsatile, but the quasi-steady state occurs for experimentally inaccessible conditions [207]. In pulsatile release, when the area increases beyond the point of rupture, a pore forms which allows some volume loss causing the membrane tension to be relieved. The line tension of the pore then drives the pore to close, resulting in a vesicle of a smaller

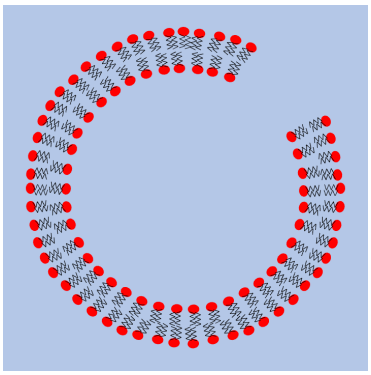

(a) Schematic of a hydrophobic defect

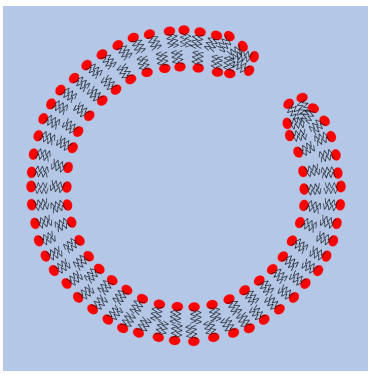

(b) Schematic of a hydrophilic pore

Figure 3.15: Schematics showing the formation of a membrane pore from a hydrophobic defect.

size. When the osmotic pressure builds up again, another pore forms and releases more of the internal volume. This cycle continues until the osmotic pressure is equilibrated across the membrane and there is no more water influx, or has reached a small enough value that the membrane can accommodate the slight difference [95, 211, 231].

Effect of Hypoosmotic Shock on Encapsulated Calcein

In order to understand how the presence of agarose affects the embedded vesicles during vesicle swelling, hypoosmotic shocks were applied to GUVs embedded into high concentration (1.0%) agarose hydrogels. Figure 3.16 shows a time series of images of both the rhodamine and calcein signals for a GUV embedded in 1.0% agarose, subjected to a hypoosmotic shock of $\Delta c = -160$ mM. A membrane pore is observed to open in Fig. 3.16c, and the fluorescence signal arising from encapsulated calcein is quickly lost following this. The calcein release profile is shown in Figure 3.16k. The drop in calcein intensity at t = 4 s is an artefact arising from the addition of the shock solution causing an out-of-focus frame at that timepoint. Similarly, the increase in intensity until t = 52 s is due only to a small amount of drift in the Z-plane, and as such is completely within the calculated experimental error.

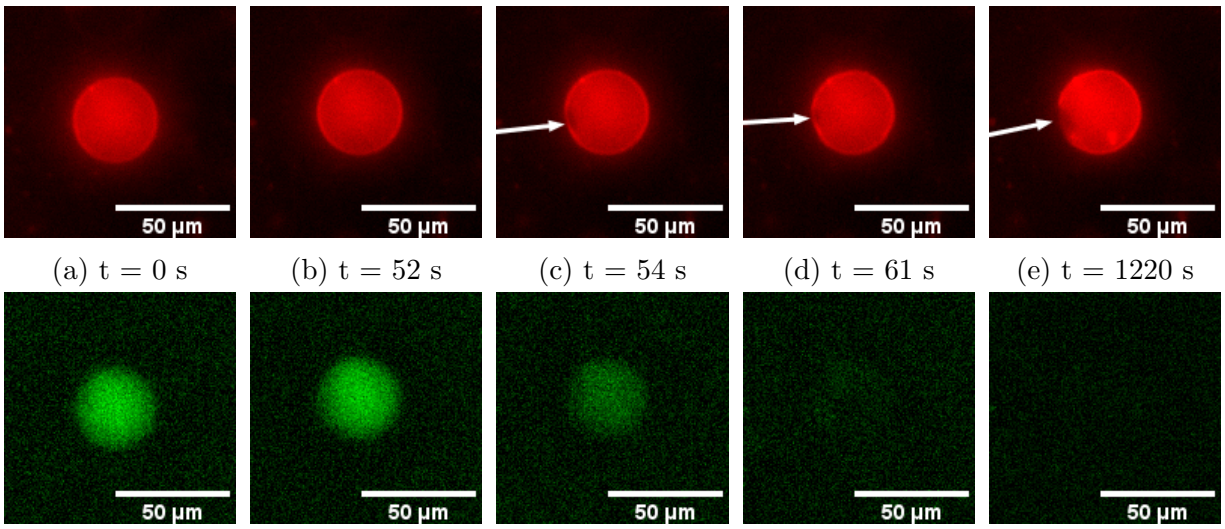

(a) t = 0 s (b) t = 52 s (c) t = 54 s (d) t = 61 s (e) t = 1220 s

(f) t = 0 s (g) t = 52 s (h) t = 54 s (i) t = 61 s (j) t = 1220 s

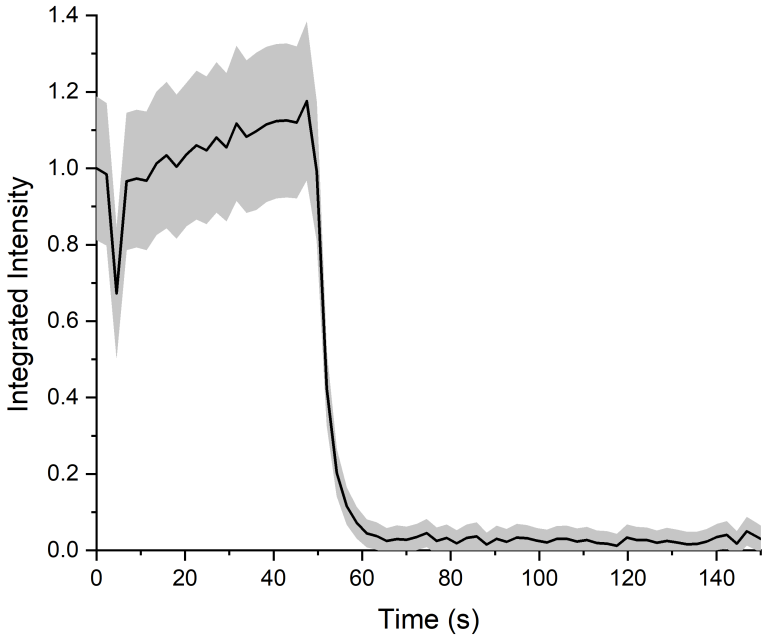

(k) Normalised integrated intensity of encapsulated calcein over time. The shaded grey region denotes the error on the intensity measurement.

Figure 3.16: Effect of hypoosmotic shock on intensity of encapsulated calcein. The gel concentration is 1.0% and the applied shock was Δc = -160 mM. White arrows show the location of a membrane pore.

Figures 3.16d-3.16e show that the membrane pore remains open over a long time period, and as shown in Figure 3.16k this results in the encapsulated calcein being released in a single burst-type profile. This is in contrast to the expected pulsatile release profile, in which a small amount of the encapsulated volume is lost ($\approx 5\%$) in each pulse [207]. From this result, we conclude that pinning of the membrane to the surrounding agarose prevents the pore from resealing, and hence the embedded vesicle cannot exhibit the pulsatile release behaviour expected of free-floating vesicles.

Effect of Hypoosmotic Shocks on the Lipid Bilayer

Pore formation and the pore morphology were then studied to further understand the membrane pinning. Figure 3.17 shows another representative time series of a hypoosmotic shock. As above, a large pore forms in the membrane in order to relieve the membrane tension and allow the release of the internal solution. The pore outline is shown in Figs. 3.17e - 3.17h.

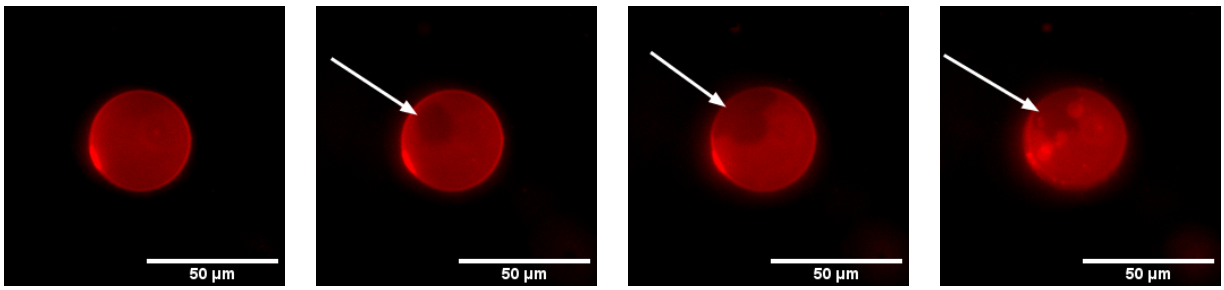

(a) Before Shock (b) t = 1 min (c) t = 10 min (d) t = 25 min

(e) Before Shock (f) t = 1 min (g) t = 10 min (h) t = 25 min

Figure 3.17: Time series of a GUV embedded in 1.0% agarose, subjected to a hypoosmotic shock of Δc = -160 mM. (a)-(d) show the original fluorescence images, with white arrows showing the location of the pore. (e)-(h) show the vesicle and pore outlines overlaid.

Generally, fluid-phase membranes have been shown to open circular pores [119, 232, 233]. However, in Figs. 3.17c and 3.17g, it becomes clear that the membrane pore of the embedded vesicle is not circular but instead resembles the "floral" pores observed for supported double bilayers reported by Gözen et al. [234–236]. The double bilayer system was formed by the fusion of a supported lipid bilayer (SLB) on a solid substrate, with a second bilayer subsequently deposited on top. The formation of non-circular pores in the upper bilayer was shown both experimentally and by peridynamic modelling to be caused by the presence of pinning between the two bilayers. Gözen et al. showed both floral pores and fractal pores for the double bilayer system, and the model revealed that the fractal pores required the membrane to have a non-zero shear modulus, whereas floral pores only appeared for membranes with zero shear modulus.

The existence of membrane pinning can also be demonstrated by membrane strands which remained adhered to the lower bilayer as pore formation proceeded, similarly to the membrane strands adhered to the agarose gel following buckling in Fig. 3.8.

The characteristic feature of the floral pores of double bilayers is a smooth, non-circular shape with "corners" where the membrane is pinned to the substrate. The agarose-embedded vesicle (Fig. 3.17) also displays this same pore shape, which further confirms the conclusion that agarose can also pin the lipid membrane in discrete positions.

3.3.5 Investigating the Mechanism of Buckling Behaviour

Since fluid-phase vesicles were not expected to be able to sustain buckled shapes, the properties of both the agarose hydrogel and the embedded lipid membrane were investigated to understand how the interaction between the gel and the membrane allows the buckling behaviour to occur.

Effect of Membrane Buckling on Gel Structure

GUVs with an external actin gel coating were previously demonstrated by Kusters et al. to exhibit buckling behaviour under hyperosmotic shock [143]. The presence of the gel

coating imparts a non-zero shear rigidity to the structure, which allows for the buckled shape to form. The following experiment was designed in order to observe whether or not the agarose gel buckles along with the lipid membrane, and hence if the shear rigidity arising from agarose is the cause of buckling.

Fluorescent tracer particles were embedded in the gel structure in the same manner as the vesicles. Relatively large tracer particles of 2 µm in diameter were chosen for these experiments, to ensure that they remain embedded within the agarose matrix and don't flow through the pores. The positions of tracer particles were tracked throughout a hyperosmotic shock experiment as well as the membrane signal in order to observe whether the tracer particles move along with the membrane during vesicle shrinking, which would imply that the gel structure buckles along with the membrane.

Firstly, no tracers were ever observed within the buckled region after vesicle shrinkage, suggesting that agarose is not pulled from its original position by the movement of the lipid membrane. Additionally, Figure 3.18 shows that the tracers do not move during vesicle shrinking. A small number of tracers that are visible in Fig. 3.18a are not visible in the subsequent frames; this is due to refocusing the confocal microscope in order to maintain the focus roughly on the equatorial plane of the irregularly-shaped deflated vesicle. As a quantitative measure of whether the tracers move relative to each other, the area between three tracers that are visible throughout the experiment is calculated and shown in Fig. 3.18e to be constant.

These results show that the bulk structure of the gel is not affected by the changing position of the lipid membrane. Therefore, the membrane likely detaches from the surrounding gel in order to form a buckled morphology, and this behaviour is not caused by a gel coating surrounding the vesicle.

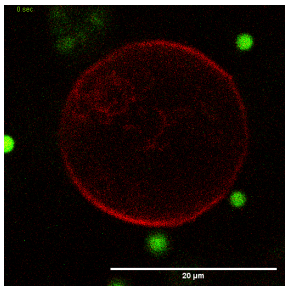

(a) Fluorescent tracer particles before application of shock to an embedded GUV

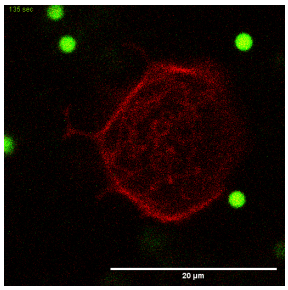

(b) Fluorescent tracer particles next to a shrinking embedded vesicle, t = 125 s after shock applied

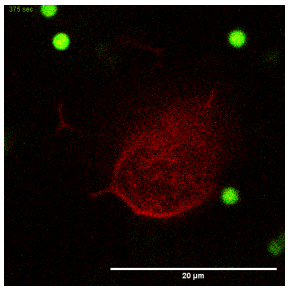

(c) Fluorescent tracer particles next to a shrinking embedded vesicle, t = 375 s after shock applied

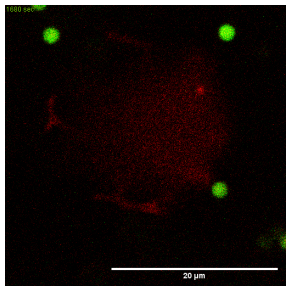

(d) Fluorescent tracer particles next to a shrinking embedded vesicle, t = 1680 s after shock applied

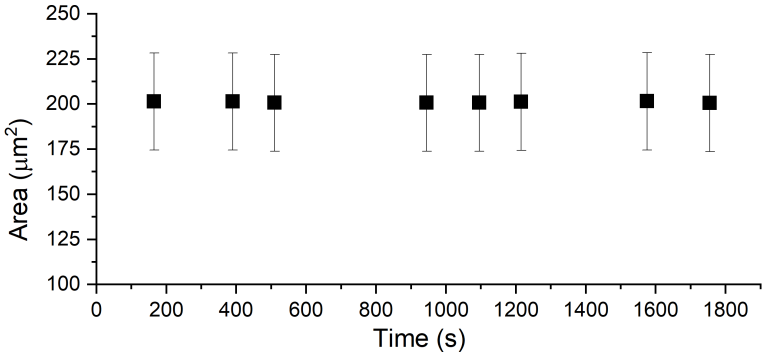

(e) Area between three tracers throughout the experiment. Error bars are calculated by propagating the error on each tracer position, taken as 2 px in any direction.

Figure 3.18: Relative positions of embedded tracer particles. The GUV is embedded in a 1.0% gel and subjected to a hyperosmotic shock of $\Delta c = +1000$ mM.

Effect of Gel Concentration on Membrane Fluctuations

Since the gel does not buckle with the membrane, Thermal Fluctuation Analysis (TFA) was used to further investigate the cause of buckling, and found that there is a strong adhesive interaction between the agarose gel and embedded lipid vesicles.

A high magnification objective (60X) was used to observe membrane fluctuations of agarose-embedded GUVs. Figure 3.19a shows a selection of three detected membrane contours of a vesicle embedded in a low concentration (0.25%) agarose gel at different timepoints overlaid into a single image. Since there are visible differences in the contours

at different times, it is clear that membrane fluctuations are not suppressed at this gel concentration. In contrast, for a GUV in a high concentration (1.0%) gel (shown in Fig. 3.19b), the membrane contours are very consistent for different timepoints. The two vesicles shown here appear to have significantly different values of the roundness R: however, this is simply due to the particular image frames of the time series chosen. In a 1.0% agarose gel (Fig. 3.19b), the vesicle maintains a very round shape over all timepoints measured. However, in a 0.25% agarose gel (Fig. 3.19a), the membrane fluctuations give the appearance of a less round vesicle. Overall, there was no general trend for the average roundness of the vesicles in different concentration gels.

Additionally, the roundness of each vesicle over time was plotted for the differing gel concentrations (Fig. 3.19c) and it is clear that although the 0.25% gel allows thermal fluctuations of the membrane, at 1.0% gel the fluctuations are significantly suppressed.

The standard deviation between all frames studied for a particular vesicle was calculated as a measure of how the roundness varies throughout an experiment. Higher standard deviation implies more shape fluctuations. Figure 3.19d confirms that standard deviation of the roundness is significantly higher ($p < 0.0001$) for 0.25% gels than for 1.0% gels.

These results show that the agarose matrix significantly suppresses membrane fluctuations at high gel concentrations. A possible mechanism for this is steric repulsion. Membrane fluctuations have been shown by multiple different methods to be suppressed close to hard walls such as solid substrates or other lipid bilayers [237]. However, the agarose hydrogel does not resemble a hard substrate. The structure of an agarose hydrogel is of bundles of agarose fibres which form junction zones. The average pore size of a 1% agarose, the most concentrated gel concentration studied here, has been reported to be on the order of a few hundred nanometres, although it is highly polydisperse and may range from 100 nm to greater than 600 nm. Both the average pore size and the polydispersity decrease as the agarose concentration is increased [46, 238].

These pore sizes are much larger than reported membrane fluctuation amplitudes. For

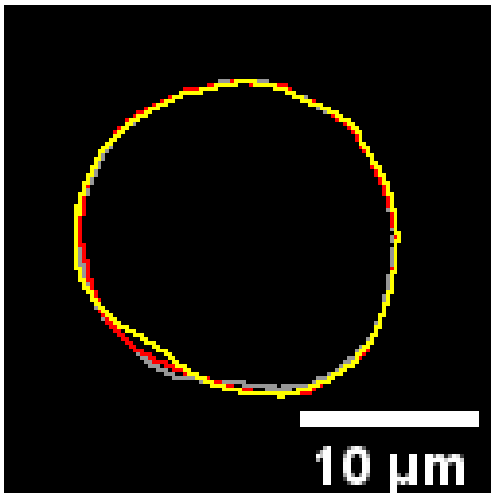

(a) Three membrane contours for a GUV embedded in 0.25% agarose.

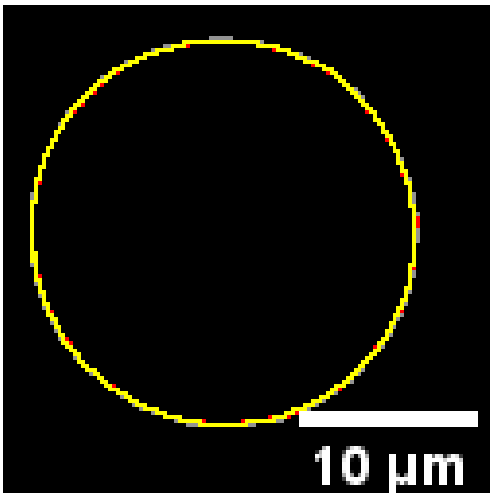

(b) Three membrane contours for a GUV embedded in 1.0% agarose.

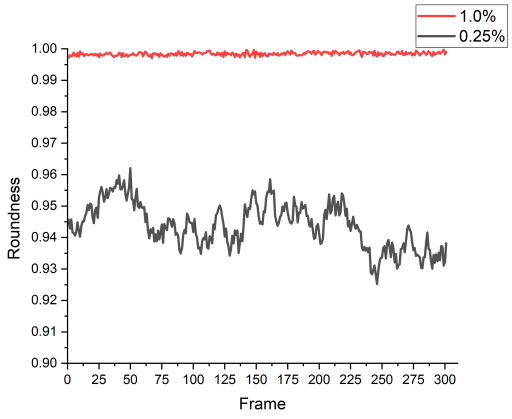

(c) Measured vesicle roundness over time for different gel concentrations.

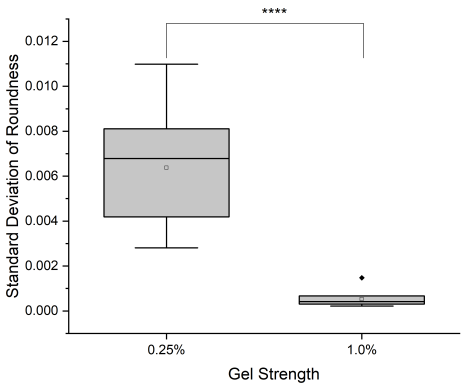

(d) Standard deviation of roundness measured for $n = 18$ vesicles.

Figure 3.19: Thermal Fluctuation Analysis (TFA) for GUVs embedded in different concentration gels.

free-floating osmotically deflated vesicles, the fluctuation amplitude has been measured to be 100 nm, whereas for deflated vesicles in the presence of a hard substrate this is reduced to 30 nm [168]. From this, it is unlikely that steric hindrance is the sole cause of the suppression of membrane fluctuations.

Increasing the agarose concentration means that the lipid membrane is in contact with a larger number of agarose bundles. This leads to a higher total adhesion strength between the gel and the membrane at high gel concentration.

Brochard and Lennon showed that membrane fluctuations are thermally driven [239]. In order for an embedded vesicle to fluctuate, parts of the membrane must detach locally from the surrounding gel or otherwise pull agarose fibres along with the membrane. Figure 3.18 showed that the movement of agarose fibres has not been observed for deflated vesicles, so it is more likely that the membrane detaches from the gel structure.

As the total adhesion strength between the gel and the lipid membrane increases, it becomes increasingly unlikely that thermal energy will be sufficient to detach the membrane from the gel in order for it to fluctuate. Therefore, it is concluded that vesicles embedded in more concentrated agarose hydrogels have stronger adhesive interactions with the gel.

Effect of Gel Concentration on Lipid Diffusion

Unlike fluid-phase membranes, gel-phase lipid vesicles have previously been shown to demonstrate buckling in response to hyperosmotic shocks [142]. Therefore, Fluorescence Recovery After Photobleaching (FRAP) was used to investigate whether the presence of the agarose gel affected the phase behaviour and hence the diffusion of lipid molecules within the DOPC membrane.

A square region in the equatorial plane of the vesicle was bleached for 10 frames, and then the recovery of the entire membrane contour was measured for 300 frames. Fig. 3.20 shows a typical recovery curve for a GUV embedded in a 1.0% agarose hydrogel. The recovery was fitted to a single exponential model using OriginPro.

Figure 3.21 shows the calculated FRAP parameters for each gel concentration studied. The mobile fraction M_f is the proportion of lipids that are free to diffuse within the membrane, i.e. those that are not pinned or somehow immobilised. This was calculated with Equation 3.7:

$$M_f = \frac{F_\infty - F_0}{F_i - F_0} \tag{3.7}$$

where F_∞ is the fluorescence intensity at the plateau, F_0 is the fluorescence immediately

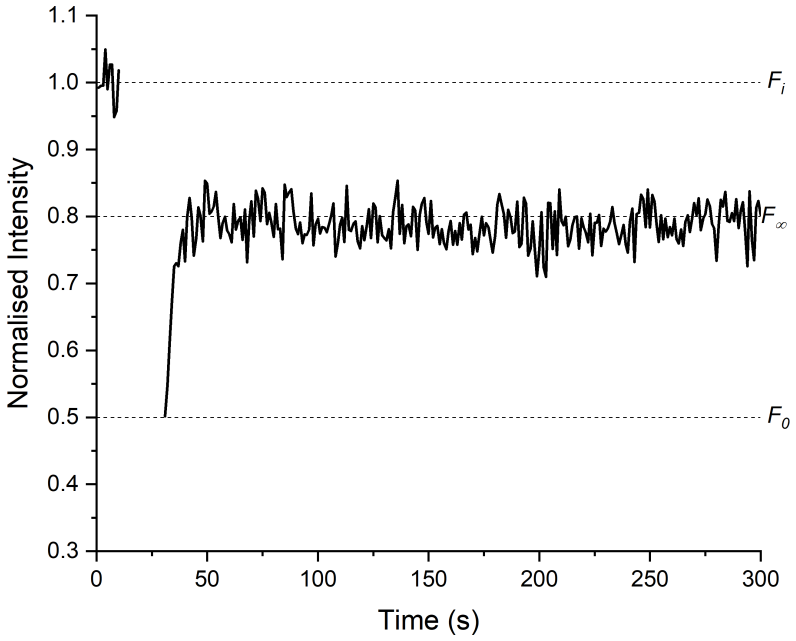

Figure 3.20: Representative recovery curve for a DOPC GUV embedded in 1.0% agarose hydrogel. The fitted parameters F_0, F_∞, and F_i are shown.

after bleaching, and F_i is the fluorescence intensity before bleaching [240]. These parameters are shown on Fig. 3.20. $t_{\frac{1}{2}}$ is the half-life of recovery, or the time taken for the fluorescence to recover to half of its final value. For fluid-phase vesicles this is typically on the order of a few seconds whereas gel-phase membranes typically recover over much longer timescales [241].

Figure 3.21 shows that $t_{\frac{1}{2}}$ does not vary with changing gel concentration. Lira et al. also found that the lipid diffusion was unaffected by the presence of the agarose hydrogel [46], which is in agreement with these results.

However, it appears that M_f decreases as the gel concentration is increased. This would suggest that the increasing contact between the membrane and the gel due to increased agarose concentration can cause increased membrane pinning. However, Analysis of Variance (ANOVA) statistical testing found that, although the difference in M_f between the 0.25% and 1.0% gels is significant at the 95% confidence level, the overall trend is only significant with 80% confidence, which is generally considered to be non-significant.

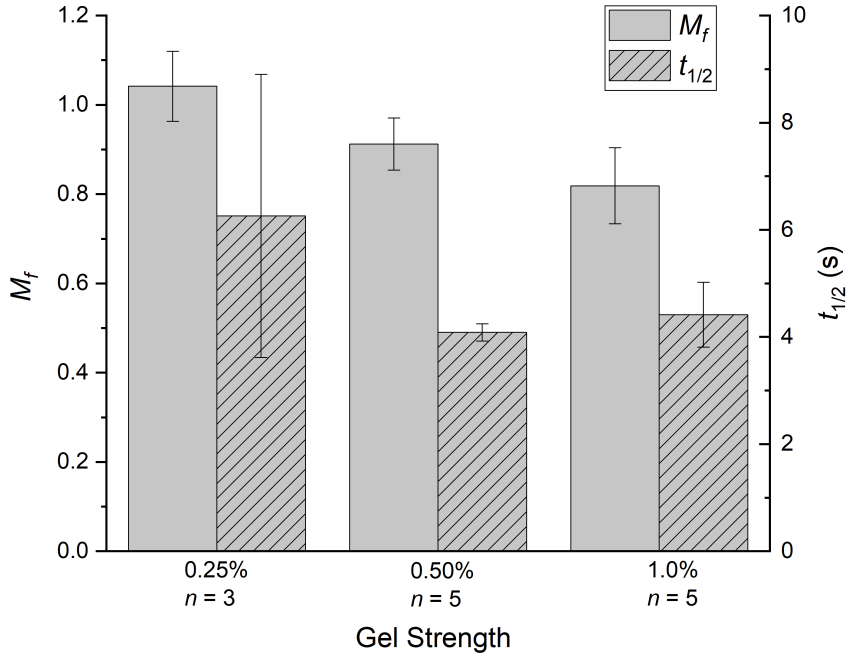

Figure 3.21: Calculated FRAP parameters for GUVs embedded in different concentration gels. $n \geq 3$ vesicles studied for each gel concentration.

Overall, the FRAP results do not show any significant effects of the agarose gel concentration on the lipid diffusion. The fact that the bleached membrane recovers quickly verifies that the membrane is still in the fluid-phase, and therefore would be expected to have zero shear modulus and be unable to sustain a buckled shape [215, 216].

However, observations from both hyperosmotic shocks and hypoosmotic shocks suggest that membrane pinning has a significant role in this system. Firstly, under hyperosmotic shocks, the membrane was shown to remain adhered strongly to the gel after buckling (Fig. 3.8). Secondly, under hypoosmotic shocks, the membrane forms floral pores resembling pinned double bilayers (Figs. 3.17).

Therefore, a decrease in the mobile fraction M_f of the membrane would be expected with increasing gel concentration. This was not found from the FRAP experiments, which may be due to the small sample numbers of vesicles measured here.

3.4 Discussion

3.4.1 Buckling of Thin Shells

As yet, buckling has only been reported for shells and capsules with a non-zero shear rigidity, as described in Section 1.3.2. The following section will consider how the fluid-phase vesicles studied in this work are able to buckle when embedded into a hydrogel matrix.

Fluid-phase vesicles are not expected to be able to sustain buckled shapes due to their lack of shear rigidity. Vesicles that were observed to buckle have shear rigidity arising from either a gel-phase membrane, or from an external gel coating. However, the vesicles used in this chapter were confirmed by FRAP (Fig. 3.20) to be in the fluid phase, and the surrounding agarose gel was shown by particle tracking not to buckle along with the membrane (Fig. 3.18). Therefore, we conclude that the agarose gel matrix interacts with the lipid membrane, causing the buckling behaviour.

In order to understand the mechanisms of buckling, we collaborated with theoreticians to numerically simulate the response of the system. The model was created by Jack Parker (PhD student in the group) and Prof. Halim Kusumaatmaja at Durham University.
The lipid bilayer is simulated as an infinitely thin sphere composed of a series of nodes connected by joints. The model accounts for the bending energy of the membrane and an adhesion energy of the membrane with its surroundings. This adhesion energy was modelled as a Lennard-Jones potential with a well depth of W, i.e. the adhesion strength, which was varied in the simulations. In some further simulations, the effects of positive spontaneous curvature are also included. The vesicle shape of lowest energy is calculated for a range of different volume reductions (V_f/V_0) and adhesion strengths W.
Figure 3.22 shows results from the model, with increasing adhesion strengths showing a transition from non-buckled to buckled shapes and increasing volume reduction (i.e.

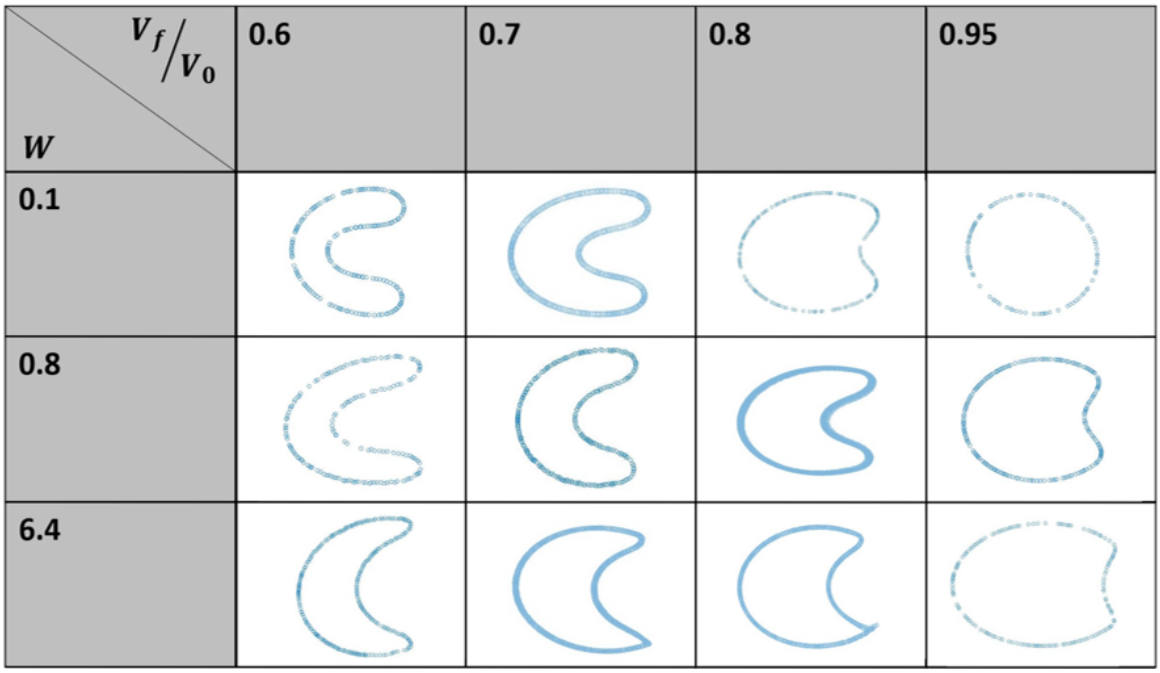

Figure 3.22: Simulated deflated vesicle cross-sections for varying adhesion strength W and final volume.

increasing shock) showing higher detachment from the substrate, in good agreement with the experimental results in Figure 3.9.

From these results, we conclude that the equilibrium shape of the deflated vesicle is determined by the competition between membrane tension, bending energy, and the adhesion energy of the membrane. Buckling of the membrane allows for volume deflation of the vesicles with only a small region of membrane detaching from the gel.

The values of W used in the model were chosen due to the similarities between the simulations and experimental results, rather than direct comparison to physical values. Consequently, the model cannot be used to infer the strength of the adhesion between the agarose and the membrane.

In order to further validate the model and conclusions, the simulations could be carried out for a wider range of input parameters and used to predict the experimental results. For example, a wider range of values of W could be simulated, and compared to a wider range of agarose concentrations.

The simulations also reveal that as the adhesion strength is increased, the curvature at the rim of the buckled region increases. This is akin to the observations on the contact angle between a vesicle and a planar adhesive substrate. Equation 3.8 shows that the curvature C_1^* depends on the adhesion energy W and the bending energy k_C [242]:

$$C_1^* = (2W/k_C)^{1/2} \tag{3.8}$$

Equation 3.8 agrees well with both the experimental (Figure 3.9) and simulation results, which show that as the adhesion energy W is increased, the curvature of the rim of the buckled region also increases. From Eq. 3.8, W could be estimated from the known value of k_C, if a sufficiently high-definition image of the rim of the buckled region were collected.

Further, the model was also used to study the effect of positive spontaneous curvature on membrane buckling. In the absence of spontaneous curvature, the vesicle buckles axis-symmetrically, shown in Figure 3.23a. However, the inclusion of a positive spontaneous curvature results in the loss of this symmetry (Fig. 3.23b); rather than forming a central indentation, the vesicle forms a crescent-shape with two lobes extending around the buckled region. These shapes are also observed experimentally for high gel concentrations (see Fig. 3.9i). This may suggest that the concentrated gels give rise to positive spontaneous curvature in the system. However, in the experimental setup, a high concentration of glucose molecules are added externally to the vesicle in order to cause the osmotic shock. Since the vesicles contain sucrose internally, this asymmetry across the membrane could also introduce spontaneous curvature to the membrane [218]. Further research could identify whether the positive spontaneous curvature is due to the presence of the agarose gel or the glucose solutes. For example, different shock solutions could be used experimentally in order to vary the spontaneous curvature.

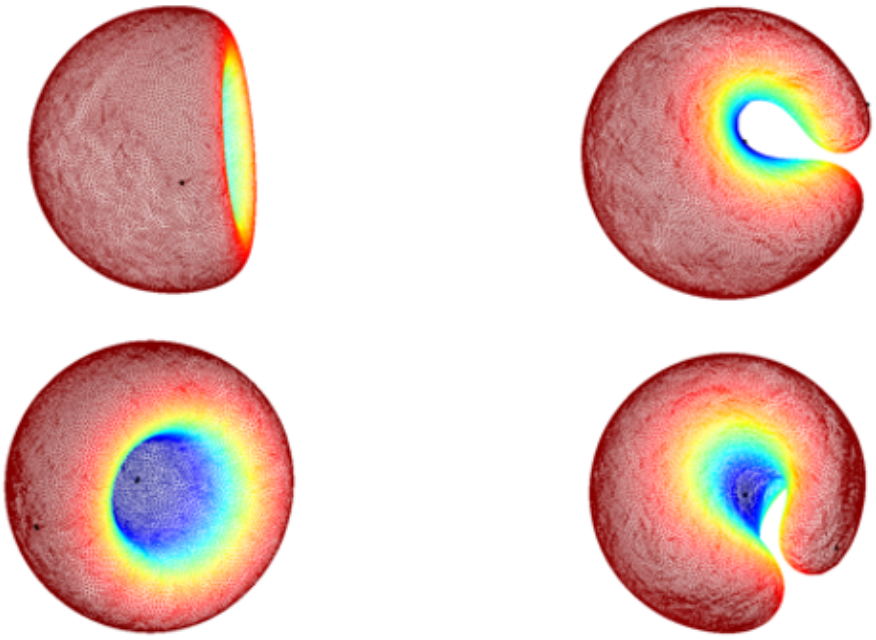

(a) Zero spontaneous curvature

(b) Positive spontaneous curvature

Figure 3.23: Effect of positive spontaneous curvature on the simulated vesicle shape. Each vesicle is shown in two orientations. The vesicles have the same final volume $V_f/V_0 = 0.75$ and adhesion strength $W = 0.1$.

The good agreement of the simulations with positive spontaneous curvature with the experimental results suggests that the experimental system also has positive spontaneous curvature. However, the formation of internal tubes and buds upon vesicle deflation (as seen in Figs. 3.7 - 3.10) is characterised by high negative spontaneous curvature [218]. Therefore, it seems likely that although the positive spontaneous curvature of the system should result in external protrusions, this is inhibited by the steric hindrance of the agarose mesh.

The formation of membrane protrusions such as tubes and blebs has been demonstrated for planar supported lipid bilayers on an elastic PDMS substrate. Compression of the substrate leads to a negative tension, resulting in the formation of either membrane caps,

buds, or tubes, depending on the compressive strain and the enclosed volume [243].
Here, the hydrogel-embedded vesicles are not compressed by the confining gel, but as the vesicle deflates, the membrane likely experiences a similar negative tension, which is relieved by the expulsion of excess membrane as either tubes or buds.

Buckled shapes similar to those in Figures 3.9 and 3.22 have also been demonstrated experimentally by vesicles confined by another lipid bilayer, and by simulations where this external lipid bilayer is modelled as a hard wall [120, 121, 244]. The model presented by Rim et al. confined vesicles in either cylindrical or spherical cavities and increased the confinement by reducing the radius of the confining shape. Under these conditions, the equilibrium shape was shown to be an invaginated shape with the geometry controlled by the strength of the adhesion to the confining surface. It was also shown that stronger adhesion produced regions of higher membrane curvature at the buckled region, as shown in Figure 3.24a [244].
Experimentally, this model was realised using Multi-Lamellar Vesicles (MLVs) by Sakashita et al. [121]. Laser illumination of the inner vesicle was used to cause an area difference between the bilayer leaflets, resulting in a shape change of the inner vesicle. Figure 3.24b shows the evolution of the buckled inner vesicle both experimentally and computationally.

So far, this discussion has only covered equilibrium energetics of the buckled shapes, but a range of non-equilibrium or dynamic effects were observed experimentally.
Firstly, the internal membrane protrusions were shown to detach from the vesicle membrane, making them inaccessible for reswelling (Figure 3.14). This is due to the dynamics of the osmotic shock: the large osmotic shocks applied result in a fast efflux of water from the vesicle, and as discussed earlier, this is faster than the relaxation time τ of the membrane.
Secondly, the shock strength Δc is inherently related to the shock rate in this experimental

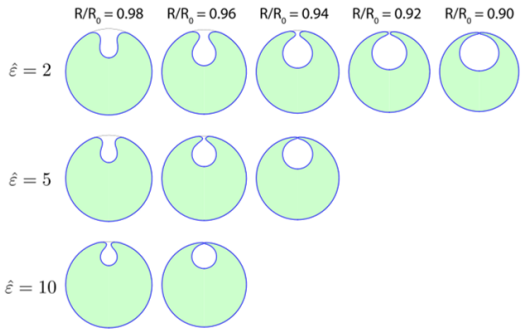

(a) Vesicles under increasing confinement (R/R_0) with different adhesion to the confining surface, $\hat{\varepsilon}$. Reprinted by permission from **Springer Nature: Springer Nature Biomechanics and Modeling in Mechanobiology**, Mechanical collapse of confined fluid membrane vesicles, Jee E. Rim et al, © (2014) [244].

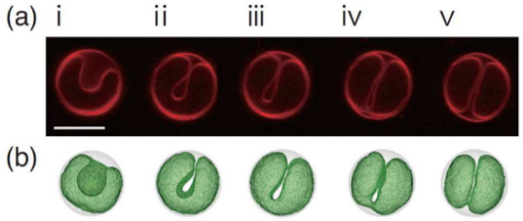

(b) Experimental and computational results showing the evolution of a buckled vesicle embedded within a confining vesicle. Scale bar = 10 µm. Reprinted figures with permission from Ai Sakashita, Masayuki Imai, and Hiroshi Noguchi, Physical Review E, 89, 040701(R), 2014. Copyright 2021 by the American Physical Society [121].

Figure 3.24: Effect of increased confinement on vesicles, by both simulation and experiments.

setup. This is likely to lead to the formation of non-equilibrium morphologies, particularly at higher values of Δc. Further developments to the setup could include smaller, step-wise increases in the osmolarity in order to promote the formation of equilibrium morphologies. There are also effects of pinning in the experimental system. As shown in Figure 3.8, membrane pinning can prevent the vesicle from detaching from the gel surface, which can lead to the formation of non-equilibrium morphologies.

To conclude, there is good agreement between the experimental and simulation results, although the wide variety of vesicle morphologies observed experimentally (including internal membrane protrusions, multiply buckled shapes, etc.) are likely due to non-equilibrium effects which are not currently captured by the model.

3.4.2 Nature of the Adhesive Interactions

In this chapter, agarose-embedded vesicles were shown to buckle when deflated by hyperosmotic shock, with increasingly non-spherical morphologies observed as the agarose concentration is increased (Figures 3.9, 3.11). This is suggested to be the effect of either

adhesive interactions between the gel and membrane, or the effect of vesicle confinement. However, the results of Thermal Fluctuation Analysis (TFA; Figure 3.19) showed a significant suppression of membrane fluctuations in the most concentrated gels, which adds further evidence of an adhesive interaction, preventing detachment of the membrane from the gel. Additionally, membrane pinning is an example of an adhesive interaction which is spatially heterogeneous, i.e. the membrane experiences a strong adhesion at discrete positions.

Previously, the interaction between lipid membranes and agarose hydrogels has only been loosely described as a weak interaction, and its nature has not been explored. This section considers how agarose may interact with the lipid membrane in order to cause the altered behaviours observed in this chapter.

Simple sugars (mono- and di-saccharides such as glucose and sucrose) are known to interact with lipid bilayers, affecting many of their mechanical properties. Sugar molecules are hydrophilic and can form hydrogen bonds both with water and with the lipid headgroups. This leads to a modification of many of the mechanical properties of the lipid membrane including the elasticity, phase behaviour, and lipid diffusivity. This effect is now understood to be concentration-dependent: at low concentrations, sugars can intercalate between lipid headgroups and form hydrogen bonds preferentially between sugars and lipids. This causes an increase in membrane area and a decrease in membrane thickness. At higher sugar concentrations (>0.2 M), sugar molecules are expelled from the membrane, and hydrogen bonds are formed preferentially from the membrane to water molecules [179].

The experiments in this chapter have an initial sugar concentration of $c_0 = 0.3$ M, so at iso-osmotic conditions and under hyperosmotic shock the system is in the high sugar concentration range. Therefore there is not likely to be any difference in the distribution of sugars in or near the bilayer due to hyperosmotic shocks.

Agarose is a polysaccharide with a repeat unit composed of an agarobiose molecule (a disaccharide). Although the agarobiose monomers cannot intercalate into the lipid membrane in the same manner as simple sugars, hydrogen bonding will certainly play a part in this system. Similarly to lipid membranes, the effect of sugars falls into two separate regimes.

The agarose gel structure is stabilised by hydrogen bonding with structured water molecules surrounding the agarose fibres [245]. In the high sugar regime, increasing the sugar concentration limits the number of water molecules available to stabilise agarose fibres, resulting in a weaker gel. However, in the low sugar regime, as the sugar concentration is increased, gel strength also increases. This is attributed to the multiple H-bonds formed between sugar molecules and water molecules, leading to a more ordered water system, which further stabilises the agarose. This effect has been evidenced by the fact that sugars with more of their hydroxyl groups in the equatorial position (e.g. trehalose), which can form more hydrogen bonds to water than sugars with axial hydroxyl groups, strengthened agarose hydrogels the most and increased their water retention capability [246–248].

As a result, we conclude that the water network which hydrates the agarose hydrogel is strongly structured by the sugar solutes, which leads to more total hydrogen-bonding between the agarose and the embedded lipid vesicles. This is manifested as an adhesive interaction between the gel and the membrane.

Electrostatic interactions are also a possible cause of the observed adhesive interactions; previously, the interaction between planar hydrogels of the charged polysaccharide chitosan and zwitterionic Small Unilamellar Vesicles (SUVs) was shown to be sufficient to cause vesicle rupture and bilayer fusion on the polymer surface. However, the same experimental setup with agarose showed no vesicle fusion, which suggests very limited electrostatic interactions [249]. Therefore it is unlikely that electrostatic attraction is the cause of the adhesion between the membrane and the agarose hydrogel

studied here; although, as suggested in Section 3.3.2, electrostatic attraction between anionic fluorophore Rh-DPPE and cationic sulfate impurities in the agarose may be the cause of membrane pinning.

In summary, although the experiments in this chapter do not allow for a direct conclusion of the cause of the adhesive interaction between the membrane and the surrounding agarose hydrogel, it seems likely that it may be due to a structuring effect of the water molecules due to hydrogen bonding between the phospholipids, agarose, water, and sugars.

3.4.3 Comparison to Cellular Responses to Osmotic Shock

The observed vesicle responses to hyperosmotic shocks, in particular the non-equilibrium responses, remarkably mimic some of the behaviours of plant cells under dehydration. Both plant and yeast cells possess a cell wall surrounding the lipid membrane, which provides mechanical support to the cell, and can also protect against pathogens, as well as osmotic pressures [13, 14].

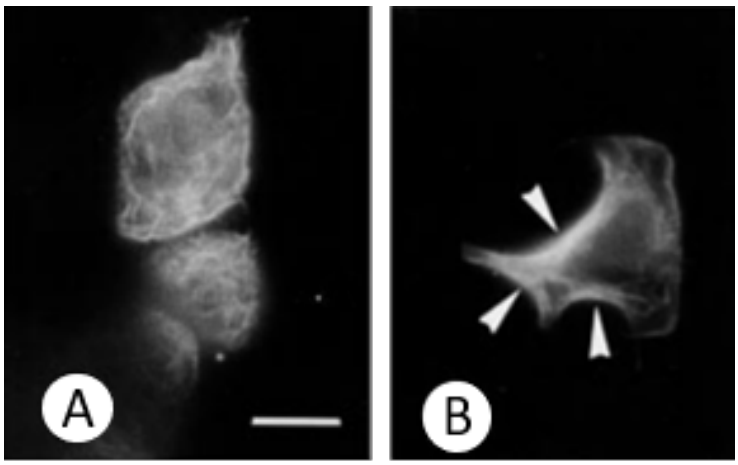

Figure 3.25: Convex (A) and Concave (B) Plasmolysis of cells. Scale bar = 10 µm. Komis, G.; Apostolakos, P., Hyperosmotic stress-induced actin filament reorganization in leaf cells of *Chlorophyton comosum*, Journal of Experimental Botany, 2002, 53, 375, 1699-1710, by permission of Oxford University Press [250].

Under hyperosmotic shock, it has been shown that the plant cell membrane detaches from the cell wall in a process known as plasmolysis. Depending on factors including the cell type, cytoplasmic viscosity, and osmotic agent used, different forms of plasmolysis have been observed [251]. Two of the predominant forms, convex and concave plasmolysis, are shown in Figure 3.25. The concave plasmolysis form displays regions of membrane buckling away from the cell wall, similar to the membrane buckling observed for agarose-embedded lipid vesicles.
Plasmolysis of plant cells is described as an active process [251] and is therefore often used as a test of cell viability [252, 253]. However, the mechanisms underlying plasmolysis appear to still be unknown. Our results demonstrate that the buckling behaviour observed in concave plasmolysis can occur as a passive membrane process which is likely related to the interaction between the membrane and surrounding cell wall, and the effect of membrane confinement.

As well as detaching from the cell wall, during plasmolysis cells can form Hechtian strands, which are membrane strands adhering the membrane to the cell wall. The strands are thin tubes of membrane material encapsulating a small volume of the cell's contents. Their size (typically in the range 30 nm - 2 µm) can change over time as strands may break or coalesce [254]. An example of Hechtian strands is shown in Figure 3.26 [253]. Figure 3.6 shows that agarose-embedded vesicles exhibit similar membrane strands to those observed in plant cells. These membrane strands have a similar appearance to Hechtian strands, although the vesicle strands form a cage-like structure on the gel surface rather than radiating through the void in the gel as Hechtian strands in plant cells [204, 255].

One role of Hechtian strands is to maintain the membrane area during plasmolysis, i.e. shrinking of the protoplast due to water efflux. Daughter vesicles can also be formed during plasmolysis and Hechtian strands can connect these daughter vesicles to the cell

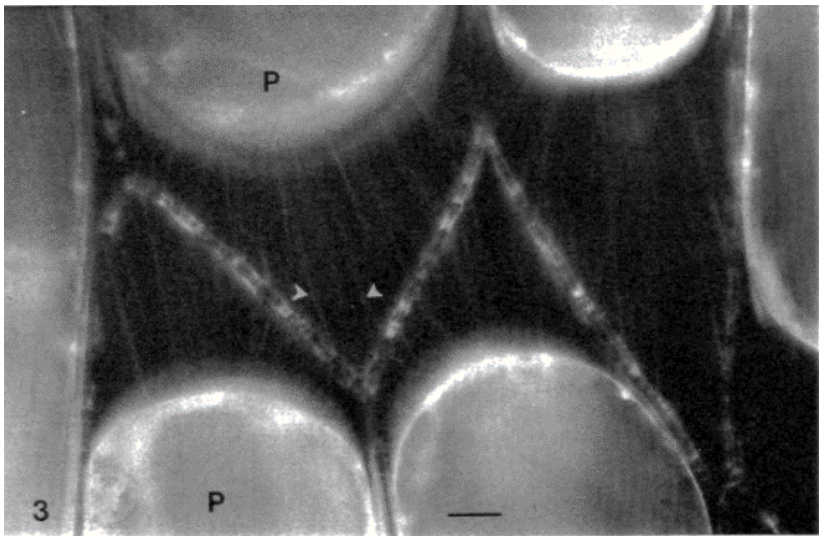

Figure 3.26: Dehydrated plant cells (onion epidermal cells) showing Hechtian strands connecting the cell membrane to the cell wall. Arrowheads highlight the presence of Hechtian strands. Scale bar = 20 µm. Reproduced with permission from Oparka et al. [253].

membrane, which also maintains the total cell membrane area. Another key function of Hechtian strands is to allow the cell membrane to return to its proper position at the cell wall upon deplasmolysis (reswelling) when there is sufficient water [202, 253].

The reversibility experiments in this chapter (Section 3.3.3) showed that agarose-embedded vesicles can lose membrane material during deflation which prevents the shrinking behaviour from being fully reversible. Relatedly, the viability of cells after dehydration and rehydration has been shown for both plant and yeast cells to be related to the rate of dehydration [202, 256]. In yeasts, fast dehydration has been shown to lead to membrane internalisation and vesiculation, and the internalised membrane is then unavailable for reswelling. When the dehydration rate is slower, the membrane was shown to form folds without internalising any membrane material, and hence was able to fully return to its original size and shape without lysing [256–258]. The reversible shrinking behaviour of yeast cells under hyperosmotic shock was hypothesised by Dupont et al. to be related to the lengthscale of membrane folds and invaginations formed. Under slow shocks, the membrane forms a small number of large membrane folds but when the shock rate is increased, the cell membrane was observed to form a higher number of smaller folds [256].

From the point of view of membrane energetics, the high shocks lead to a large proportion of the cell membrane adopting an unfavourable highly curved configuration, and as the authors point out, the membrane folds are likely brought into close contact with each other. This means that while the cells are maintained in the shocked state, the membrane rearranges into a lower energy configuration of internalised daughter vesicles without any regions of high membrane curvature. The internalised vesicles are then unavailable for reswelling of the cell, leading to cell death on rehydration. As discussed earlier, a similar behaviour is also observed for vesicles; fast changes to the surface area to volume ratio can lead to irreversible membrane budding which leaves some of the membrane material inaccessible for reswelling.

Plant cells exhibit a different behaviour during dehydration and rehydration cycles. As described above, the formation of Hechtian strands means that the cell membrane can remain connected to any daughter vesicles formed during plasmolysis and then use them as a reservoir of membrane lipids for reswelling. It has been suggested that for successful reswelling (deplasmolysis) of the cells, the rate of reincorporation of lipids into the cell membrane must at least equal the rate of surface area increase [253]. When the cell membrane remains connected via Hechtian strands to the lipid reservoir, this property must be related to the fluidity of the membrane. However if any daughter vesicles are formed and not connected to the cell membrane via Hechtian strands, then their incorporation into the membrane relies on membrane fusion once the membrane and daughter vesicle are brought into contact.

The formation of Hechtian strands depends on a pinning or strong adhesion of the membrane to the cell wall. Lang et al. have suggested that Hechtian strands are adhered to the cell wall by cellulose microfibrils, which are formed at the membrane by cellulose synthase complexes (CSCs), and may entangle with the cellulose structure of the cell wall leading to membrane pinning [254]. CSCs are complexes of different cellulose synthase

proteins, which are membrane-bound and, in plants, contain eight transmembrane domains. The structures of the cellulose synthase proteins depend significantly on the plant, and therefore there are many possible frunctional groups that may be binding to the cell wall [259–261].

Since the localisation of CSCs has been suggested to be regulated by cortical microtubules in the cytoskeleton [262], this membrane pinning is closely linked to active processes, in contrast to the agarose-embedded lipid vesicles which exhibit membrane pinning in a purely passive system.

The deflated agarose-embedded vesicles studied in this chapter closely resemble plant cells under plasmolysis, which can buckle (concave plasmolysis) and form membrane strands (Hechtian strands). This may explain why the buckling behaviour was not observed to be fully reversible due to the fast shock rate applied which formed daughter vesicles which made some of the membrane area unavailable for reswelling. It is also possible that the reversibility is due to active processes present within plant cells [263], which are absent in the model system.

To summarise, this model system for plant cell plasmolysis demonstrates that the formation of Hechtian strands due to hyperosmotic shock is a passive membrane process which relies on the interactions of the membrane with its surroundings. As the number of intact Hechtian strands formed by plasmolysis is known to decrease over time [254], this model system could be used to study whether strand coalescence or breakage are also passive processes, as well as the conditions under which they are observed.

3.4.4 Application to Food Systems

This section will discuss how this system may be useful to study and develop the use of embedded lipid vesicles for the encapsulation of flavours or other actives in food products. Since lipid vesicles are widely used for encapsulation, they may be used within foods to encapsulate active ingredients and therefore protect them from degradation [264]. The

experimental system studied in this chapter is useful for understanding how this might be useful for gel-based products, such as confectionery gels.

The osmolarity of a sample is determined by the concentration of osmotic agents, which for foods includes sugars and salts. For typical confectionery gels, sugars are the main ingredient, and can contribute well over 50% of the final mass [265].
The composition of saliva varies from person to person and also depending on factors including the method of stimulation (contact, sight of food, odours), etc. [266, 267], so it is difficult to know its exact osmolarity. However, some papers report that it is below 100 mOsm [268].
As a result, if this system were to be used in confectionery products, during consumption the embedded vesicles would be subjected to a hypoosmotic shock much higher than the shocks studied in this chapter. Therefore, it should be expected that the osmotic shock would cause rupture of the vesicles and a burst release of the encapsulated actives, similar to the release of calcein demonstrated in Fig. 3.16.
Additionally, Figure 3.3 demonstrated that the embedded vesicles remain intact in iso-osmotic conditions. As a result, actives can be stably encapsulated over long timescales (such as during transportation and storage), and not released until exposed to saliva during consumption.

Another potential cause of osmotic shocks in a confectionery system could be dehydration upon storage. Evaporation of the external solution, perhaps caused by temperature fluctuations, would lead to a hyperosmotic shock on embedded vesicles.
Figure 3.4b shows that the initial internal osmolarity of the embedded vesicles affects the final volume after hyperosmotic shocks. It can be seen that at high values of c_0, small shock strengths Δc result in very small volume changes. Similarly, the higher c_0 is, the higher the hypoosmotic shock the GUV can accommodate without membrane rupture. If embedded vesicles are used in confectionery gels, then the high initial osmolarity c_0

means that the vesicles will be more resistant to osmotic shocks, particularly of the shock strengths studied here. In order to be able to use embedded vesicles for such products, then further work would be required to understand what strength of osmotic shocks are likely to be experienced by the products, and therefore whether the vesicles will behave in a similar manner as observed in this chapter.

3.4.5 Further Work

A useful extension to this work would be to further develop the computational model in order to account for the effects of membrane pinning. This could be introduced as discrete points on the confining surface with much higher membrane adhesion than the general Lennard-Jones potential interaction energy. This extension to the model would then help to further understand the separate effects of membrane adhesion and membrane pinning.

Experimentally, it would be useful to vary the type of shock solution used in order to better control the effect of spontaneous curvature. The use of sucrose shock solutions instead of glucose would still lead to some spontaneous curvature due to the difference in concentrations across the bilayer [163], but this would eliminate the effect of the different sized sugar molecules which also contribute to spontaneous curvature.
Additionally, further experiments could decouple the effect of shock magnitude and shock rate, by adding smaller shocks (e.g. 100 mM) step-wise and allowing the system to equilibrate at each step, up to the same high shock magnitude (1000 mM). These experiments should remove the dynamic/non-equilibrium effects of tube and daughter vesicle formation before buckling, and should further improve the agreement between experiments and simulations.

A further extension to this work could be to synthesise fluorescent agarose to be used as the gel matrix as in the work of Horger et al. [269]. This would reveal if there is an interfacial layer of agarose bound to the membrane that buckles along with the vesicle, or

whether the membrane detaches cleanly.

Another area for further work would be to study further the biological relevance of the agarose matrix as a model cell wall. For example, the membrane composition could be varied to more accurately represent the composition of cell membranes, including for example different lipid headgroups and/or a mixture of lipid tail lengths. This would alter the phase behaviour and water permeability of the membrane [270], which may be related to how plant cells survive dehydration.

3.5 Conclusions

The experiments in this chapter show that fluid-phase vesicles can buckle in response to volume reduction, if they are embedded into agarose hydrogels. Specifically, under hyperosmotic shocks, the embedded vesicles shrink by membrane buckling, which is a behaviour that is not expected of a fluid-phase vesicle since it has no shear rigidity. Shape analysis of the deflated vesicles shows a dependence on both the gel concentration and the osmotic shock strength. This result shows that there is a significant adhesion energy between the lipid membrane and the agarose, and comparison with computational results shows that the buckling behaviour is controlled by the ratio of adhesion and bending energies of the membrane.

In addition to the interaction energy between agarose and the lipid bilayer, membrane pinning was also observed for hyperosmotic and hypoosmotic shocks. After hypoosmotic shocks, the membrane pores formed had a non-circular shape resembling the "floral" pores of Gözen et al. [234–236]. This membrane pinning is not included in the computational model and is likely a cause of the non-equilibrium effects observed.
Membrane pinning also has implications for the use of embedded vesicles for controlled release, since pinning prevents pore closure. The release of calcein through a membrane

pore was demonstrated after hypoosmotic shocks. Due to membrane pinning, the pore did not reseal and the encapsulated calcein was lost in a single burst. If embedded vesicles are to be used as an encapsulation system, this shows that the nature of membrane pinning needs to be investigated further in order to understand how it will affect the release profile of the encapsulated actives.

Under hyperosmotic shocks the agarose-embedded GUVs mimic the behaviour of plasmolysed plant cells, which suggests that, with further comparison between simulation and experimental results to elucidate the strength of the interactions, they may make a promising model system. The membrane is strongly pinned to its surrounding agarose which leads to the formation of membrane tubes which closely resemble Hechtian strands. Reversibility experiments also showed similar behaviours as the large shock values led to irreversible membrane vesiculation rather than reversible tubulation [256–258]. This model system demonstrates that the formation of buckled morphologies and Hechtian strands by lipid bilayers is a passive membrane process, despite differences in the chemical structures used and hence differences in the cause of membrane pinning.

The following chapter will further this work by investigating mechanical compression of hydrogel-embedded vesicles as a method to cause vesicle deformation and volume loss. The experiments will highlight how the membrane - gel adhesion shown here can support highly deformed vesicles and study whether this can be applied as a controlled release system.

Chapter 4

Mechanical Compression of Hydrogel-Embedded Vesicles

4.1 Introduction

By embedding vesicles into hydrogels, a hybrid material with a prolonged release profile of encapsulated actives can be achieved [86, 109, 206]. Alternatively, this release can be triggered by utilising stimuli-responsive hydrogels, such as p(NIPAM) [111].

Lipid vesicles can be deformed by a variety of methods, such as atomic force microscopy, electrodeformation, optical tweezers [74, 271, 272], or by mechanical compression via either microfluidics or responsive hydrogels [128, 129]. Since the lipid membrane has a high energy cost for stretching [273], this shape deformation away from the equilibrium spherical shape is associated with a loss of volume from the vesicle core. For hydrogel-embedded vesicles, mechanical compression may therefore be a suitable trigger for release of encapsulated actives, as compression of the gel should cause deformation of the embedded vesicles. This deformation would be associated with volume loss which might arise from the release of only intravesicle water or by the release of encapsulated actives. In this chapter, agarose-embedded vesicles are compressed with a well-defined magnitude and rate of compression using a micromanipulator.

Previously, compression of free-floating vesicles has been shown to cause significant vesicle deformation and volume loss. Using a microfluidic stamp, Robinson et al. demonstrated that under uniaxial compression vesicles lose volume via water efflux through the bilayer. The deformation behaviour was found to be strongly dependent on the absence of osmotic agents in the vesicle and its surroundings. In the presence of sugars, water efflux from the vesicle during compression was suppressed by the osmotic pressure building up across the membrane, eventually leading to vesicle rupture [128].
Jia et al. prepared a pH-responsive hydrogel template and used it to compress vesicles biaxially. By changing the pH, the gel swelled which caused compression of the trapped vesicles, and by patterning the vesicle traps within the hydrogel, non-circular vesicle cross-sections were achieved [129]. The pH-responsive hydrogel chosen in this case was bovine serum albumin, which is frequently used to prevent non-specific binding of vesicles to substrates [274]; as such, the embedded vesicles were not subject to a vesicle-gel adhesion which might affect the formed vesicle shapes.
Both of these experimental setups reached similarly high levels of vesicle deformation, exceeding those found for other methods of vesicle deformation such as electrodeformation or by optical tweezers [271, 272]. Additionally, both experiments demonstrated a change in membrane phase behaviour due to the compression [128, 129].
However, none of these systems included interactions between the vesicle and its surroundings, which would affect the vesicle's response to compression. In particular, Chapter 3 showed that there is a significant adhesion between lipid membranes and agarose hydrogels, which is sufficient to stabilise non-spherical vesicle morphologies.

In addition to free-floating vesicles, mechanical compression is also used to study cell behaviours. Cells are often embedded into agarose hydrogels for 3D scaffolding experiments and to study the effects of compression on cell behaviours such as calcium signaling, cytoskeleton organisation, and cell metabolism [275–277]. Agarose has low

adhesion to cells [278], whereas the results of Chapter 3 showed that lipid vesicles have a significant adhesion to agarose hydrogels. Therefore, the use of vesicles as model cells may depend on understanding how this adhesion affects the lipid bilayer during hydrogel compression. Also, agarose has been shown to exhibit stress relaxation due to the ability of its physical crosslinks to rearrange under static compression [279, 280]. This behaviour may affect how embedded vesicles respond to compression, and as a result may have a bearing on the compression-induced release of vesicle contents.

The aim of this chapter is to investigate the behaviour of hydrogel-embedded GUVs in response to mechanical compression and specifically to examine whether this can be used as a trigger for volume loss. The experiments in the previous chapter showed that for agarose-embedded GUVs, there is a significant adhesion of the lipid bilayer to the surrounding gel which can sustain the membrane in energetically unfavourable morphologies. Therefore it is expected that the adhesion with agarose may also be able to support vesicles which are deformed by compression of the agarose.
Additionally, these experiments will use vesicles encapsulating calcein as a model active in order to study the mechanism of volume loss of the vesicle in response to compression.

4.2 Experimental

4.2.1 Sample Preparation

DOPC GUVs were prepared as described in Chapter 2. External calcein was removed by dispersing the GUVs into 300 mM glucose (without calcein) and collecting the GUVs after they had settled to the bottom of the solution. This was repeated 5x to give sufficient contrast between the encapsulated calcein and background fluorescence.
Samples of vesicles embedded in agarose were then prepared as in Chapter 3, except that the agarose was dissolved in glucose solution rather than sucrose solution. This resulted in GUVs gradually sedimenting towards the bottom of the gel during gelation,

Figure 4.1: Photograph of the compression device located above the objective of an inverted microscope imaging a hydrogel sample.

which minimises the effect of the GUV height within the gel on its response to mechanical compression.

The gel concentration of 1% was chosen as it withstands higher compression magnitudes or rates without breaking or flowing compared to lower gel concentrations. However, this does result in some vesicles being ruptured or deformed during the gelation step as this is the higher end of the range of gel concentrations suitable for embedding vesicles [46].

4.2.2 The Compression Device

The gel samples were directly compressed by a compressing arm made of Teflon and controlled by a micromanipulator (MP-225, Sutter Instruments, USA). The micromanipulator controls the position of the Teflon arm in 3 dimensions with a resolution of 62.5 nm. A python code was used to define the movement of the micromanipulator, with fixed distance and speed. Fig. 4.1 shows a photograph of the device in its position above a large gel sample being imaged on an inverted microscope. By using an inverted microscope, the compressor did not interfere with the optical path and so it is possible to image fluorescent vesicles during the compression experiments.

Figure 4.2 shows a typical compression pattern alongside schematics of the system during each phase of the experiment. In a typical experiment, a chosen vesicle was imaged before any compression began. The compressing arm was then gradually lowered into position whilst live imaging the vesicle, until either a small movement of tracer particles or small deformation or motion of the vesicle was observed, which indicates the arm had come into contact with the sample. The vesicle was imaged again, and then the compression was started using the python code to compress by a known distance (ΔZ) in the vertical direction with a set speed (v_Z). After the motion of the compressing arm finished, it was held in place (stationary phase) for a period of at least 5 minutes with images of the vesicle membrane and encapsulated calcein collected every 30 s.
The standard compression parameters were a compression of $\Delta Z = 100$ µm over a time of 136 s, which equals a downward speed of $v_Z = 0.73$ µm/s. For repeated compressions, the vesicle was compressed further following the stationary phase, with the same compression parameters. Under these conditions, any deformation of the glass slide which supports the gel is assumed to be negligible compared to the compression of the hydrogel.

4.2.3 Imaging

Fluorescence images were collected using an inverted Nikon Ti-E widefield epifluorescence microscope. The objective used had 40X magnification, Numerical Aperture = 0.6, working distance = 2.8 mm. The exposure time was 200 ms and Neutral Density (ND) filters were added into the optical path to prevent photobleaching of calcein. An ANDOR Neo sCMOS camera was used to acquire images. 2x2 pixel binning was used to further increase the signal to noise ratio.

4.2.4 Image Analysis

Image analysis was carried out in ImageJ as described in Chapter 2. Firstly, the rhodamine (membrane) image was smoothed by applying the mean filter (radius = 2 px), which was

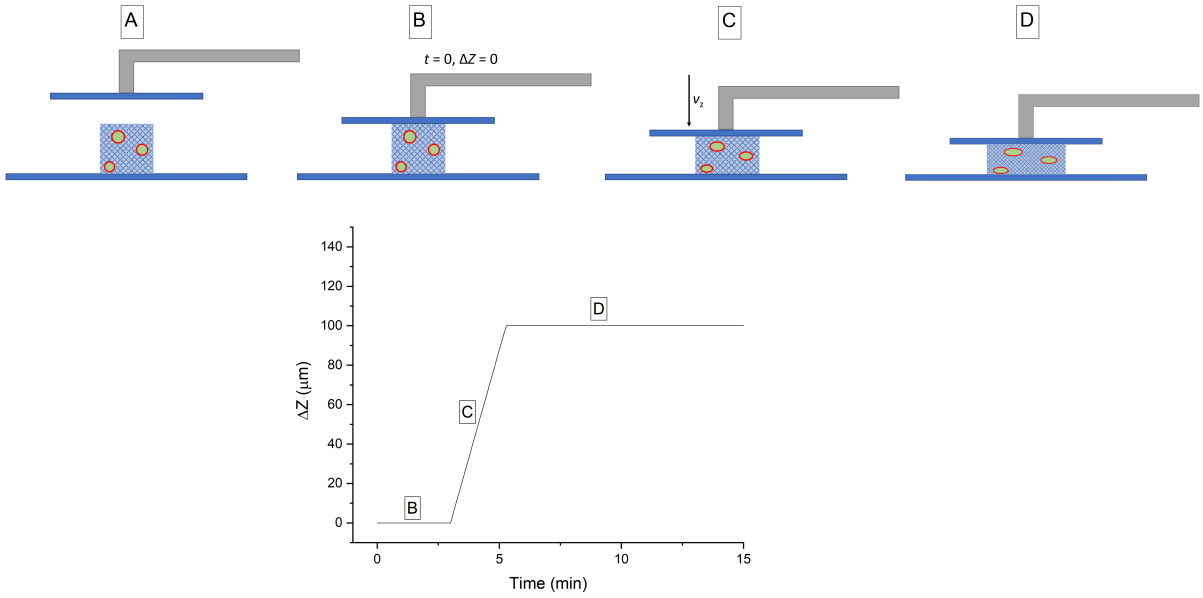

Figure 4.2: Compression protocol for a typical experiment. A: The compressing piece starts at an unknown distance above the gelled sample. B: The compressing piece is slowly brought into contact with the gel surface by manual control of the micromanipulator. The point of contact is determined by observing when either embedded vesicles or tracer particles first begin to move. This point is taken as the zero of time and compression. In some cases, this position is held for the 'contact phase'. C: The compressing piece is moved downwards for a fixed distance (ΔZ) with a known velocity (v_Z). This is termed the 'compression phase'. D: The compressing piece is held at a constant position, termed the 'stationary phase'.

found to improve the detection of the membrane contour. In the calcein channel, the background fluorescence was subtracted using the rolling ball algorithm (radius = 200 px) in order to eliminate fluorescence signal arising from the environment rather than from the vesicle.

In each frame, the vesicle was detected and measured. The measurements included the intensity of the calcein channel, the area and perimeter of the vesicle detected in the rhodamine channel, and the shape descriptors of the vesicle.

There are two measurements of fluorescence intensity which may be used: the integrated intensity, which is the sum of grey values of all pixel values within the region of interest (ROI), or the mean intensity. In these experiments, the vesicle projected area changes,

which can change the mean intensity due to redistribution of the calcein into the new vesicle area.

Since images were captured using an epifluorescence microscope, the measured calcein intensity is due to photons arriving at the detector from the entire vesicle, not just those in the focal plane. Therefore, when the vesicle is compressed, the integrated intensity ought to stay the same if there has been no loss of calcein, or if there is calcein loss then the integrated intensity should decrease. Errors on the measured values were calculated as described in Chapter 2.

4.2.5 Particle Tracking

Blue-fluorescent polystyrene tracer particles were embedded into the gel in order to study changes in the gel structure during compression. The suspension of tracer particles was vortexed briefly in order to break up any aggregates of particles. The tracer particles were added at a concentration of 5 µL/mL to the hot solution of agarose before gelation. Relatively large tracer particles with diameter = 2 µm were chosen, as their size significantly exceeds the typical pore size of agarose hydrogels (approx 600 nm for a 1% low-melting agarose gel [281]) and so they remain successfully immobilised into the gel matrix during gel compression.

The tracer particles were imaged using the DAPI filter set (λ_{em} = 375 nm, λ_{ex} = 460 nm) during compression to analyse the movement of the gel during compressions. Images were typically collected every 1.2 s. The MOSAIC plugin in ImageJ [282] was used to identify trajectories of individual particles. For effective tracking of 2.0 µm polystyrene beads at 40X magnification, the input parameters were: Kernel radius = 8 px, Cut-off radius = 0.0 px, Percentile = 0.1, Displacement = 10 px, Link Range = 10 frames. These parameters were found to give good identification of particles at small separations. A high link range was used so that if particles went out of focus during the experiment, the trajectory once back in focus would be linked back to the original trajectory, rather than

being labelled as a new particle trajectory. Occasionally there were still some mislabelled trajectories, so these were identified by eye and removed before further analysis.

4.3 Results

4.3.1 Effect of Hydrogel Compression on the Lipid Membrane

Vesicle Shape

Firstly, agarose hydrogels containing embedded vesicles were compressed in order to study what effect this has on the lipid bilayer. The compression was applied by either manual control of the micromanipulator giving an undefined compression magnitude and rate, or by using the python code to control the movement of the micromanipulator giving a well-defined magnitude and rate of compression. Shape analysis was then carried out on a range of compressed vesicles to understand further how the compression causes changes to the vesicle morphology.

Figure 4.3 shows a collection of vesicles displaying a range of different shapes after compression. Some vesicles are observed to remain roughly circular in the focal plane (Fig. 4.3a, roughly 50% of compressions), some adopt an elliptical shape (Fig. 4.3b, roughly 41% of compressions), and a small number display very irregular shapes with membrane strands (Fig. 4.3c, approximately 9% of occurrences. This shape will be discussed further later in this section).

The roundness values R of vesicles imaged before and after compression are plotted in Figure. 4.4. It can be seen that before compression, most vesicles are nearly perfectly round ($R = 1.0$) with a small distribution of values. After compression, the distribution is much wider: there are still some vesicles with R close to 1.0, whereas some are much more elliptical or irregular with lower values of R. The statistical significance of this effect was studied with a Welch's t-test and the effect was found to be significant at $p < 0.001$.

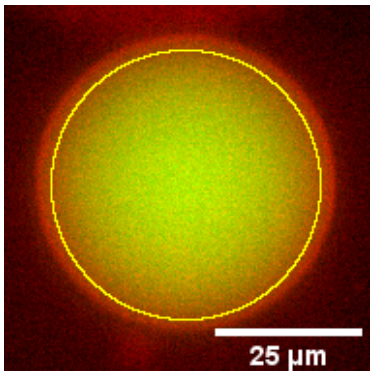

(a) Vesicle displaying a circular projected area after compression. This occurs for approximately 50% of compressions. $R = 1.000$.

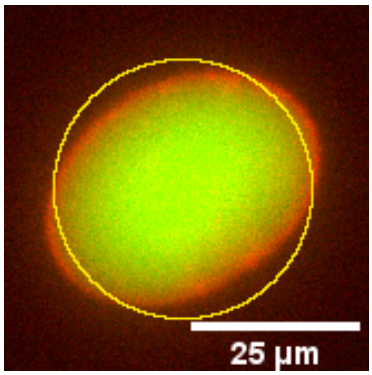

(b) Vesicle displaying an elliptical projected area after compression. This occurs for approximately 41% of compressions. $R = 0.995$.

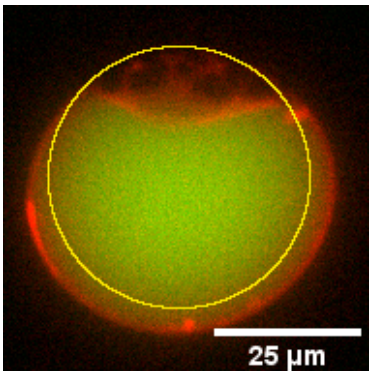

(c) Vesicle displaying irregular shape after compression. This occurs for approximately 9% of compressions. $R = 0.832$.

Figure 4.3: DOPC GUVs embedded in agarose, displaying different membrane shapes in response to compression. In each image, the yellow outline shows the size and shape of the vesicle before compression. The roundness values R for the compressed vesicles are also shown.

The wide distribution of roundness values, along with images of vesicles post-compression (Fig. 4.3), shows that there can be both prolate and oblate vesicle shapes forming due to the compression. This is attributed to the different compressive forces experienced at different positions within the gel. Vesicles close to the centre of the gel and located centrally under the compressing piece form oblate shapes, where the height is reduced. Conversely, prolate shapes are likely to be due to vesicles closer to the edge of the gel where the compression causes motion in both the Z direction and the X-Y plane. During these experiments, although vesicles obviously close to the edge of the gel were ignored, it was not possible to identify the exact centre of the gel and hence to quantify the proximity of chosen vesicles to the centre of the gel. As such, it is not possible to predict what shape will be adopted by a given vesicle under compression.

It is also possible that differences in the local gel structure could cause the different behaviour in response to compression, as agarose gels are known to be structurally heterogeneous over lengthscales of tens of micrometres [221, 225, 226, 246].

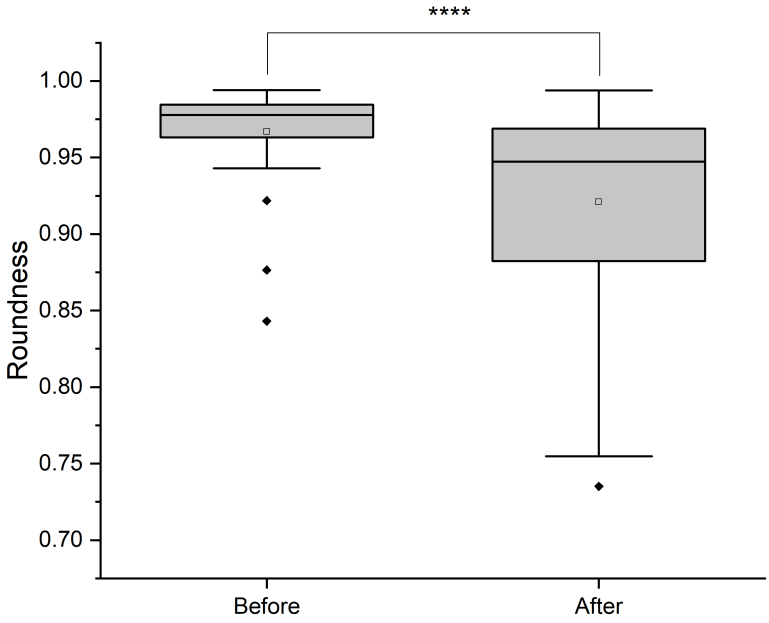

Figure 4.4: Roundness values R of vesicles embedded in 1% agarose hydrogel, before and after any compression, $n = 33$ vesicles. Outliers are shown as black circles outside of the box plots.

Projected Vesicle Area

Controlled compressions of a fixed magnitude ($\Delta Z = 100$ µm) and speed ($v_Z = 0.73$ µm/s) were then carried out on embedded vesicles in order to elucidate how the compression affects the vesicles. The compression protocol is shown in Fig. 4.2. The vesicle was imaged every 30 s for 3 minutes in the pre-compression phase and every 30 s for >5 minutes in the stationary phase. The gel height was approximately 400 µm so the value of $\Delta Z = 100$ µm corresponds to a reduction in the height of the gel of approximately 25%.

Figure 4.5 shows the projected area (i.e. its area in the X-Y plane) for a representative vesicle throughout a single controlled compression experiment. The projected area is increased after the compression, and remains constant (within experimental error) throughout the stationary phase.

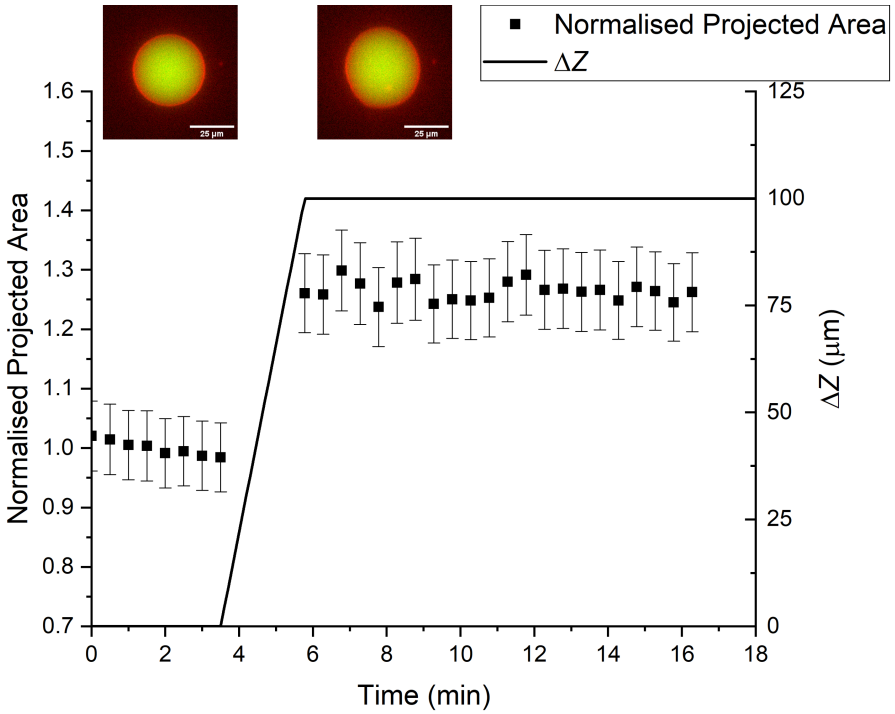

Figure 4.5: Projected area for a representative vesicle throughout a single compression experiment with $\Delta Z = 100$ µm and $v_Z = 0.73$ µm/s. The solid black line shows the position of the compressor. Error bars show the error due to thresholding, as described in Chapter 2. Inset are representative images from each phase.

To study the reproducibility of this result, the same compression protocol was then applied to multiple vesicles ($n = 22$). The chosen compression parameters were kept constant, and were found to visibly deform vesicles in many cases, yet there was no gel rupture and also the motion was slow enough to track a single vesicle throughout the experiment.

In order to compare the projected area before and after compression, the weighted average and weighted error were calculated for the contact phase (before compression) and stationary phase (after compression). These were then normalised to the value in the contact phase such that a normalised projected area of 1.0 corresponds to an undeformed vesicle. Figure 4.6a shows the increase in projected vesicle area for a series

of different vesicles undergoing the same compression protocol. Although the collection of vesicles showed a wide range of area changes, the average increase in projected area due to compression was 1.14 with a standard deviation of 0.15. For these compression parameters, all vesicles studied were observed to remain intact after compression and throughout the entire stationary phase.

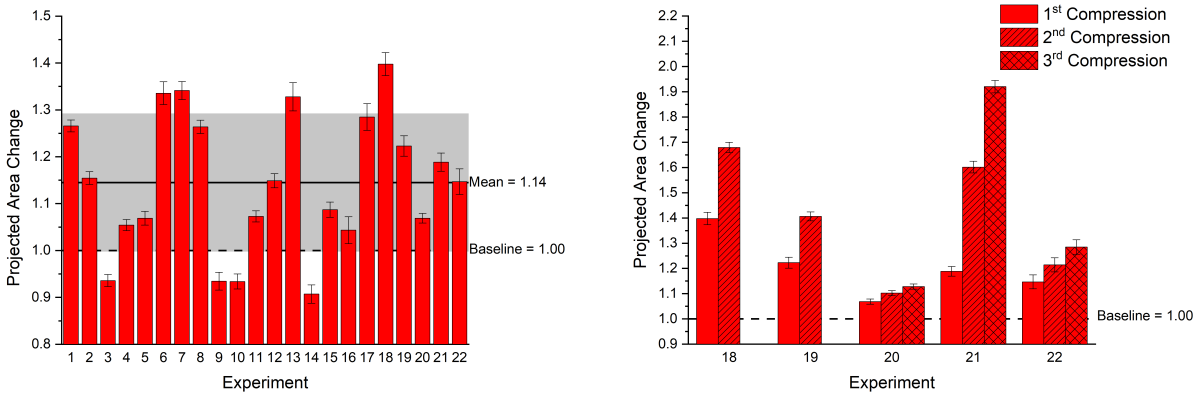

(a) Area change for single compression experiments.

(b) Area change due to multiple compression steps.

Figure 4.6: Change in vesicle due to compression of agarose-embedded vesicles. Each compression had $\Delta Z = 100$ µm and $v_Z = 0.73$ µm/s. The error bars are the weighted errors for each experiment calculated from all timepoints after compression. In both graphs the solid horizontal line refers to the mean area change for all single compression experiments and the grey region shows 1 standard deviation from the mean. The dashed horizontal line denotes the baseline value of 1.0, i.e. no area change.

Since the embedded vesicles are clearly compressed along with the hydrogel, their response to further compression was also studied. Figure 4.6b shows, for five separate experiments (with either two or three compression phases), how the projected area of the vesicle changes throughout an experiment of multiple compressions. Each compression phase had identical compression parameters ΔZ and v_Z. The projected area is normalised against its initial value in the contact phase before the first compression phase.

Each experiment shows an increase in the projected vesicle area in the X-Y plane after a compression step, which is to be expected after a compression in the Z direction. It is also

observed that after each compression phase the increase in projected area is not constant, either between experiments or between different compression phases of the same vesicle. The variability between the deformation shown by different experiments is likely due to the fact that different positions within the gel will experience different compressive forces.

Then, the projected area values were used to study whether the deformation of the vesicles caused any volume loss. Vesicle deformation may occur with constant volume, where the whole vesicle deforms elastically, but this would require an increase in the surface area of the membrane. Alternatively, the vesicle may deform with constant surface area, which causes volume loss from the vesicle core.

Assuming the vesicle volume remains constant, the height of the vesicle was calculated from the initial and final projected areas. This was then used to calculate the final surface area of the vesicle, and the amount by which this had increased in comparison to the initial state.
For single compressions, the largest increase in projected area was a factor of 1.42 ± 0.08, and for multiple compressions, this was 1.93 ± 0.08. The corresponding surface area change values (shown in Table 4.1) are 5% and 20%, which are well above the values of membrane area change of 3% which is typically shown to cause membrane rupture or poration [19]. The vesicles were observed to remain intact over a timescale of minutes after the compression finished. This shows that the constant volume assumption cannot be valid, as such large increases in surface area would cause membrane lysis.

Instead, it is likely that the vesicle does lose some of its internal volume and the surface area remains constant. To calculate the volume loss, the surface area was calculated from the initial projected area. The height of the deformed vesicle was then calculated using the constant surface area and the deformed projected area. The results in Table 4.1 show that these projected area changes correspond to a significant amount of volume loss from

the vesicle. Later, in Section 4.3.2, the calcein fluorescence will be used to investigate whether this volume loss arises from the loss of the encapsulated calcein and sugars, or solely from the loss of water.

Table 4.1: Surface area increase or volume loss of vesicles with the largest change in projected area. The surface area changes and volume changes are shown relative to their values before compression.

Experiment	**Projected Area Change**	**Surface Area Change (Constant Volume)**	**Volume Change (Constant Surface Area)**
Single Compression	1.42 ± 0.08	5%	-12%
Multiple Compression	1.93 ± 0.08	20%	-74%

Formation of Large Membrane Defects

Although the majority of vesicles displayed a circular or elliptical projected area after compression, a small number of vesicles showed an irregular shape with large, visible, membrane defects. These irregular shapes generally occurred after larger deformations. Fig. 4.7 shows a series of images of a single vesicle during a multiple compression experiment (3x compressions, $\Delta Z = 100$ µm and $v_Z = 0.73$ µm/s each. The compression pattern is shown in Figure 4.7e).

During the first compression and stationary phases, the vesicle's shape was elliptical, as observed in the majority of experiments. However, during both the second and third compressions, defects are observed to be formed in the membrane as the vesicle deviates from an elliptical shape. In the second compression, the membrane buckles and appears to 'peel away' from the gel but leaves strands of membrane connected to the gel surface. Then during the following stationary phase, the membrane returns along the strands to an intact ellipse with no strands. In the third compression phase, a similar effect is observed, and during compression the vesicle again peels away from the gel, this time leaving external daughter vesicles. These are then re-absorbed into the membrane during the stationary phase as the vesicle returns towards a spherical circular shape.

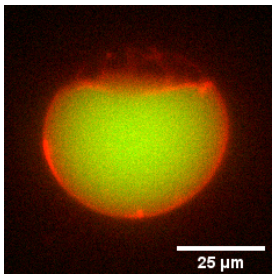

(a) At the end of the second compression phase, point A in Fig. 4.7e

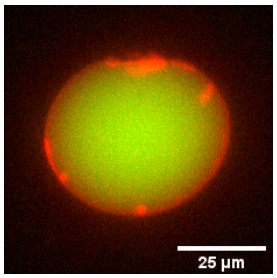

(b) At the end of the second stationary phase, point B in Fig. 4.7e

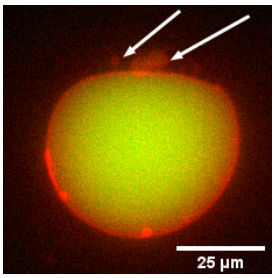

(c) At the end of the third compression phase, point C in Fig. 4.7e

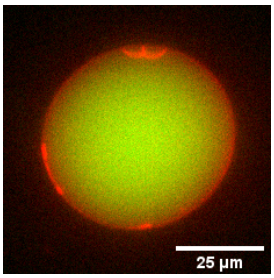

(d) At the end of the third stationary phase, point D in Fig. 4.7e

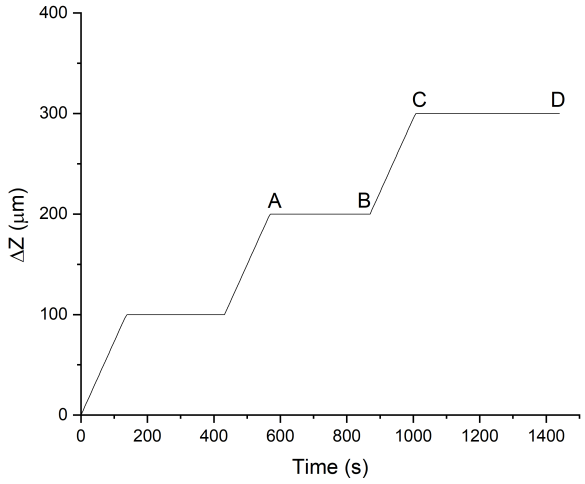

(e) Compression pattern for the above experiment

Figure 4.7: Time series of a membrane during a multiple compression experiment. Each compression was of $\Delta Z = 100$ µm and at $v_Z = 0.73$ µm/s. This is Experiment 21 in Figs. 4.6 and 4.9. White arrows show the location of daughter vesicles external to the vesicle.

As shown in Chapter 3, when the vesicle volume is reduced, it can buckle away from the gel matrix. This effect is seen most frequently at high gel concentrations of 1%, which is the same gel concentration used in this chapter. In Fig. 4.7, a similar effect is observed: as the vesicle is compressed, the water efflux causes a decrease in volume, which then causes the membrane to buckle away from the gel. Energetically, the regions of high membrane curvature formed by buckling are unfavourable and so during the stationary phase, the vesicle relaxes towards a spherical shape in order to minimise the effect of curvature. This is likely accompanied by an influx of water which reduces the osmotic

pressure on the vesicle imposed by compression.

After both the second and third compression phases, buckled vesicles were observed to recover towards an elliptical morphology during the stationary phase, despite there being no movement of the compressor. Since agarose is known to exhibit stress relaxation during static compression, over a timescale of a few minutes [279], it appears that this relaxation of the gel structure surrounding the vesicle may be related to the vesicle's return to a non-buckled morphology.

However, the healing behaviour is not always observed for buckled membranes, and can remain stable for >5 minutes, as shown in Fig. 4.8. In this case, the membrane maintains a buckled shape with external membrane strands in contact with the gel.

In addition, in both of these experiments (Figs. 4.7 and 4.8), a significant calcein signal remains within the defected vesicles. This suggests that, as with hydrogel-embedded vesicles subjected to hyperosmotic shocks, the buckled membrane shape is formed by an intact membrane. However, from these static images it is unclear whether or not the membrane has transiently formed pores which have subsequently resealed. In order to answer this question, the fluorescence intensity of encapsulated calcein was studied throughout the course of the compression experiments to determine whether any calcein has been lost from the embedded vesicles.

4.3.2 Effect of Hydrogel Compression on Encapsulated Calcein

If the buckled vesicles observed in Figs. 4.7 - 4.8 are formed of an intact membrane, then the question arises as to how volume is lost from the vesicles. Volume loss could occur either via the formation (and subsequent closure) of membrane pores or via transport through the lipid bilayer. In the first case, if membrane pores are formed, then large molecules can be lost from the vesicle, whereas this is very unlikely in the second case of transport through the bilayer. The fluorophore calcein was encapsulated within vesicles

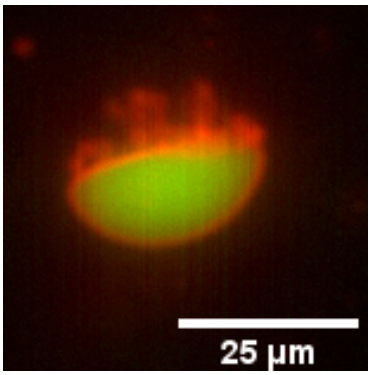

(a) Buckled vesicle immediately after compression stops

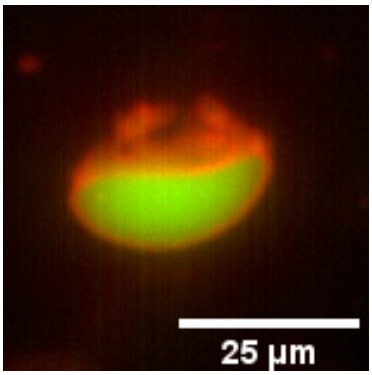

(b) Buckled vesicle 5 minutes after compression stops

Figure 4.8: Long-lasting buckled vesicle.

to study which of these mechanisms occurs during compression.

The integrated calcein intensity was measured at each timepoint, and then a weighted average was calculated for both the contact phase (before compression) and stationary phase (after compression). The data was then normalised to its value in the contact phase. Figure 4.9a shows the change in integrated calcein intensity after compression for a collection of vesicles under the same conditions.

The average integrated intensity across all single compression experiments was consistent with the baseline value before compression, with an average integrated intensity change of 0.99 and standard deviation of 0.09. This suggests that there is no release of calcein molecules during compression; however, there is significant variation between experiments with some vesicles showing a decrease in integrated intensity after compression. This is attributed to residual motion of the vesicles after compression, which causes vesicles to drift slightly out of the focal plane resulting in a lower calcein intensity.

A pairwise t-test was used to find out whether this set of intensity changes was statistically significant. For each compression, the difference in integrated intensity before (I_{before}) and after (I_{after}) compression was calculated. The null hypothesis H_0 was that there is no difference in the intensity before and after compression; i.e. $I_{after} - I_{before} = 0$.

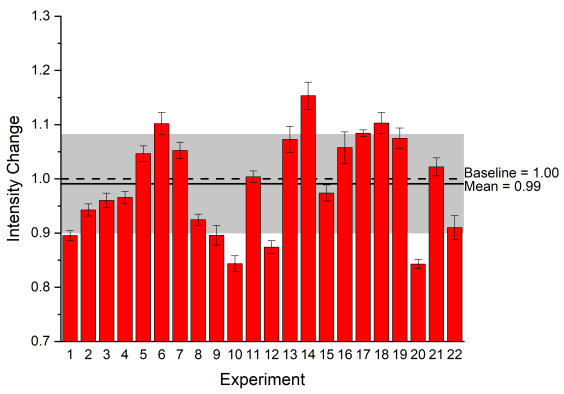

(a) Intensity change for single compression experiments.

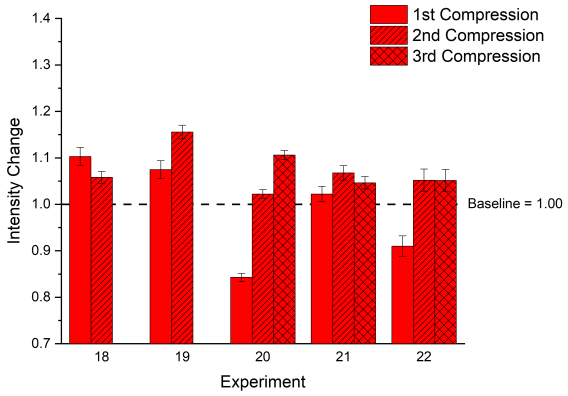

(b) Intensity change due to multiple compression steps.

Figure 4.9: Change in normalised calcein intensity due to compression of agarose-embedded vesicles. Each compression had $\Delta Z = 100$ µm and $v_Z = 0.73$ µm/s. The solid horizontal line corresponds to the mean intensity change between single compression experiments and the grey region shows 1 standard deviation from the mean. The error bars are the weighted errors for each experiment calculated from all timepoints after compression. The dashed horizontal line denotes the baseline value of 1.0, i.e. no intensity change.

Although the vesicles were shown earlier to be significantly deformed, there was found to be no statistically significant change in the integrated intensity due to compression. This implies that the amount of encapsulated calcein remains constant throughout the experiment and the volume loss is due to transport of water molecules across the bilayer.

Experiments were also carried out in which the same vesicle was deformed further using multiple compression phases. (A compression pattern for three compressions is shown in Fig. 4.7e.) The integrated intensity during each phase for a collection of vesicles undergoing two or three compressions is shown in Fig. 4.9b. Similarly to the results for single compressions (Fig. 4.9a), there is no loss in calcein when vesicles are subjected to further compressions. This also adds evidence that the irregular membrane shapes observed in Fig. 4.7 consist of an intact bilayer which has buckled away from its spherical shape.

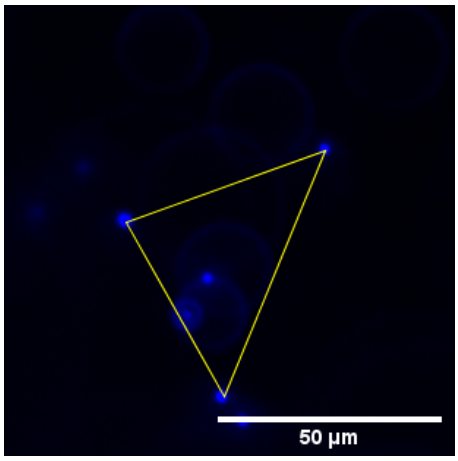

(a) Before compression begins.

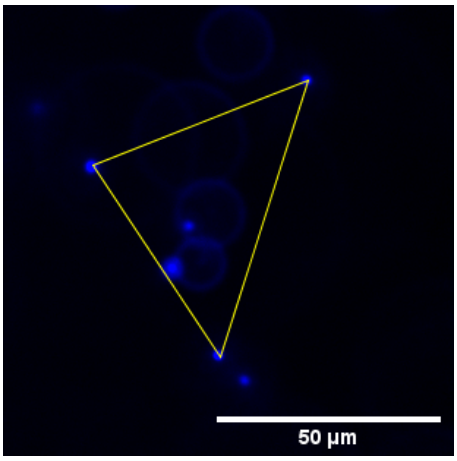

(b) After compression of $\Delta Z = 80$ µm, $v_Z = 0.73$ µm/s.

Figure 4.10: Representative images of an ROI defined by three tracer particles, before and after a controlled compression experiment.

Therefore, we conclude that when embedded vesicles are deformed by compression, they lose volume via the permeation of water molecules through the bilayer, rather than the formation of membrane pores and release of encapsulated model actives.

4.3.3 Particle Tracking During Compression

Particle tracking experiments were used to characterise the compression behaviour of the agarose hydrogels, and to explain the differences in vesicle behaviours due to compression. Blue-fluorescent polystyrene tracer particles were embedded into the gel in the same manner as vesicles.

The compressor was moved in the Z-direction causing the hydrogel to expand in the X-Y plane. This is demonstrated in Fig. 4.10 which shows the area of an ROI (triangle defined by three tracer beads) changing over time during the compression phase ($\Delta Z = 80$ µm and $v_Z = 0.73$ µm/s). The area strain ε is calculated by:

$$\varepsilon = \frac{A_t - A_0}{A_0} \tag{4.1}$$

where A_t is the area of the ROI at time t, and A_0 is the initial ROI area. ε is averaged over 10 different ROIs within the same field of view.

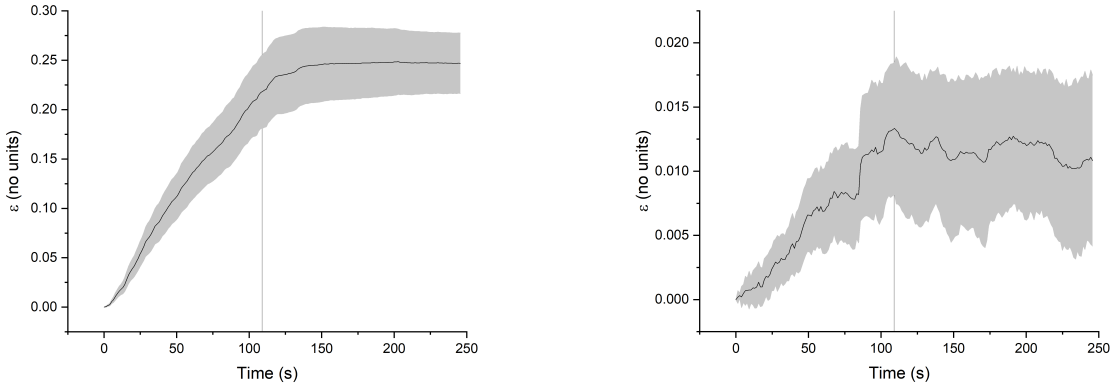

(a) Experiment 1

(b) Experiment 2

Figure 4.11: Area strains ε plotted during the course of two separate particle tracking experiments, each with ΔZ = 80 µm and v_Z = 0.73 µm/s. Note the different y-axis scales. The vertical line shows the time at which compression stopped. The solid black line represents the mean value for 5 ROIs and the grey filled area shows the standard deviation between ROIs.

Figure 4.11 shows that ε increases during the compression phase. It can also be seen that the motion of the beads continues for a short time into the stationary phase before coming to rest. However, for repeated experiments of the same compression parameters, the area strain plots are not always reproducible. Fig. 4.11b shows a repeat experiment on a different gel sample, also with ΔZ =80 µm and v_Z = 0.73 µm/s. The plateau area strain is much smaller in Fig. 4.11b than Fig. 4.11a. Additionally, the variability is a lot larger, suggesting that not all ROIs within the field of view increased by the same extent. The results of Figure 4.11 confirm that compression in the Z direction causes a measurable expansion in the gel structure in the X-Y plane. Further, they show that there is significant variability in the plateau value of ε between experiments, which is attributed to different positions within the gel experiencing different compression. This also supports the explanation that the variability in the deformation of vesicles (Fig. 4.6a) is due to differences in the extent of compression experienced.

The heterogeneity of agarose structure is known to vary on a lengthscale of tens of micrometres, and increases as the gel concentration increases [225]. As such, it would be likely that by reducing the agarose concentration, the variability in the compression plateau would also reduce. A further possibility would be to embed lipid vesicles into a covalently-crosslinked hydrogel, such as poly(acrylamide), which would have less structural heterogeneity [225], and therefore should compress all embedded vesicles equally.

4.4 Discussion

4.4.1 Water Loss, Deformation, and Rupture

The results of this chapter show that agarose-embedded vesicles are significantly deformed upon gel compression. This deformation is accompanied by the release of water from the vesicle, but no release of the encapsulated model active, calcein, was observed.

Previous experiments subjecting free-floating vesicles to an increased hydrostatic pressure have demonstrated water loss from the vesicle core [125, 283]. Vesicles were imaged during pressure changes and were observed to maintain a spherical shape whilst decreasing in volume, which is attributed to water loss via permeation of water molecules through the bilayer. In some cases, water loss from vesicles has been attributed to the formation of transient membrane pores [230, 284, 285], but in these cases the vesicles exhibited water loss around the phase transition temperature, which is known to lead to the formation of pores or defects at the boundaries between domains of different co-existing lipid phases [88, 89].
This supports the hypothesis that the hydrogel compression leads to water loss by permeation of water molecules through the bilayer, which is why there is no associated loss of calcein (as described in Section 4.3.2).

The agarose-embedded vesicles exhibited a significant increase in projected area

during compression (Figure 4.6), which is associated with a change from a spherical morphology to either an elliptical or irregular morphology (Figure 4.3).

Previously, deformation of free-floating vesicles has been achieved by a microfluidic stamp. It was found that the presence of sugars within the vesicle caused vesicles to rupture in response to compression on a timescale of < 3 minutes whereas vesicles in the absence of sugars are stably deformed. The reason given for this result was that as the vesicle is compressed, it loses water, causing a volume loss that allows for the increased surface area of the compressed ellipsoid compared to the spherical shape pre-compression. However, in the presence of sugars, water efflux is suppressed in order to maintain osmotic pressure balance across the lipid membrane. Therefore as the vesicle is compressed, the volume stays constant but the surface area increases beyond the lysis area increase and hence ruptures [128].

This is in contrast to the results shown here, where water loss is not inhibited by the presence of sugars in the system. The compressed hydrogel-embedded vesicles experience increased hypoosmotic pressure as water is released from the vesicle interior during deformation. Therefore, we conclude that the presence of external agarose supports the lipid membrane during compression, giving it increased mechanical stability to withstand the imposed osmotic pressure. Here, the sugar concentration was maintained at 300 mM whereas in the work of Robinson et al. the sugar concentration was much higher at 900 mM.

Since the results of Chapter 3 have shown that the adhesion strength between the embedded vesicle and surrounding gel depends on the agarose concentration, we hypothesise that as the gel concentration increases, so does the ability of the gel to stabilise non-spherical vesicle morphologies against osmotic pressure. Therefore, as the gel concentration increases, the amount of deformation that a vesicle can sustain in the presence of osmolytes including sugars should increase. Further experiments could investigate whether there is a relation between the sugar concentration, the gel concentration, and the rupture of deformed vesicles.

Hydrogels have previously been shown to add mechanical stability to lipid membranes using studies on Gel-Filled Vesicles (GFVs) [39, 62, 286] and for planar supported lipid bilayers (SLBs) on hydrogel substrates [287, 288]. GUVs prepared from hydrogel films have also been demonstrated to alter the mechanical properties of the membrane, specifically the response of the membrane to deformation by electric pulses [289]. Experiments by the same group found that electrodeformation of agarose-embedded GUVs showed no qualitative difference in the mechanical properties of embedded vesicles to those of free-floating GUVs, but the lifetime of membrane pores was significantly increased by the presence of a 0.5% agarose hydrogel [46].

The results of this chapter give further evidence that the agarose matrix can impart mechanical stability to the embedded lipid membrane, by supporting significantly non-spherical shapes with high degrees of deformation.

4.4.2 Mechanical Properties of Agarose Hydrogels

The behaviour of hydrogel-embedded vesicles has been shown in this chapter to be significantly different to that of free-floating vesicles, specifically in that they are stabilised against rupture in response to compression. This section will consider how the mechanical properties of agarose may be related to the observed behaviours.

Agarose hydrogels are formed by physical interactions between polysaccharide chains at temperatures below the gelation temperature [225, 290, 291]. The mechanical properties of agarose hydrogels are dependent on a range of factors, including the presence of co-solutes such as sugars [246, 292] and the thermal history and gelation rate [197, 226]. Typical elastic moduli of agarose hydrogels are on the order of $10^4 - 10^5$ kPa, with elastic modulus increasing as gel concentration is increased [293–295].

Additionally, structural heterogeneity in agarose hydrogels has been reported by

multiple authors [221, 225, 226, 246]. The inclusion of sucrose has been shown to reduce structural heterogeneity [246] to some extent. Another method of reducing structural heterogeneity is to cool the gels more rapidly [226], for example by gelling at a lower temperature, but for embedding vesicles, this reduced the amount of vesicles surviving the gelation process.

This heterogeneity is another potential source of variation in experiments that may cause different vesicles to adopt different deformed morphologies or to be deformed to different extents.

Agarose Hydrogels Under Compression

Due to their biocompatibility and similarity to soft tissue, agarose hydrogels have been suggested to be suitable scaffolds for seeding chondrocytes as a method for cartilage repair [196]. As cartilage undergoes significant mechanical compression and other stresses in the body [296], the behaviour of agarose under compression has been well characterised.

When hydrogels are compressed, they may respond either linearly (i.e. equal strain throughout the gel) or non-linearly (position-dependent strain). For agarose hydrogels, it has been found that this response is dependent on the loading rate, i.e. the rate of compression v_Z [297, 298]. At high loading rates, the response is non-linear, whereas slower loading results in a linear compression. In this chapter, the compression rate was $v_Z = 0.73$ µm/s. This value was chosen for experimental reasons – to maintain the imaged vesicle within the field of view throughout the experiment – and is much lower than many loading rates used in the literature. Therefore, we assume that the compression would be linear throughout the samples studied here. However, developments to the experimental protocol might allow for this to be studied further and to confirm this assumption.

The nature of the interface between the gel and its supporting surface (a glass slide, in this case) is also known to affect its behaviour under compression. If the interface is

lubricated, for example with oil, then as the compression proceeds, the contact surface between the gel and the slide increases. If, however, the gel is bonded with an adhesive to the glass surface, then the contact area stays constant, and the edges of the gel will bulge outwards as the gel is compressed [299].

In this work, the interface was neither lubricated nor bonded. This case typically gives behaviour in between the lubricated and bonded cases, with the gel initially sticking and acting as a bonded sample, followed by sliding as a lubricated sample. Within this case, it is difficult to know the exact shape of the sample at a given time during the compression [300, 301]. Therefore, in any further experiments, it would be useful to lubricate the interface to ensure that the compression is reproducible between experiments.

Filled Gels

Inclusions (such as emulsion droplets, solid particles, vesicles, etc.) within a hydrogel structure are collectively known as filler particles. Depending on the strength of interactions between the filler particle and the surrounding matrix, these are classified as either active or passive fillers, and have differing effects on the properties of the overall composite material. Passive fillers are those which do not interact with the gel matrix, and these tend to weaken the gel network. As the gel is sheared or compressed, passive fillers act as voids within the structure. In contrast, active fillers interact more strongly with the gel and are sheared or compressed along with it. The effect of active fillers on the mechanical properties of the gel depends further on the relative moduli of the fillers and the matrix as well as the volume fraction of fillers [302, 303].

In 3D cell culture experiments, increasing the amount of cells included in an agarose hydrogel has been shown to decrease the dynamic modulus and equilibrium modulus [196], suggesting that cells interact only weakly with the gel and act as passive fillers. However, for hydrogel-embedded vesicles, the results depend on the chemistry of both the membrane and gel. Charged vesicles within hyaluronic acid hydrogels increased the strength of the

hydrogel network [304], and thus acted as active fillers. However, egg phosphatidylcholine (EPC) liposomes have been demonstrated to decrease the strength of pNIPAM gels [111] and were therefore passive fillers.

Chapter 3 discussed the observed adhesion between the agarose and the embedded vesicles, and its possible origins. This interaction would cause the vesicles used here to act as active filler particles, and most likely increase the elastic modulus of the composite material. Since the vesicles are active fillers in this system, this allows them to be deformed along with the hydrogel, rather than acting as voids within the structure. Therefore we conclude that the adhesion between the gel and the lipid membrane is what causes the vesicles to adopt the significantly deformed morphologies under compression.

Stress Relaxation

Agarose has previously been shown to exhibit a large degree of stress relaxation during static unconfined compression experiments [279, 280, 305]. This was demonstrated to be in contrast to covalently crosslinked PEG hydrogels which did not show any significant stress relaxation under similar compression conditions [279]. This is attributed to two factors: firstly, the hydrogels were unconfined in directions perpendicular to the compression, which allows water to be lost from the hydrogel during compression. Secondly, the relatively weak nature of physical crosslinks compared to covalent crosslinks, as well as the fact that non-covalent interactions can fluctuate over time [306], means that, during static compression, the physical interactions in agarose hydrogels can be broken and reformed, whereas covalent bonds cannot. Hence, physically crosslinked hydrogels show stress relaxation behaviour but chemically crosslinked hydrogels do not [279]. The stress relaxation behaviour also depends on the gel concentration: both the maximum stress experienced due to compression and the relaxed stress value increase with gel concentration for a fixed deformation. The timescale of the relaxation also increases with gel concentration [280]. Again, this result is attributed to the rearrangement of hydrogen bonds within the gel structure.

The stress relaxation appears to occur over a timescale of minutes [279]. Therefore this behaviour could be closely related to the observation of membrane defects healing during the stationary phase of compression shown here in Figure. 4.7, which also occurs on a similar timescale. As the agarose structure rearranges, it allows the embedded vesicle to relax towards a more spherical shape.

The relaxation behaviour of the vesicle is likely to be accompanied by the influx of water, partially returning the osmolarity to its initial value following the loss of water during compression. As discussed in Chapter 3, membrane permeation can occur very quickly for water in comparison with larger molecules. Free-floating vesicles subjected to a small osmotic shock can equilibrate the osmotic pressure by water loss (or gain) within a timescale of just 1 minute [124]. Therefore, it is probable that as the gel relaxes over a few minutes, water permeates across the bilayer to counteract the buildup of osmotic pressure over a similar timescale.

4.4.3 Application to Food Systems

A possible application of this system to foods would be for controlled release from embedded vesicles during chewing. Firstly, Figure 4.9 shows that embedded vesicles do not release their encapsulated contents in response to mild compressions. Although they can be significantly deformed by mechanical compression under the parameters studied here, the associated volume loss occurs via permeation of water molecules through the lipid bilayer, rather than the formation of membrane pores which would allow for the release of larger encapsulated molecules.

Although this means that mechanical compression of embedded vesicles is unlikely to be useful for controlled release, this also suggests that under the conditions studied here, the encapsulation of actives within the vesicles is highly stable, due to the stabilising effect of the external agarose.

Rates of strain or deformation experienced by gel samples during compression in chewing are difficult to quantify [307], and as a result there is a wide range of values reported. Ostry et al. found measured chewing magnitudes of ≈ 0.5 cm, rates of ≈ 5 cm/s, and times of approximately 300 ms [308]. During chewing, foods also experience shear forces in addition to unidirectional compression [309]. The compression experiments in this chapter used a compression magnitude of $\Delta Z = 100$ µm and compression rate of $v_Z = 0.73$ µm/s, which equates to a compression time of 136 s. These parameters were chosen to ensure that the vesicle would remain within the microscope field of view without the need for significant movement of the stage in the X-Y plane, which would introduce a possible effect of shear. As such, in order to more accurately mimic the embedded vesicle behaviour during chewing, the compression rates and magnitudes would need to be significantly increased and account for shearing motion as well as compressive motion.

Additionally, confectionery recipes are much more complex than the simple agarose and sugar system studied here. Firstly, the sugar concentration used in these experiments is relatively low, at 300 mM sucrose within the vesicles and 300 mM glucose in the gel structure. Typical confectionery gels have a very low water content of <20%, with a significant amount of the remaining formulation being sugars, mainly sucrose and glucose syrup [310].

Other biopolymers such as starch, gelatin, and pectin are typically used in confectionery products [265]. Starch and pectin are both polysaccharides: the repeat units of the polymer chains are sugar groups, as in agarose [195, 311, 312]. In contrast, gelatin is a polypeptide derived from the protein collagen [313]. These biopolymers also have differing gelation mechanisms: starch and gelatin both demonstrate thermal gelation behaviour, requiring heating in water to a high temperature and then cooling to form a gel, but pectin may additionally require high sugar concentration and low pH in order to gel [265]. Further work in applying this system to foods would require studying whether these different biopolymer structures and gelation mechanisms can stably embed vesicles

at appropriate gel concentrations.

Further, to be used in food products, the effect of simultaneous mechanical and osmotic stresses would need to be understood. In the previous chapter, hypoosmotic shocks were shown to cause a single burst release of the encapsulated model active, calcein. This is influenced by the interaction of the gel with the membrane, which inhibits pore sealing and therefore prevents the pulsatile release often observed for free-floating vesicles [95, 207, 211]. Hypoosmotic shocks could be caused by the addition of saliva to the system. In contrast, hyperosmotic shocks and mechanical compression were shown to release only water from the vesicle without the formation of membrane pores and release of calcein. During chewing, foods would be subjected simultaneously to compressive forces, shown to release water but not larger molecules, and hypoosmotic shocks, which have been shown to release large molecules through the formation of membrane pores.

In summary, the results of this chapter show that agarose-embedded vesicles are stable against loss of encapsulated actives due to mild gel compression; however, further work is required to understand if this conclusion applies at higher rates and magnitudes of compression and for other gel-based systems.

4.4.4 Further Work

As mentioned above, the vesicle shape is subject to significant changes due to compression of the surrounding gel matrix. Confocal microscopy could be used to image the vesicle membrane in more detail by taking Z stacks and using them to study the 3D shape of the vesicle after compression. This would allow the vesicle volume to be calculated directly, and the effect of the agarose gel on the lipid membrane to be understood in more detail.

For controlled release applications, further experiments could include using a variety of different hydrogels, for example using biopolymers with ionic gelation rather than thermal

gelation or using covalently crosslinked gels, in order to modulate the strength of adhesion between the gel and the membrane and to understand further how this allows the vesicle to be stably deformed. Further, varying the composition of the membrane would affect membrane properties such as the rigidity and fluidity, which could affect the deformation of the vesicles and their stability once deformed.

It would also be interesting to study lipophilic model actives, as many food flavourings are either partially or fully lipophilic [314]. Since these reside within the hydrophobic region of the bilayer rather than within the aqueous core [315], they have been shown to have different release kinetics to hydrophilic actives due to their ability to diffuse through the membrane [316]. Therefore, upon deformation of the bilayer membrane, this may promote the release of lipophilic actives without the need for membrane pore formation.

4.5 Conclusions

Agarose-embedded lipid vesicles have been shown to adopt highly deformed shapes under mechanical compression, which are stabilised by the adhesion between the lipid membrane and the agarose gel matrix. The shape change was accompanied by a volume change which was shown to be due to water efflux through the bilayer rather than the formation of membrane pores. As a result, the encapsulated model active calcein was retained within the vesicle. This result contrasts with previous literature stating that the presence of sugars during (free-floating) vesicle compression causes vesicle rupture; this is attributed to the stabilising effect of the agarose hydrogel on the lipid membrane.

Chapter 5

Stimuli-Responsive Gel-Filled Vesicles

5.1 Introduction

Gel-Filled Vesicles (GFVs) are widely investigated for their use in encapsulation and controlled release applications, since they can encapsulate both hydrophilic and hydrophobic actives, and have been shown to display sustained release profiles in comparison to either fluid-filled vesicles or uncoated hydrogels [66, 67, 112–115]. In addition, the coupling between the membrane and hydrogel opens up the possibility for new controlled release mechanisms, including the poration mechanism as defined by Kazakov [39]. In this mechanism, swelling of the internal hydrogel causes the lipid bilayer to stretch beyond its lysis point, resulting in the formation of membrane pores which can release actives encapsulated within the gel [39]. This behaviour is analogous to the behaviour of planar lipid bilayers supported on elastic substrates; on expansion of the substrate, the membrane formed reversible, stable membrane pores. This was found to depend on a range of parameters including the substrate hydrophilicity, pH of the environment, and the strain rate of the substrate [119, 317].

However, the poration mechanism of GFVs has not as yet been realised experimentally.

This chapter will attempt to form GFVs with a relevant stimulus-responsive hydrogel core, and utilise this for triggered release.

As well as encapsulation systems, GFVs are also of interest as model cells to study what effect the hydrogel-like cytoskeleton has on the membrane. For example, the inclusion of internal actin filaments has been shown to decrease the water permeability of the membrane and increase the area compressibility modulus [72, 74]. GFVs with a poly(*N*-isopropylacrylamide) core, which are known to exhibit a strong non-specific adhesion between the gel and the membrane, exhibit an increased stability against solubilisation by detergents and reduced lipid mobility [69, 76]. These results all demonstrate that coupling a vesicle membrane to an internal hydrogel can alter membrane properties.

Additionally, Chapter 3 demonstrated that the presence of an external hydrogel caused membrane pinning, which prevents pore closure. Therefore in order to use GFVs for controlled release, it will be important to understand whether coupling a lipid membrane to a hydrogel, rather than a solid substrate, still allows for the formation of reversible membrane pores.

The aim of this chapter is to investigate whether GFVs can reversibly open membrane pores on gel expansion, comparable to the behaviour of planar SLBs on elastic substrates, and further, whether this behaviour can be exploited for the poration mechanism of controlled release by tuning the magnitude of gel deformation.

5.2 Methods

5.2.1 Hydrogel Synthesis and Characterisation

Poly(acrylamide-*co*-acrylic acid) (p(AM-*co*-AA)) hydrogels were prepared using photo-initiated free radical polymerisation. The pre-gel solution contained acrylamide

(non-responsive monomer), acrylic acid (thermoresponsive monomer), bisacrylamide (crosslinking monomer), and diethoxyacetophenone (DEAP, photoinitiator) mixed in a 500 mM NaCl solution. Both the concentrations of the crosslinker and the relative concentrations of acrylamide and acrylic acid were varied.

As an example, 2 mL of a pre-gel solution of 25%mol acrylic acid, 3%mol crosslinker, 1 M total concentration contains:

- 259 µL acrylamide solution (40%)
- 33 µL acrylic acid
- 463 µL bisacrylamide solution (2%)
- 2 µL DEAP photoinitiator
- 1245 µL NaCl solution (500 mM)

Gelation was carried out using UV illumination (18 W, $\lambda = 365$ nm) for 30 minutes. Photopolymerisation was chosen as a more appropriate method of gelation than thermal gelation, as it maintains the polymer in its swollen state throughout polymerisation, which reduces any effects of precipitation or phase separation which may occur in thermal polymerisation [318].

For bulk hydrogels, the pre-gel solution was photopolymerised within a polypropylene tube. The gel cylinders were removed and cut into slices approximately 5 mm thick. These were immersed into a bath of swelling solution (500 mM NaCl) for 24 h to remove any unreacted monomers, and then re-immersed into a bath of fresh swelling solution for measurements. After 24 h of equilibration at 21 °C, each gel slice was blotted with laboratory tissue to remove any excess solution and then weighed and returned to the swelling solution. The samples were then sealed within a petri dish to prevent evaporation of the solution, and transferred to an oven at 40 °C for 24 h to equilibrate before being re-weighed in the same manner. The swelling ratio Q was then calculated according to

Equation 5.1 [319]:

$$Q = \frac{m_{40} - m_{21}}{m_{21}} \tag{5.1}$$

where m_{40} and m_{21} are the masses of the gels at 40 °C and 21 °C respectively. These temperatures were chosen to fall either side of the critical temperature, $T_c \approx 25 - 35$ °C [199]. $Q = 0$ refers to a non-responsive gel, and increasing values of Q refer to a larger water uptake of the gel.

5.2.2 Confirming the GFV Structure

In order to confirm that GFVs were successfully prepared, two tests were employed. Firstly, the integrity of the lipid coating was tested using a calcein permeation assay, and secondly, the gelation of the GFV core was tested using a detergent assay.

Proof of Bilayer Integrity

To test whether the lipid coating was an intact lipid bilayer, a calcein permeation assay was employed. The GFVs were placed into a bath of calcein solution (0.02 mg/mL calcein in a solution iso-osmolar to the GFV core).

The GFVs were then imaged on a confocal microscope ($\lambda_{ex} = 470$ nm, $\lambda_{em} = 510$ nm). If the lipids have formed a defect-free bilayer surrounding the core, then there is zero calcein signal within the core. However, if the lipids form another structure, such as a supported vesicle layer (SVL), or patches of a lipid bilayer with defects in between, then calcein will be able to permeate into the core giving a non-zero signal.

Proof of Gelation

Gelation of the GFV core was tested using a detergent assay. GFVs were imaged using brightfield microscopy to visualise the cores. The detergent SDS (10% solution) was added to the sample to remove the lipid bilayer, and once equilibrated the GFVs were imaged again. If the core is successfully gelled, then following removal of the bilayer, the gel core is

still visible in brightfield microscopy. However, if the core has not gelled, then disruption of the bilayer leads to mixing of the internal and external solutions, and there is no visible structure remaining [71].

5.3 Results

5.3.1 Choice of Gel Chemistry

Although a wide variety of stimuli-responsive hydrogels have been reported [320, 321], many of these would be inapplicable for the aim of designing GFVs to display the poration mechanism. The stimulus needs to be felt by the gel core, and for chemical stimuli, such as pH, ionic strength, etc., this relies on a molecule or ion passing through the lipid bilayer. The impermeability of the lipid bilayer is one of its most desirable characteristics when considering GFVs for controlled release applications, yet it is a considerable limitation into the use of responsive gel cores with chemical stimuli.

As an illustration of this, Kiser et al. used a pH-responsive hydrogel encompassed in a DPPC/DPPG/cholesterol bilayer. Although uncoated microgels swelled when placed into a solution of lower pH, the GFVs remained stable at their original size due to the impermeability of the bilayer to H^+ ions. When the membrane was porated by electroporation, hydrogen ions were able to permeate the gel, causing gel swelling which then led to further membrane poration as the gel swelling continued [68, 117].
Similarly, Wang et al. demonstrated that nanogels of poly(acrylic acid) were both pH-responsive and responsive to ionic strength, whereas GFVs of the same gel composition were not responsive under the same condition, due to the inability of ions to cross the bilayer [114]. These reports demonstrate the inapplicability of chemical triggers such as pH or ionic strength for gel swelling for the poration mechanism.

Therefore, physical stimuli such as temperature are better candidates for designing

GFVs to exhibit the poration mechanism, since no chemical species needs to cross the bilayer.

Thermoresponsive hydrogels can either display Lower Critical Solution Temperature (LCST) or Upper Critical Solution Temperature (UCST) behaviour. LCST gels (also termed negatively thermoresponsive [107]) are those which exhibit a discrete volume transition to smaller volumes as the temperature is increased above a critical transition temperature, T_c [322]. UCST gels (positively thermoresponsive gels) show an increase in volume above T_c [323].

Poly(acrylamide-*co*-acrylic acid) (p(AM-*co*-AA)) has been shown to exhibit UCST behaviour [199, 324], although this only occurs at high ionic strengths (>400 mM NaCl) or low pH values (pH < 4) [325]. The transition temperature T_c can be tuned by both the molar ratio of acrylamide (AM) to acrylic acid (AA) and the degree of crosslinking, with experimentally accessible values in the range 21 °C to above 32 °C [324].

Poly(*N*-isopropylacrylamide) (p(NIPAM)) is a widely-studied hydrogel with LCST behaviour. It also has a tuneable transition temperature of around 32 °C [326]; however, p(NIPAM) becomes almost fully hydrophobic above T_c [327] and therefore is not a suitable substrate for a lipid bilayer in this condition [41]. Therefore it would not be possible to assemble a bilayer on the shrunken hydrogel at high temperatures and use a drop in temperature below T_c to trigger membrane poration.

As a result, p(AM-*co*-AA) hydrogels were chosen as a suitable choice for the gel core, since the UCST transition temperature is experimentally accessible, and the gel core should be a suitable substrate for a lipid bilayer in both the shrunken and swollen states.

5.3.2 Gel Characterisation

To investigate their applicability as responsive gel cores, bulk gels of p(AM-*co*-AA) were prepared and their UCST behaviour in 500 mM NaCl was characterised using the swelling ratio as described in Equation 5.1. It has previously been shown for p(NIPAM) hydrogels

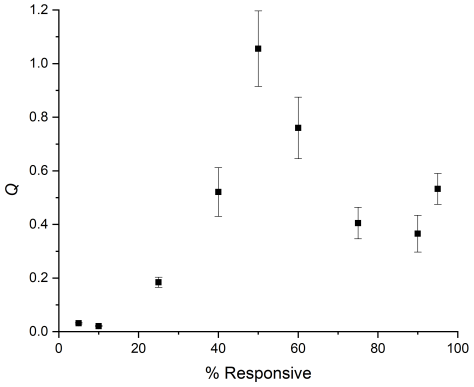

(a) Effect of the ratio of responsive to non-responsive co-monomers on swelling ratio Q. All gels have total monomer concentration of 1 M and crosslinker concentration of 3% mol.

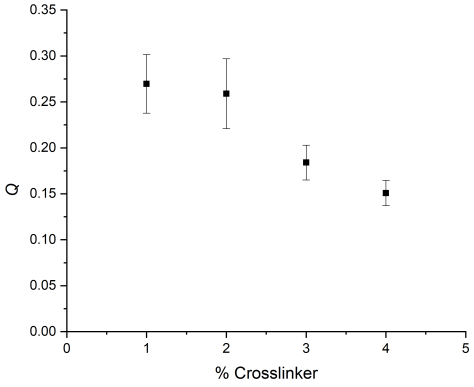

(b) Effect of the concentration of crosslinking co-monomer on Q. All gels have total monomer concentration of 1 M and acrylic acid concentration of 25% mol.

Figure 5.1: Effect of the relative amounts of responsive, non-responsive, and crosslinking co-monomers on the swelling ratio, Q. All gels are submerged in 500 mM NaCl. Error bars are the standard error of $n > 7$ gel slices.

that the swelling ratio Q of GFVs is independent of the initial size and agrees well with Q as measured on bulk hydrogels [77].

Figure 5.1 shows how the temperature-responsive swelling can be modulated by varying the ratio of responsive (acrylic acid) to non-responsive (acrylamide) co-monomers and varying the concentration of the crosslinking co-monomer, bisacrylamide.

Firstly, Figure 5.1a shows that the maximum swelling ratio (for a given crosslinker concentration) occurs at 50% responsive monomer, i.e. a 1:1 molar ratio of acrylic acid to acrylamide monomers. This result has previously been found for microgels of interpenetrating networks (IPNs) of poly(acrylamide) and poly(acrylic acid) as well as copolymer microgels [328–330]. At a 1:1 molar ratio, there is maximum hydrogen bonding between acrylamide and acrylic acid monomers within the gel, giving the smallest equilibrium size at low temperature [329]. Therefore, when these hydrogen bonds are replaced with hydrogen bonds to water molecules as the temperature is increased [330],

there is a more pronounced increase in size resulting in a higher value of Q.

Secondly, Figure 5.1b shows that, as expected, increasing the concentration of the crosslinking monomer bisacrylamide causes a reduction in the maximum swelling ratio. Similar results have been demonstrated for other hydrogels such as p(NIPAM) and poly(*N*-vinylcaprolactam) [331, 332]. As the amount of crosslinker increases, the mesh size of the hydrogel decreases, which reduces the mobility of the polymer between the crosslinks. This inhibits how much extra water can be taken up by the hydrogel in its swollen state, and therefore reduces the swelling ratio [199, 333, 334].

These results show that, firstly, p(AM-*co*-AA) hydrogels exhibit UCST behaviour in 500 mM NaCl solution, and secondly, that the degree of swelling can be tuned by altering either the relative concentrations of responsive and non-responsive monomers or by changing the crosslinker concentration. Therefore this gel composition would be suitable for inclusion within GFVs in order to demonstrate the poration mechanism of controlled release from GFVs.

5.3.3 Preparation of GFVs

Liposomal Reactor Method

Firstly, the liposomal reactor method for forming GFVs was used. In this method (shown in Figure 5.2), vesicles encapsulating a pre-gel solution are prepared, and then the vesicle core is caused to gel by a method appropriate for the gel chemistry. For p(AM-*co*-AA), gelation was induced by UV illumination, which causes the photoinitiator DEAP in the pre-gel solution to form free radicals which initiate the gelation reaction.

Since UV illumination is known to cause chemical damage to phospholipids [335], it is possible that this choice of method could affect the GFV membrane properties. However,

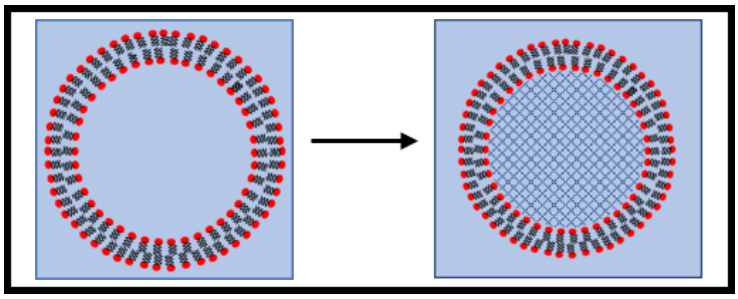

Figure 5.2: Schematic showing the basis of the liposomal reactor method of forming GFVs.

this wavelength of UV illumination (365 nm) has previously been successfully used for GFVs at a much higher power (100 W, in comparison to 18 W used here) [114]. Further, for pNIPAM-filled vesicles formed by this same method, the same membrane behaviours were observed for both saturated lipid membranes and unsaturated membranes, from which the authors concluded that the UV illumination had not initiated any chemical reactions [71]. Therefore, the photopolymerisation parameters used here are unlikely to impede the formation of lipid bilayers or to affect their properties in GFVs.

For the p(AM-*co*-AA) pre-gel solution (i.e. solution of monomers, crosslinker, and initiator in salt solution), hydration-based methods (including electroformation) of vesicle formation were found to be unsuccessful. Hydration-based methods are known to be sensitive to the hydration solution [96] and in particular, high concentrations of salts in the solution are known to prevent detachment of the hydrated vesicles from the substrate [187].

To overcome this, the Emulsion Phase Transfer (EPT) method of vesicle formation was utilised, as described in Chapter 2. This method relies on the formation of a phospholipid-stabilised water-in-oil (W/O) emulsion containing the aqueous pre-gel solution, and then transferring the emulsion droplets through a planar lipid monolayer of phospholipids, which forms an intact lipid bilayer surrounding the emulsion droplets. A notable benefit of this method is its inherent asymmetry: the internal aqueous solution is different to the external aqueous solution [189, 336]. This allows for the internal aqueous

solution to be gelled, for example by exposure to UV illumination, without causing gelation of the external aqueous phase.

Figure 5.3a shows that this method was able to successfully prepare lipid vesicles encapsulating the pre-gel solution. UV illumination was then used to gel the core. Following this, the detergent SDS was added in order to test the gelation. Figure 5.3b shows that the core gelation was unsuccessful as there was no structure remaining visible under bright-field illumination.

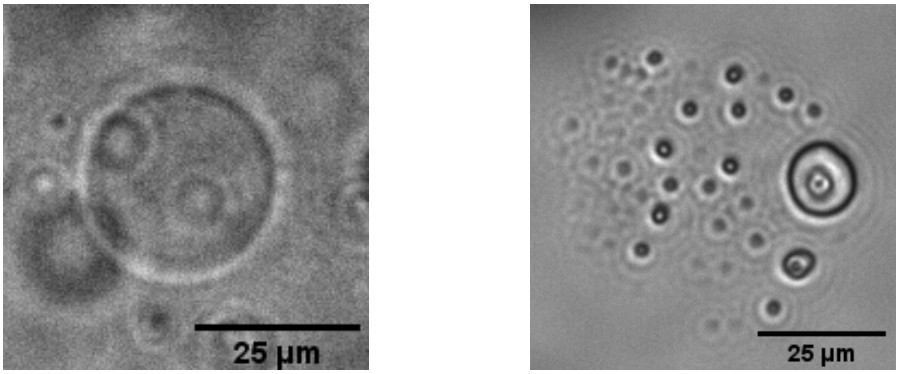

(a) Before addition of detergent

(b) After addition of detergent

Figure 5.3: Detergent assay for core gelation.

Emulsion Reactor Method

In order to overcome the issue with gelation within the vesicle core, an emulsion reactor method was used instead. Similarly to the liposomal reactor method used above, the emulsion reactor method also begins with the formation of a lipid-stabilised W/O emulsion containing the pre-gel solution. However, the aqueous droplets are gelled in the emulsion state before transferring the gelled droplets through the planar monolayer to form vesicles [66], and therefore this may be more successful than gelation within the vesicle core. Figure 5.4 shows a schematic of this method.

Firstly, it was found that gelation within the W/O emulsion droplets was successful,

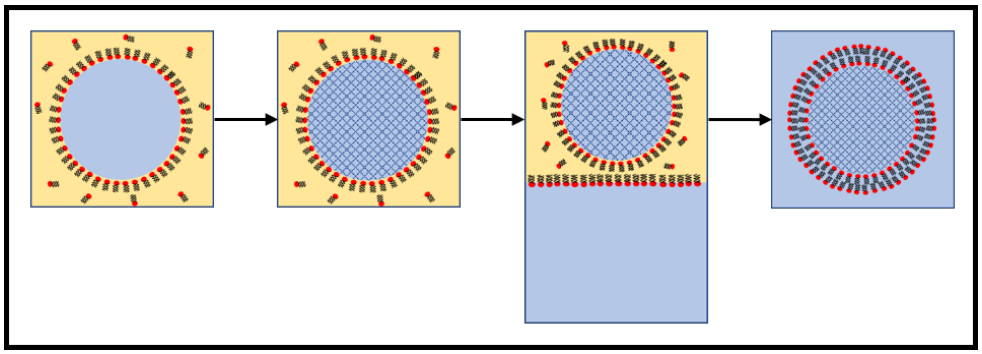

Figure 5.4: Schematic showing the Emulsion Reactor method of forming GFVs.

and gels survived the detergent assay. However, Figure 5.5 shows that calcein is able to permeate the gel core, and hence there was no complete bilayer surrounding the gel. As a control experiment, sucrose-filled GUVs were prepared by the same method. These showed zero calcein intensity within the vesicle core (Figs. 5.5b & 5.5d), indicating that gelation of the core may prevent intact bilayer formation. Alternatively, it may be that the density difference between the gelled emulsion droplets and the external aqueous phase is insufficient for the droplet transfer step.

Previously, Shen et al. have demonstrated that p(AM-*co*-AA) microgels (prepared by emulsion templating) have a higher equilibrium volume once transferred to aqueous solution than in the original emulsion, i.e. the microgel sizes are larger than the preceding emulsion droplets [337]. This means that as the gel cores are transferred through the planar monolayer into the external aqueous phase, they may swell and would therefore have a higher surface area, requiring a larger concentration of phospholipids to fully coat the gel core and form a bilayer.

5.4 Discussion and Further Work

For Emulsion Phase Transfer (EPT) methods, increasing the density gradient between the internal and external aqueous phases has been shown to improve the efficiency of transfer of emulsion droplets to vesicles [147, 336]. In these experiments, although there

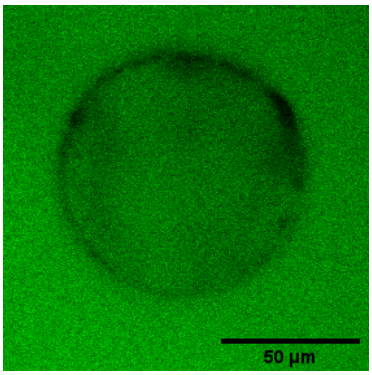

(a) Calcein permeation assay for a GFV

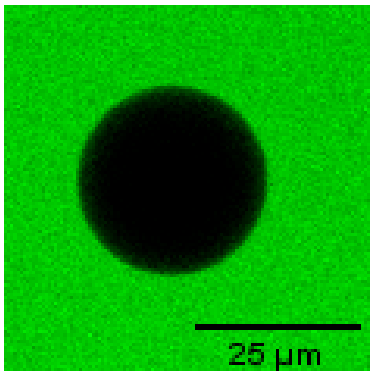

(b) Calcein permeation assay for a sucrose-filled GUV

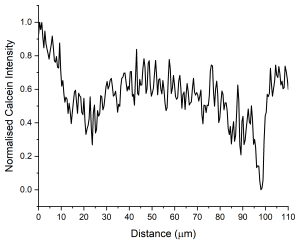

(c) Calcein profile across the centre of the GFV shown in Fig. 5.5a

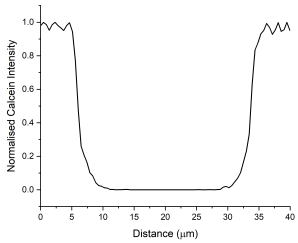

(d) Calcein profile across the centre of the vesicle shown in Fig. 5.5b

Figure 5.5: Calcein permeation assay for a representative Gel-Filled Vesicle and sucrose-filled vesicle.

was a density difference between the (internal) gel and the external aqueous phase, this could be increased by, for example, including sucrose in the internal phase and glucose in the external phase, alongside the salt solution required for gel swelling. If this improves the transfer efficiency and successfully forms GFVs, then the effect of including sugars on the gel's thermoresponsivity would need to be studied further, as it has previously been shown that the thermal swelling of p(AM-*co*-AA) is highly dependent on its aqueous environment [325].

Additionally, further work could investigate if there are differences in the equilibrium sizes of the emulsion droplets and microgels, which would lead to an increased interfacial area between the aqueous and oil phases after gelation. This higher interfacial area would require a larger concentration of phospholipids in order to form an intact monolayer stabilising the interface. Therefore, changing the concentration of phospholipids at each

stage of the EPT method could improve the formation of an intact bilayer surrounding the gel cores.

Alternatively, a different method of forming GFVs could be used. In the bilayer fusion method, polymer microgels are first formed (e.g. by emulsion templating), then lipids are adsorbed onto the gel surface in the form of SUVs and caused to rupture into a bilayer [338]. The adsorption step can be promoted by the inclusion of charged monomers [63], which could make this method particularly suitable for p(AM-*co*-AA) hydrogels, since the acrylic acid moiety is positively charged at pH $\lesssim$ 5.8 [339].
The final step of this method involves rupture of the adhered SUVs into a bilayer covering the gel surface, which may be promoted by freeze-thaw cycles to destabilise the adsorbed SUVs [198, 340]. However, in some cases, lipid SUVs are stable on the microgel surface and do not rupture [182]. Also, bilayers formed by this method have been shown to be partially permeable to small model actives [63], which could mean that the bilayer is not completely covering the gel surface, and would be inappropriate for controlled release studies.

5.5 Conclusions

In summary, the hydrogel poly(acrylamide-*co*-acrylic acid) was identified and characterised as a gel core for GFVs which could demonstrate the poration mechanism of controlled release. However, attempts to include this hydrogel within lipid vesicles were so far unsuccessful, by both the liposomal reactor and emulsion reactor methods. This is likely to be due to the concentrations of solutes in the emulsion phases: either due to the density gradient between aqueous phases or the phospholipid concentration in the oil phase. Optimising the method to account for this should allow for p(AM-*co*-AA)-filled vesicles to be formed, such that the response of the membrane to temperature-responsive gel swelling can be studied.

Chapter 6

Conclusions and Further Work

6.1 Thesis Overview

Broadly, this thesis considers two different composite structures formed of hydrogels and lipid vesicles, in order to investigate gel - membrane interactions and how these affect membrane behaviours. Both hydrogel-embedded vesicles and Gel-Filled Vesicles (GFVs) were investigated for their applicability as encapsulation and controlled-release systems.

Firstly, Chapter 3 explored the behaviour of agarose-embedded vesicles in response to osmotic shocks. Under hyperosmotic shocks, vesicles embedded in high-concentration hydrogels were observed to shrink via buckling, whereas those in lower-concentration gels maintained a spherical morphology. The encapsulated calcein was retained within the vesicle, confirming that the buckled vesicles consisted of an intact bilayer and had not formed membrane pores during buckling.

Under hypoosmotic shocks, membrane pores were formed as expected for free-floating vesicles; however the release profile of calcein showed a single burst release rather than the pulse-wise release that is observed for free-floating vesicles. Additionally, the membrane pores exhibited a non-spherical shape, similar to the floral pores demonstrated by Gözen et al. for pinned membranes [234].

The results from this chapter, as well as a collaborative study including simulations of embedded vesicles, showed that there is a significant adhesion between the lipid membrane and the external agarose gel. In addition to this non-specific adhesion, there is also membrane pinning at defined positions within the gel, which leads to the formation of membrane strands during vesicle shrinking. This membrane pinning and formation of membrane strands under vesicle deflation mimics the behaviour of plant cells during plasmolysis, and therefore hydrogel-embedded vesicles may provide insights on the passive mechanism of Hechtian strand formation in plants, and the conditions that can lead to their coalescence or breakage.

In Chapter 4, the same system of agarose-embedded vesicles was used in order to study whether mechanical compression of the gel can be used to control the release of actives encapsulated within the embedded vesicles. A compression device was designed, utilising a micromanipulator in order to give a well-defined rate and magnitude of compression in the Z-direction.

Compression was shown to significantly deform the embedded vesicles, with an increase in vesicle projected area in the X-Y plane. Simultaneously, the vesicle was shown to have lost volume, and analysis of calcein fluroescence showed that this loss of vesicle volume was due to efflux of water molecules through the lipid bilayer rather than the formation of membrane pores and release of encapsulated calcein.

Previously, Robinson et al. reported that mechanical compression of free-floating vesicles in the presence of sugars resulted in vesicle rupture due to the imposed osmotic stress [128]. However, the results of Chapter 4 illustrate that the presence of an external agarose hydrogel can stabilise the vesicle such that no rupture was observed due to compression.

Finally, Chapter 5 investigated the preparation of GFVs for the poration mechanism of controlled release as defined by Kazakov [39]. UCST-type thermoresponsive gels were considered to be the most applicable hydrogels for the core due to the possibility of the

gel core to "feel" the effect of the stimulus without the need for a chemical stimulus to cross the bilayer. Bulk poly(acrylamide-*co*-acrylic acid) hydrogels were synthesised and the swelling ratio Q was characterised. In good agreement with previous results, Q was found to decrease with increasing crosslinker content, and was maximised for a 1:1 molar ratio of acrylamide (non-responsive) to acrylic acid (responsive) monomers [329–332]. However, attempts to include these hydrogels within vesicles were unsuccessful.

Altogether, these results demonstrate that coupling a lipid membrane to a hydrogel (either internally or externally) can significantly affect membrane properties and behaviours. For example, as well as affecting the vesicle shape after deflation, membrane pinning to the agarose hydrogel was shown to prevent closure of membrane pores after vesicle swelling. Also, the stabilising effect of agarose on embedded lipid membranes was shown to prevent the rupture of the embedded vesicles under compression in the presence of sugars. These altered behaviours will affect the use of either GFVs or hydrogel-embedded vesicles as an encapsulation system: the fact that membrane pinning prevents pore closure results in a single burst of encapsulated actives rather than the burst profile expected for free-floating vesicles.

6.2 Further Work

In the following section, some possible extensions to this work are suggested.

Synthesis of Fluorescent Agarose

Particle tracking experiments were used in Chapters 3 and 4 of this thesis in order to study how the agarose gel structure changed during either osmotic shock or mechanical compression. Due to the porous nature of agarose, large tracer particles were used such that they were immobilised within the matrix and not freely-floating in the aqueous solution.

The use of fluorescent agarose, as synthesised by Horger et al. [269], would be able to give more detail into the structural changes of the gel during either of these experiments. For example, this could reveal whether an interfacial layer of agarose remains adhered to the lipid membrane during buckling. The use of fluorescent agarose might also be used to confirm whether the stress-relaxation behaviour of agarose [279, 280] is responsible for the observation that buckled vesicles may return to a spherical shape during the stationary phase of compression.

Dependence on Sugar Concentration

In Chapter 4, agarose-embedded vesicles were stably deformed by mechanical compression, in the presence of 300 mM sugars. However, Robinson et al. had shown previously that the compression of free-floating vesicles in the presence of 900 mM sugars caused vesicle rupture [128], and therefore we conclude that the agarose has a stabilising effect on the lipid membrane. This has been reported for other hydrogels in various systems [62, 286–288], but has not been quantified. In order to understand this effect, further experiments could include varying the initial sugar concentration as well as the gel concentration, and studying how far the vesicles can be mechanically deformed before rupturing in each condition.

Simultaneous Osmotic and Mechanical Stresses

The two different stresses studied in this thesis - osmotic shocks and mechanical compression - were both shown to cause volume loss from agarose-embedded vesicles. As described in Chapter 4, the use of this system for encapsulation in confectionery systems would require further understanding of the interplay between mechanical and osmotic effects. Similar compression setups have been used for hydrogel-embedded cells submerged in a buffer solution [341, 342] - for vesicles, rather than a buffer solution a suitable shock solution could be used to study the effects of simultaneous osmotic shock and mechanical compression on the lipid bilayer. Particularly, this would show whether volume loss occurs

via efflux of water molecules through the bilayer, as observed for compression experiments, or via the formation of membrane pores and release of encapsulated actives, as observed for hypoosmotic shocks.

Membrane - Gel Interactions

Many of the membrane properties and behaviours studied in this thesis were found to depend on the adhesion strength to the coupled hydrogel - for example, the frequency of the buckling behaviour in Chapter 3 increases with gel concentration. Section 1.1.3 also discussed two examples of p(NIPAM)-filled vesicles from the literature which were prepared by different methods and, as a result, experienced different membrane-gel interaction strengths and membrane behaviours upon gel shrinking. Therefore, a useful extension to this work would be to systematically prepare GFVs with varying gel and bilayer compositions and by a range of methods, in order to compare membrane behaviours.

For GFVs, the adhesion strength between the gel and the membrane can be measured by micropipette aspiration. Kremer et al. showed that the force required to delaminate the membrane from the gel core could be used to calculate the adhesion strength for both p(NIPAM)-filled vesicles as well as red blood cells [76].

Previously, electrostatic attraction between the membrane and a charged hydrogel has been shown to significantly pin the membrane [343]. Therefore we expect that the different types of interactions arising from different hydrogel chemistries may result in different amounts of membrane pinning. The presence of membrane pinning was suggested in Chapter 3 to be related to the pore formation and the release profile of the encapsulated actives (i.e. burst release rather than pulse-wise release), and so this may have significant impact on the use of both GFVs and hydrogel-embedded vesicles for controlled release.

Membrane pinning was also suggested to be the reason that deflating embedded vesicles can form membrane strands similar to Hechtian strands in plasmolysed plants. For this

reason, understanding how the pinning arises from different membrane - gel interactions can inform further experiments on the pinning sites within cells. Measuring the effect of pinning could be carried out using Fluorescence Recovery After Photobleaching (FRAP), to observe how the mobile fraction of lipids M_f is affected by different hydrogels or preparation methods.

Food-Grade Systems

In order to apply these results to confectionery, further work would be needed such that the agarose-embedded vesicles system more closely resembles a relevant confectionery recipe, and that the system can be prepared on a kitchen-scale rather than a lab-scale. Some preliminary experiments were carried out in this area.

Firstly, in place of the synthetic phospholipid DOPC, soya lecithin was used. Similarly to egg lecithin, this is a food-grade reagent derived from natural sources, and contains a variety of lipid headgroups and chain lengths. Soya lecithin is already used within the food industry as an emulsifier in chocolate [344]. Soya lecithin vesicles were successfully prepared via the EPT method, using an internal aqueous phase of 300 mM sucrose, and external aqueous phase of 300 mM dextrose.

Two further extensions to this work are necessary. Confectionery recipes typically contain very high levels of sugar, corresponding to low water levels. Since the lipid bilayer structure self-assembles due to the hydrophobic effect and hydrogen bonding of lipid headgroups to water molecules, it may not be possible to form vesicles at such high sugar levels, as other lipid phases may be preferred [345]. Therefore, the formation of lipid vesicles in low-water environments would need to be studied.

Finally, the gel matrix would need to be of an industry-relevant ingredient. Agarose is the gelling fraction of agar, which also contains the non-gelling fraction agaropectin. Agar is the more commonly used ingredient in the food industry, and so characterising the effect of changing from agarose to agar would be required. Moreover, both gelatin and pectin

are more widely used for confectionery than agar, and so might be a preferable gel matrix to study. These have different gelation mechanisms to agar, which could affect whether vesicles can be stably embedded within.

6.3 Conclusions

Although vesicles are used already in some food applications, their use in confectionery systems as hydrogel-embedded vesicles is likely to be limited by the low water activity of such foods, which may promote the formation of other phospholipid structures rather than lipid vesicles. However, this work has shown that embedded vesicles can encapsulate model actives very stably when embedded into hydrogels, suggesting that, if the low water activity problem can be overcome, then hydrogel-embedded vesicles could be utilised for the encapsulation of flavour molecules. Additionally, Chapter 3 has shown that despite their stability against hyperosmotic shocks and mechanical compression, the embedded vesicles can release their encapsulated actives in response to hypoosmotic shocks, such as the addition of saliva.

Since flavours can be some of the more expensive ingredients within confectionery, the fact that they can be stably encapsulated over long timescales against degradation may present a cost benefit as well as the opportunity for novel consumer experiences based on the triggered release of flavours.

Similarly, GFVs could present a route to triggered release of flavours within foods. Many of the reports of controlled release from GFVs so far have referred to delayed or prolonged release, where diffusion of the encapsulated active out of the lipid bilayer is slowed by the presence of the hydrogel core. There are very few reports of triggered release from GFVs, and seemingly none that utilise the membrane poration mechanism, which would allow for sequential, non-destructive release from the GFV. This thesis has begun to identify the barriers, and their solutions, to forming GFVs that display this

specific behaviour.
However, the implementation of GFVs in the food industry (or other industries) will be constrained by the limitations outlined above for hydrogel-embedded vesicles, as well as by the requirement for more complex preparation methods.

In total, the investigations within this thesis have shown that the combination of lipid vesicles and hydrogels offer multiple routes towards controlled release systems, with differing triggers for release. Various interactions between the gel and the lipid bilayer under a range of conditions have been discussed, and the steps required to implement these systems in the food industry have been considered.

Bibliography

1. Chan, Y.-H. M. & Boxer, S. G. Model Membrane Systems and Their Applications State of the field. *Current Opinion in Chemical Biology* **11,** 581–587 (2007).

2. Wagner, A. & Vorauer-Uhl, K. Liposome Technology for Industrial Purposes. *Journal of Drug Delivery* **2011,** 1–9 (2011).

3. Ota, S., Yoshizawa, S. & Takeuchi, S. Microfluidic formation of monodisperse, cell-sized, and unilamellar vesicles. *Angewandte Chemie - International Edition* **48,** 6533–6537 (2009).

4. Karamdad, K. *et al.* Engineering thermoresponsive phase separated vesicles formed: Via emulsion phase transfer as a content-release platform. *Chemical Science* **9,** 4851–4858 (2018).

5. Immordino, M. L., Dosio, F. & Cattel, L. Stealth liposomes: review of the basic science, rationale, and clinical applications, existing and potential. *International Journal of Nanomedicine* **1,** 297–315 (2006).

6. Dittrich, P. S., Heule, M., Renaud, P. & Manz, A. On-chip extrusion of lipid vesicles and tubes through microsized apertures. *Lab on a Chip* **6,** 488–493 (2006).

7. Sackmann, E. Membrane bending energy concept of vesicle- and cell-shapes and shape-transitions. *FEBS Letters* **346,** 3–16 (1994).

8. Hynes, R. O. The Extracellular Matrix: Not Just Pretty Fibrils. *Science* **326,** 1216–1219 (Nov. 2009).

9. Mecham, R. P. Overview of Extracellular Matrix. *Current Protocols in Cell Biology,* 1–10 (1998).

10. Rosso, F., Giordano, A., Barbarisi, M. & Barbarisi, A. From Cell-ECM Interactions to Tissue Engineering. *Journal of Cellular Physiology* **199,** 174–180 (2004).

11. Reuzeau, C. & Pont-Lezica, R. F. Comparing plant and animal extracellular matrix-cytoskeleton connections - are they alike? *Protoplasma* **186,** 113–121 (1995).

12. Vorwerk, S., Somerville, S. & Somerville, C. The role of plant cell wall polysaccharide composition in disease resistance. *Trends in Plant Science* **9,** 203–209 (2004).

13. Stewart, G. G. in *Brewing and Distilling Yeasts* 55–75 (Springer, 2017).

14. Burton, R. A., Gidley, M. J. & Fincher, G. B. Heterogeneity in the chemistry, structure and function of plant cell walls. *Nature Chemical Biology* **6,** 724–732 (2010).

15. Read, S. M. & Bacic, A. in *Plant Cell Wall Analysis* 63–80 (Springer, 1996).

16. Watt, F. M. The extracellular matrix and cell shape. *Trends in Biochemical Sciences* **11,** 482–485 (1986).

17. Scheffers, D.-J. & Pinho, M. G. Bacterial Cell Wall Synthesis: New Insights from Localization Studies. *Microbiology and Molecular Biology Reviews* **69,** 585–607 (2005).

18. Fletcher, D. A. & Mullins, R. D. Cell mechanics and the cytoskeleton. *Nature* **463,** 485–492 (2010).

19. Hamill, O. P. & Martinac, B. Molecular basis of mechanotransduction in living cells. *Physiological Reviews* **81,** 685–740 (2001).

20. Murrell, M. *et al.* Spreading dynamics of biomimetic actin cortices. *Biophysical Journal* **100,** 1400–1409 (2011).

21. Étienne, J. & Duperray, A. Initial dynamics of cell spreading are governed by dissipation in the actin cortex. *Biophysical Journal* **101,** 611–621 (2011).

22. Kanchanawong, P. *et al.* Nanoscale architecture of integrin-based cell adhesions. *Nature* **468,** 580–584 (2010).

23. Pizzo, A. M., Kokini, K., Vaughn, L. C., Waisner, B. Z. & Voytik-Harbin, S. L. Extracellular matrix (ECM) microstructural composition regulates local cell-ECM biomechanics and fundamental fibroblast behavior: A multidimensional perspective. *Journal of Applied Physiology* **98,** 1909–1921 (2005).

24. Schlie-Wolter, S., Ngezahayo, A. & Chichkov, B. N. The selective role of ECM components on cell adhesion, morphology, proliferation and communication in vitro. *Experimental Cell Research* **319,** 1553–1561 (2013).

25. Takagi, A., Hokonohara, H. & Kawai, T. Flat hydrogel substrate for atomic force microscopy to observe liposomes and lipid membranes. *Analytical and Bioanalytical Chemistry* **395,** 2405–2409 (2009).

26. McCabe, I. P. & Forstner, M. B. Polymer Supported Lipid Bilayers. *Open Journal of Biophysics* **03,** 59–69 (2013).

27. Hennink, W. E. & Van Nostrum, C. F. Novel crosslinking methods to design hydrogels. *Advanced Drug Delivery Reviews* **54,** 13–36 (2002).

28. Gupta, P., Vermani, K. & Garg, S. Hydrogels: From controlled release to pH-responsive drug delivery. *Drug Discovery Today* **7,** 569–579 (2002).

29. Ionov, L. Hydrogel-based actuators: Possibilities and limitations. *Materials Today* **17,** 494–503 (2014).

30. Suri, A. *et al.* Liposome-doped hydrogel for implantable tissue. *Soft Matter* **7,** 7071–7077 (2011).

31. Fels, J., Orlov, S. N. & Grygorczyk, R. The hydrogel nature of mammalian cytoplasm contributes to osmosensing and extracellular pH sensing. *Biophysical Journal* **96,** 4276–4285 (2009).

32. Li, J. & Mooney, D. J. Designing hydrogels for controlled drug delivery. *Nature Reviews Materials* **1,** 16071 (Dec. 2016).

33. Zhang, H., Zhai, Y., Wang, J. & Zhai, G. New progress and prospects: The application of nanogel in drug delivery. *Materials science & engineering. C, Materials for biological applications* **60,** 560–568 (2016).

34. Marras-Marquez, T., Peña, J. & Veiga-Ochoa, M. D. Agarose drug delivery systems upgraded by surfactants inclusion: Critical role of the pore architecture. *Carbohydrate Polymers* **103,** 359–368 (2014).

35. Caliari, S. R. & Burdick, J. A. A practical guide to hydrogels for cell culture. *Nature Methods* **13,** 405–414 (2016).

36. Van Vlierberghe, S., Dubruel, P. & Schacht, E. Biopolymer-based hydrogels as scaffolds for tissue engineering applications: A review. *Biomacromolecules* **12,** 1387–1408 (2011).

37. Ullah, F., Othman, M. B. H., Javed, F., Ahmad, Z. & Akil, H. M. Classification, processing and application of hydrogels: A review. *Materials Science and Engineering C* **57,** 414–433 (2015).

38. Patel, A. & Mequanint, K. in *Biomedical Engineering: Frontiers and Challenges* 275–296 (United Trade Press, 1967).

39. Kazakov, S. in *Liposomes* 49–93 (InTech, 2017).

40. Dou, Y., Li, J., Yuan, B. & Yang, K. Lipid merging, protrusion and vesicle release triggered by shrinking/swelling of poly(N-isopropylacrylamide) microgel particles. *Applied Surface Science* **296,** 95–99 (2014).

41. Lu, N. *et al.* Controlled drug loading and release of a stimuli-responsive lipogel consisting of poly(N-isopropylacrylamide) particles and lipids. *Journal of Physical Chemistry B* **117,** 9677–9682 (2013).

42. Ivashkov, O. V. *et al.* On the mechanism of payload release from liposomes bound to temperature-sensitive microgel particles. *Colloids and Surfaces A: Physicochemical and Engineering Aspects* **570,** 396–402 (2019).

43. Wang, M. *et al.* Assembling responsive microgels at responsive lipid membranes. *Proceedings of the National Academy of Sciences of the United States of America* **116,** 5442–5450 (2019).

44. Simon, C. *et al.* Actin dynamics drive cell-like membrane deformation. *Nature Physics* **15,** 602–609 (2019).

45. Zhao, Y. *et al.* Surface-anchored framework for generating RhD-epitope stealth red blood cells. *Science Advances* **6,** 1–12 (2020).

46. Lira, R. B., Steinkühler, J., Knorr, R. L., Dimova, R. & Riske, K. A. Posing for a picture: Vesicle immobilization in agarose gel. *Scientific Reports* **6,** 1–12 (2016).

47. Cohen, S., Bañó, M. C., Chow, M. & Langer, R. Lipid-alginate interactions render changes in phospholipid bilayer permeability. *Biochimica et Biophysica Acta - Biomembranes* **1063,** 95–102 (1991).

48. DiTizio, V. *et al.* Localized drug delivery using crosslinked gelatin gels containing liposomes: Factors influencing liposome stability and drug release. *Journal of Biomedical Materials Research* **51,** 96–106 (2000).

49. Jensen, B. E. B. *et al.* Lipogels: surface-adherent composite hydrogels assembled from poly(vinyl alcohol) and liposomes. *Nanoscale* **5,** 6758 (2013).

50. Lee, S., Lee, J. & Choi, Y. W. Skin permeation enhancement of ascorbyl palmitate by liposomal hydrogel (Lipogel) formulation and electrical assistance. *Biological and Pharmaceutical Bulletin* **30,** 393–396 (2007).

51. Nie, S., Hsiao, W. W., Pan, W. & Yang, Z. Thermoreversible pluronic® F127-based hydrogel containing liposomes for the controlled delivery of paclitaxel: In vitro drug

release, cell cytotoxicity, and uptake studies. *International Journal of Nanomedicine* **6,** 151–166 (2011).

52. Gao, W. *et al.* Hydrogel containing nanoparticle-stabilized liposomes for topical antimicrobial delivery. *ACS Nano* **8,** 2900–2907 (2014).

53. Tsumoto, K., Oohashi, M. & Tomita, M. Monitoring of membrane collapse and enzymatic reaction with single giant liposomes embedded in agarose gel. *Colloid and Polymer Science* **289,** 1337–1346 (2011).

54. Sá-Lima, H., Tuzlakoglu, K., Mano, J. F. & Reis, R. L. Thermoresponsive poly(N-isopropylacrylamide)- g- methylcellulose hydrogel as a three-dimensional extracellular matrix for cartilage-engineered applications. *Journal of Biomedical Materials Research - Part A* **98 A,** 596–603 (2011).

55. Cavo, M. *et al.* Microenvironment complexity and matrix stiffness regulate breast cancer cell activity in a 3D in vitro model. *Scientific Reports* **6,** 1–13 (2016).

56. Wickremasinghe, N. C., Kumar, V. A. & Hartgerink, J. D. Two-step self-assembly of liposome-multidomain peptide nanofiber hydrogel for time-controlled release. *Biomacromolecules* **15,** 3587–3595 (2014).

57. Mart, R. J., Liem, K. P. & Webb, S. J. Magnetically-controlled release from hydrogel-supported vesicle assemblies. *Chemical Communications,* 2287–2289 (2009).

58. Rose, J. C. *et al.* Biofunctionalized aligned microgels provide 3D cell guidance to mimic complex tissue matrices. *Biomaterials* **163,** 128–141 (2018).

59. Kazakov, S., Kaholek, M., Teraoka, I. & Levon, K. UV-induced gelation on nanometer scale using liposome reactor. *Macromolecules* **35,** 1911–1920 (2002).

60. Viallat, A., Dalous, J. & Abkarian, M. Giant Lipid Vesicles Filled with a Gel: Shape Instability Induced by Osmotic Shrinkage. *Biophysical Journal* **86,** 2179–2187 (2004).

61. Jesorka, A., Markström, M., Karlsson, M. & Orwar, O. Controlled hydrogel formation in the internal compartment of giant unilamellar vesicles. *Journal of Physical Chemistry B* **109,** 14759–14763 (2005).

62. Saleem, Q., Liu, B., Gradinaru, C. C. & Macdonald, P. M. Lipogels: Single-Lipid-Bilayer-Enclosed Hydrogel Spheres. *Biomacromolecules* **12,** 2364–2374 (June 2011).

63. Helwa, Y., Dave, N. & Liu, J. Electrostatically directed liposome adsorption, internalization and fusion on hydrogel microparticles. *Soft Matter* **9,** 6151–6158 (2013).

64. De Geest, B. G. *et al.* Self-exploding lipid-coated microgels. *Biomacromolecules* **7,** 373–379 (2006).

65. Kang, I. *et al.* Stable vesicle assemblies on surfaces of hydrogel nanoparticles formed from a polysaccharide modified with lipid moieties. *Chemical Engineering Journal* **263,** 38–44 (2015).

66. Campbell, A., Taylor, P., Cayre, O. J. & Paunov, V. N. Preparation of aqueous gel beads coated by lipid bilayers. *Chemical Communications* **10,** 2378–2379 (2004).

67. Jin, T., Pennefather, P. S. & Lee, P. I. Lipobeads: A hydrogel anchored lipid vesicle system. *FEBS Letters* **397,** 70–74 (1996).

68. Kiser, P. F. *et al.* A synthetic mimic of the secretory granule for Drug Delivery. *Time,* 459–462 (1998).

69. Stauch, O. *et al.* Mimicking a cytoskeleton by coupling poly(N-isopropylacrylamide) to the inner leaflet of liposomal membranes: Effects of photopolymerization on vesicle shape and polymer architecture. *Biomacromolecules* **3,** 324–332 (2002).

70. Noireaux, V. & Libchaber, A. A vesicle bioreactor as a step toward an artificial cell assembly. *Proceedings of the National Academy of Sciences* **101,** 17669–17674 (2004).

71. Campillo, C. C., Pépin-Donat, B. & Viallat, A. Responsive viscoelastic giant lipid vesicles filled with a poly(N-isopropylacrylamide) artificial cytoskeleton. *Soft Matter* **3,** 1421 (2007).

72. Yoshitani, T. & Yamazaki, M. Water permeability of lipid membranes of GUVs and its dependence on actin cytoskeletons inside the GUVs. *2008 International Symposium on Micro-NanoMechatronics and Human Science, MHS 2008,* 130–134 (2008).

73. Tsai, F. C., Stuhrmann, B. & Koenderink, G. H. Encapsulation of active cytoskeletal protein networks in cell-sized liposomes. *Langmuir* **27,** 10061–10071 (2011).

74. Schäfer, E., Kliesch, T. T. & Janshoff, A. Mechanical properties of giant liposomes compressed between two parallel plates: Impact of artificial actin shells. *Langmuir* **29,** 10463–10474 (2013).

75. Ramos, J., Imaz, A. & Forcada, J. Temperature-sensitive nanogels: poly(N-vinylcaprolactam) versus poly(N-isopropylacrylamide). *Polym. Chem.* **3,** 852–856 (2012).

76. Kremer, S., Campillo, C. C., Pepin-Donat, B., Viallat, A. & Brochard-Wyart, F. Nanotubes from gelly vesicles. *EPL* **82** (2008).

77. Campillo, C. C., Schröder, A. P., Marques, C. M. & Pépin-Donat, B. Volume transition in composite poly(NIPAM)–giant unilamellar vesicles. *Soft Matter* **4,** 2486 (2008).

78. Campillo, C. C., Schroder, A. P., Marques, C. M. & Pépin-Donat, B. Composite gel-filled giant vesicles: Membrane homogeneity and mechanical properties. *Materials Science and Engineering C* **29,** 393–397 (2009).

79. Edris, A & Bergnståhl, B. Encapsulation of orange oil in a spray dried double emulsion. *Nahrung/Food* **2,** 133–137 (2001).

80. Shahidi, F. & Han, X. Q. Encapsulation of Food Ingredients. *Critical Reviews in Food Science and Nutrition* **33,** 501–547 (1993).

81. Huynh, C. T. & Lee, D. S. in *Encyclopedia of Polymeric Nanomaterials* 1–12 (Springer Berlin Heidelberg, Berlin, Heidelberg, 2014).

82. Schultz, P. & Kleinebudde, P. A new multiparticulate delayed release system. Part I: Dissolution properties and release mechanism. *Journal of Controlled Release* **47,** 181–189 (1997).

83. Billard, A. *et al.* Liposome-loaded chitosan physical hydrogel: Toward a promising delayed-release biosystem. *Carbohydrate Polymers* **115,** 651–657 (2015).

84. Qin, S., Geng, Y., Discher, D. E. & Yang, S. Temperature-controlled assembly and release from polymer vesicles of poly(ethylene oxide)-block-poly(N-isopropylacrylamide). *Advanced Materials* **18,** 2905–2909 (2006).

85. Zhang, W. *et al.* Osmotic Pressure Triggered Rapid Release of Encapsulated Enzymes with Enhanced Activity. *Advanced Functional Materials* **27,** 1–7 (2017).

86. Popescu, M. T., Mourtas, S., Pampalakis, G., Antimisiaris, S. G. & Tsitsilianis, C. PH-responsive hydrogel/liposome soft nanocomposites for tuning drug release. *Biomacromolecules* **12,** 3023–3030 (2011).

87. Nii, T. & Ishii, F. Encapsulation efficiency of water-soluble and insoluble drugs in liposomes prepared by the microencapsulation vesicle method. *International Journal of Pharmaceutics* **298,** 198–205 (2005).

88. Papahadjopoulos, D., Jacobson, K., Nir, S. & Isac, I. Phase transitions in phospholipid vesicles Fluorescence polarization and permeability measurements concerning the effect of temperature and cholesterol. *Biochimica et Biophysica Acta - Biomembranes* **311,** 330–348 (1973).

89. Cruzeiro-Hansson, L. & Mouritsen, O. G. Passive ion permeability of lipid membranes modelled via lipid-domain interfacial area. *Biochimica et Biophysica Acta - Biomembranes* **944,** 63–72 (1988).

90. Westhaus, E. & Messersmith, P. B. Triggered release of calcium from lipid vesicles: A bioinspired strategy for rapid gelation of polysaccharide and protein hydrogels. *Biomaterials* **22,** 453–462 (2001).

91. Barbet, J., Machy, P., Truneh, A. & Leserman, L. D. Weak Acid-Induced Release of Liposome-Encapsulated Carboxyfluorescein. *Biochimica et Biophysica Acta* **772,** 347–356 (1984).

92. Wehunt, M. P. *et al.* Controlled drug-release system based on pH-sensitive chloride-triggerable liposomes. *Journal of Liposome Research* **23,** 37–46 (2013).

93. Koçer, A. A remote controlled valve in liposomes for triggered liposomal release. *Journal of Liposome Research* **17,** 219–225 (2007).

94. Ambroggio, E. E., Separovic, F., Bowie, J. H., Fidelio, G. D. & Bagatolli, L. A. Direct visualization of membrane leakage induced by the antibiotic peptides: Maculatin, citropin, and aurein. *Biophysical Journal* **89,** 1874–1881 (2005).

95. Idiart, M. A. & Levin, Y. Rupture of a liposomal vesicle. *Physical Review E - Statistical Physics, Plasmas, Fluids, and Related Interdisciplinary Topics* **69,** 8 (2004).

96. Chiba, M., Miyazaki, M. & Ishiwata, S. Quantitative analysis of the lamellarity of giant liposomes prepared by the inverted emulsion method. *Biophysical Journal* **107,** 346–354 (2014).

97. Karami, N., Moghimipour, E. & Salimi, A. Liposomes as a novel drug delivery system: Fundamental and pharmaceutical application. *Asian Journal of Pharmaceutics* **12,** S31–S41 (2018).

98. Gouin, S. Microencapsulation: Industrial appraisal of existing technologies and trends. *Trends in Food Science and Technology* **15,** 330–347 (2004).

99. Lamichhane, N. *et al.* Liposomes: Clinical applications and potential for image-guided drug delivery. *Molecules* **23,** 1–17 (2018).

100. Beltrán-Gracia, E., López-Camacho, A., Higuera-Ciapara, I., Velázquez-Fernández, J. B. & Vallejo-Cardona, A. A. *Nanomedicine review: Clinical developments in liposomal applications* **1,** 1–40 (Springer Vienna, 2019).

101. Hoare, T. R. & Kohane, D. S. Hydrogels in drug delivery: Progress and challenges. *Polymer* **49,** 1993–2007 (2008).

102. McClements, D. J. Designing biopolymer microgels to encapsulate, protect and deliver bioactive components: Physicochemical aspects. *Advances in Colloid and Interface Science* **240,** 31–59 (2017).

103. Kenawy, E. R., El-Newehy, M. H. & Al-Deyab, S. S. Controlled release of atenolol from freeze/thawed poly(vinyl alcohol) hydrogel. *Journal of Saudi Chemical Society* **14,** 237–240 (2010).

104. Schmaljohann, D. Thermo- and pH-responsive polymers in drug delivery. *Advanced Drug Delivery Reviews* **58,** 1655–1670 (2006).

105. Pelton, R. Temperature-sensitive aqueous microgels. *Advances in Colloid and Interface Science* **85,** 1–33 (2000).

106. Zhang, B. Y. *et al.* Reducibly degradable hydrogels of PNIPAM and PDMAEMA: Synthesis, stimulus-response and drug release. *Journal of Polymer Science, Part A: Polymer Chemistry* **48,** 3604–3612 (2010).

107. Satarkar, N. S. & Hilt, J. Z. Magnetic hydrogel nanocomposites for remote controlled pulsatile drug release. *Journal of Controlled Release* **130,** 246–251 (2008).

108. Hosny, K. M. Optimization of gatifloxacin liposomal hydrogel for enhanced transcorneal permeation. *Journal of Liposome Research* **20,** 31–37 (2010).

109. Gordon, S. *et al.* Chitosan hydrogels containing liposomes and cubosomes as particulate sustained release vaccine delivery systems. *Journal of Liposome Research* **22,** 193–204 (2012).

110. Ciobanu, B. C., Cadinoiu, A. N., Popa, M., Desbrières, J. & Peptu, C. A. Modulated release from liposomes entrapped in chitosan/gelatin hydrogels. *Materials Science and Engineering C* **43,** 383–391 (2014).

111. Liu, Y., Li, Z. & Liang, D. Behaviors of liposomes in a thermo-responsive poly(N-isopropylacrylamide) hydrogel. *Soft Matter* **8,** 4517–4523 (2012).

112. Monshipouri, M. & Rudolph, A. S. Liposome-encapsulated alginate: Controlled hydrogel particle formation and release. *Journal of Microencapsulation* **12,** 117–127 (1995).

113. Tiwari, S. *et al.* Development and characterization of novel carrier gel core liposomes based transmission blocking malaria vaccine. *Journal of Controlled Release* **140,** 157–165 (2009).

114. Wang, Y., Tu, S., Pinchuk, A. N. & Xiong, M. P. Active drug encapsulation and release kinetics from hydrogel-in-liposome nanoparticles. *Journal of Colloid and Interface Science* **406,** 247–255 (2013).

115. Obuobi, S., Julin, K., Fredheim, E. G., Johannessen, M. & Škalko-Basnet, N. Liposomal delivery of antibiotic loaded nucleic acid nanogels with enhanced drug loading and synergistic anti-inflammatory activity against S. aureus intracellular infections. *Journal of Controlled Release* **324,** 620–632 (2020).

116. Liu, J., Stace-Naughton, A., Jiang, X. & Brinker, C. J. Porous Nanoparticle Supported Lipid Bilayers (Protocells) as Delivery Vehicles. *J. Am. Chem. Soc.,* 1354–1355 (2009).

117. Kiser, P. F., Wilson, G. & Needham, D. Lipid-coated microgels for the triggered release of doxorubicin. *Journal of Controlled Release* **68,** 9–22 (2000).

118. Liu, Z. W., Zeng, X. A., Sun, D. W. & Han, Z. Effects of pulsed electric fields on the permeabilization of calcein-filled soybean lecithin vesicles. *Journal of Food Engineering* **131,** 26–32 (2014).

119. Stubbington, L., Arroyo, M. & Staykova, M. Sticking and sliding of lipid bilayers on deformable substrates. *Soft Matter,* 181–186 (2016).

120. Kavčič, B., Sakashita, A. A., Noguchi, H. & Ziherl, P. Limiting shapes of confined lipid vesicles. *Soft Matter* **15,** 602–614 (2019).

121. Sakashita, A., Imai, M. & Noguchi, H. Confinement-induced shape transitions in multilamellar vesicles. *Physical Review E* **89,** 040701 (Sept. 2018).

122. Seifert, U., Berndl, K. & Lipowsky, R. Shape transformations of vesicles: Phase diagram for spontaneous- curvature and bilayer-coupling models. *Physical Review A* **44,** 1182–1202 (1991).

123. Döbereiner, H. G. Properties of giant vesicles. *Current Opinion in Colloid and Interface Science* **5,** 256–263 (2000).

124. Sakashita, A., Urakami, N., Ziherl, P. & Imai, M. Three-dimensional analysis of lipid vesicle transformations. *Soft Matter* **8,** 8569–8581 (2012).

125. Perrier-Cornet, J. M., Baddóuj, K. & Gervais, P. Pressure-induced shape change of phospholipid vesicles: Implication of compression and phase transition. *Journal of Membrane Biology* **204,** 101–107 (2005).

126. Döbereiner, H. G., Evans, E., Kraus, M., Seifert, U. & Wortis, M. Mapping vesicle shapes into the phase diagram: A comparison of experiment and theory. *Physical Review E - Statistical Physics, Plasmas, Fluids, and Related Interdisciplinary Topics* **55,** 4458–4474 (1997).

127. Menger, F. M. & Keiper, J. S. Chemistry and physics of giant vesicles as biomembrane models. *Current Opinion in Chemical Biology* **2,** 726–732 (1998).

128. Robinson, T. & Dittrich, P. S. Observations of Membrane Domain Reorganization in Mechanically Compressed Artificial Cells. *ChemBioChem* **20,** 2666–2673 (2019).

129. Jia, H. *et al.* Shaping Giant Membrane Vesicles in 3D-Printed Protein Hydrogel Cages. *Small* **16,** 1–10 (2020).

130. Srividya, N. & Muralidharan, S. Determination of the Line Tension of Giant Vesicles from Pore-Closing Dynamics. *The Journal of Physical Chemistry B* **112,** 7147–7152 (2008).

131. Wullschleger, L. & Meyer-Piening, H. R. Buckling of geometrically imperfect cylindrical shells - Definition of a buckling load. *International Journal of Non-Linear Mechanics* **37,** 645–657 (2002).

132. Zoelly, R. Uber ein Knickungsproblem an der Kugelschale. *Zürich* (1915).

133. Timoshenko, S. P., Gere, J. M. & Prager, W. *Theory of Elastic Stability, Second Edition* 2nd. **1,** 220–221 (Courier Corporation, Mar. 1962).

134. Hutchinson, J. W. Buckling of spherical shells revisited. *Proceedings of the Royal Society A: Mathematical, Physical and Engineering Sciences* **472** (2016).

135. Knoche, S. & Kierfeld, J. The secondary buckling transition: Wrinkling of buckled spherical shells. *European Physical Journal E* **37,** 1–21 (2014).

136. Mitchell, R. F. Tubing buckling - The state of the art. *SPE Drilling and Completion* **23,** 361–370 (2008).

137. Osgood, W. R., Carlson, R. L., Sendelbeck, R. L. & Hoff, N. J. Experimental studies of the buckling of complete spherical shells. *Experimental Mechanics* **8,** 281–282 (1968).

138. Zhang, X. W., Fu, R. & Yu, T. X. *Experimental study on static/dynamic local buckling of ping pong balls compressed onto a rigid plate* in *Fourth International Conference on Experimental Mechanics* **7522** (2009), 75220Z.

139. Zhang, J., Zhang, M., Tang, W., Wang, W. & Wang, M. Buckling of spherical shells subjected to external pressure: A comparison of experimental and theoretical data. *Thin-Walled Structures* **111,** 58–64 (2017).

140. Shorter, R., Smith, J. D., Coveney, V. A. & Busfield, J. J. C. Axial Compression of Hollow Elastic Spheres. *Journal of Mechanics of Materials and Structures* **5,** 693–705 (2010).

141. Gao, C., Donath, E., Moya, S., Dudnik, V. & Möhwald, H. Elasticity of hollow polyelectrolyte capsules prepared by the layer-by-layer technique. *European Physical Journal E* **5,** 21–27 (2001).

142. Quemeneur, F., Quilliet, C., Faivre, M., Viallat, A. & Pépin-Donat, B. Gel phase vesicles buckle into specific shapes. *Physical Review Letters* **108,** 1–5 (2012).

143. Kusters, R. *et al.* Actin shells control buckling and wrinkling of biomembranes. *Soft Matter* **15,** 9647–9653 (2019).

144. Helfer, E. *et al.* Buckling of actin-coated membranes under application of a local force. *Physical Review Letters* **87,** 881031–881034 (2001).

145. Litvinchuk, S., Lu, Z., Rigler, P., Hirt, T. D. & Meier, W. Calcein release from polymeric vesicles in blood plasma and PVA hydrogel. *Pharmaceutical Research* **26,** 1711–1717 (2009).

146. Alam, J. M., Kobayashi, T. & Yamazaki, M. The single-giant unilamellar vesicle method reveals lysenin-induced pore formation in lipid membranes containing sphingomyelin. *Biochemistry* **51,** 5160–5172 (2012).

147. Moga, A., Yandrapalli, N., Dimova, R. & Robinson, T. Optimization of the Inverted Emulsion Method for High-Yield Production of Biomimetic Giant Unilamellar Vesicles. *ChemBioChem* **20,** 2674–2682 (2019).

148. Grandgirard, J., Poinsot, D., Krespi, L., Nénon, J. P. & Cortesero, A. M. Measurement of Cell Volume Changes by Fluorescence Self-Quenching. *Entomologia Experimentalis et Applicata* **103,** 239–248 (2002).

149. Bonora, M. *et al.* Comprehensive analysis of mitochondrial permeability transition pore activity in living cells using fluorescence-imaging-based techniques. *Nature Protocols* **11,** 1067–1080 (2016).

150. Maherani, B., Arab-Tehrany, E., Kheirolomoom, A., Geny, D. & Linder, M. Calcein release behavior from liposomal bilayer; Influence of physicochemical/mechanical/structural properties of lipids. *Biochimie* **95,** 2018–2033 (Nov. 2013).

151. Binder, W. H. Polymer-induced transient pores in lipid membranes. *Angewandte Chemie - International Edition* **47,** 3092–3095 (2008).

152. Simões, M. G., Alves, P., Carvalheiro, M. & Simões, P. N. Stability effect of cholesterol-poly(acrylic acid) in a stimuli-responsive polymer-liposome complex obtained from soybean lecithin for controlled drug delivery. *Colloids and Surfaces B: Biointerfaces* **152,** 103–113 (2017).

153. Loura, L. M. & Prates Ramalho, J. P. Fluorescent membrane probes' behavior in lipid bilayers: Insights from molecular dynamics simulations. *Biophysical Reviews* **1,** 141–148 (2009).

154. Loura, L. M. & Ramalho, J. P. Recent developments in molecular dynamics simulations of fluorescent membrane probes. *Molecules* **16,** 5437–5452 (2011).

155. Chen, H. H., Lin, Y. Z. & Luo, Y. Isotropic differential phase contrast microscopy for quantitative phase bio-imaging. *Journal of Biophotonics* **11,** 1–7 (2018).

156. Lipowsky, R. & Erich, S. *Structure and dynamics of membranes: I. from cells to vesicles/II. generic and specific interactions.* (Elsevier, 1995).

157. Gupta, S., De Mel, J. U. & Schneider, G. J. Dynamics of liposomes in the fluid phase. *Current Opinion in Colloid and Interface Science* **42,** 121–136 (2019).

158. Svetina, S. & Žekš, B. Membrane bending energy and shape determination of phospholipid vesicles and red blood cells. *European Biophysics Journal* **17,** 101–111 (1989).

159. Svetina, S. S. S. S., Zeks, B., Bŏtjaňeǩ & Zeks, B. Shape behavior of lipid vesicles as the basis of some cellular processes. *Anatomical Record* **268,** 215–225 (2002).

160. Janmey, P. A. & Kinnunen, P. K. Biophysical properties of lipids and dynamic membranes. *Trends in Cell Biology* **16,** 538–546 (2006).

161. Boal, D. in *Mechanics of the Cell* 137–174 (Cambridge University Press, 2001).

162. Maleki, M., Seguin, B. & Fried, E. Kinematics, material symmetry, and energy densities for lipid bilayers with spontaneous curvature. *Biomechanics and Modeling in Mechanobiology* **12,** 997–1017 (Oct. 2013).

163. Rózycki, B. & Lipowsky, R. Membrane curvature generated by asymmetric depletion layers of ions, small molecules, and nanoparticles. *Journal of Chemical Physics* **145** (2016).

164. Akimov, S. A. *et al.* Pore formation in lipid membrane II: Energy landscape under external stress. *Scientific Reports* **7,** 1–20 (2017).

165. Dimova, R. Recent developments in the field of bending rigidity measurements on membranes. *Advances in Colloid and Interface Science* **208,** 225–234 (2014).

166. Pan, J., Tristram-Nagle, S., Kučerka, N. & Nagle, J. F. Temperature dependence of structure, bending rigidity, and bilayer interactions of dioleoylphosphatidylcholine bilayers. *Biophysical Journal* **94,** 117–124 (2008).

167. Faizi, H. A., Reeves, C. J., Georgiev, V. N., Vlahovska, P. M. & Dimova, R. Fluctuation spectroscopy of giant unilamellar vesicles using confocal and phase contrast microscopy. *Soft Matter* (2020).

168. Monzel, C. & Sengupta, K. Measuring shape fluctuations in biological membranes. *Journal of Physics D: Applied Physics* **49** (2016).

169. Lipowsky, R. The morphology of lipid membranes. *Current Opinion in Structural Biology* **5,** 531–540 (1995).

170. Rawicz, W, Olbrich, K. C., Mcintosh, T, Needham, D & Evans, E. Effect of Chain Length and Unsaturation on Elasticity of Lipid Bilayers. **79,** 328–339 (2000).

171. Akimov, S. A. *et al.* Pore formation in lipid membrane I: Continuous reversible trajectory from intact bilayer through hydrophobic defect to transversal pore. *Scientific Reports* **7,** 1–20 (2017).

172. Karatekin, E. *et al.* Cascades of transient pores in giant vesicles: Line tension and transport. *Biophysical Journal* **84,** 1734–1749 (2003).

173. Förtig, A. *et al.* Solid-supported biomimetic membranes with tailored lipopolymer tethers. *Macromolecular Symposia* **210,** 329–338 (2004).

174. Li, S., Hu, P. C. & Malmstadt, N. Imaging molecular transport across lipid bilayers. *Biophysical Journal* **101,** 700–708 (2011).

175. Israelachvili, J. N., Mitchell, D. J. & Ninham, B. W. Theory of self-assembly of lipid bilayers and vesicles. *Biochimica et Biophysica Acta - Biomembranes* **470,** 185–201 (1977).

176. Jeffrey, G. A. & Saenger, W. *Hydrogen Bonding in Biological Structures* (Springer Berlin Heidelberg, June 1991).

177. May, S & S.˜May. A molecular model for the line tension of lipid membranes. *The European Physical Journal E* **3,** 37–44 (2000).

178. Strauss, G & Hauser, H. Stabilization of lipid bilayer vesicles by sucrose during freezing. *Biophysics* **83,** 24222426 (1986).

179. Andersen, H. D., Wang, C., Arleth, L., Peters, G. H. & Westh, P. Reconciliation of opposing views on membrane-sugar interactions. *Proceedings of the National Academy of Sciences of the United States of America* **108,** 1874–1878 (2011).

180. Schneemilch, M. & Quirke, N. Free energy of adsorption of supported lipid bilayers from molecular dynamics simulation. *Chemical Physics Letters* **664,** 199–204 (2016).

181. Cevc, G. & Marsh, D. *Phospholipid Bilayers* (Wiley, 1987).

182. MacKinnon, N. *et al.* Triggered instability of liposomes bound to hydrophobically modified core-shell PNIPAM hydrogel beads. *Langmuir* **26,** 1081–1089 (2010).

183. Tsumoto, K., Matsuo, H., Tomita, M. & Yoshimura, T. Efficient formation of giant liposomes through the gentle hydration of phosphatidylcholine films doped with sugar. *Colloids and Surfaces B: Biointerfaces* **68,** 98–105 (Jan. 2009).

184. Hope, M. J., Bally, M. B., Mayer, L. D., Janoff, A. S & Cullis, P. R. Generation of Multilamellar and Unilamellar Phospholipid Vesicles. *Chemistry and Physics of Lipids* **40,** 89–107 (1986).

185. Angelova, M. I. & Dimitrov, D. S. Liposome electroformation. *Faraday Discussions of the Chemical Society* **81,** 303–311 (1986).

186. Politano, T. J., Froude, V. E., Jing, B. & Zhu, Y. AC-electric field dependent electroformation of giant lipid vesicles. *Colloids and Surfaces B: Biointerfaces* **79,** 75–82 (2010).

187. Stein, H., Spindler, S., Bonakdar, N., Wang, C. & Sandoghdar, V. Production of Isolated Giant Unilamellar Vesicles under High Salt Concentrations. *Frontiers in Physiology* **8,** 63 (2017).

188. Méléard, P., Bagatolli, L. A. & Pott, T. Giant Unilamellar Vesicle Electroformation. From Lipid Mixtures to Native Membranes Under Physiological Conditions. *Methods in Enzymology* **465,** 161–176 (2009).

189. Pautot, S., Frisken, B. J. & Weitz, D. A. Engineering asymmetric vesicles. *Proceedings of the National Academy of Sciences* **100,** 10718–10721 (2003).

190. Fang, Y. & Dalgleish, D. G. Comparison of the effects of three different phosphatidylcholines on casein-stabilized oil-in-water emulsions. *Journal of the American Oil Chemists' Society* **73,** 437–442 (1996).

191. Borden, E. C., Gary, G. W. & Murphy, F. A. Comparison of agar and agarose preparations for mengovirus plaque formation. *Applied microbiology* **20,** 289–291 (1970).

192. McIlvain, G. *et al.* Reliable preparation of agarose phantoms for use in quantitative magnetic resonance elastography. *Journal of the Mechanical Behavior of Biomedical Materials* **97,** 65–73 (2019).

193. Cuatrecasas, P. Agarose derivatives for purification of protein by affinity chromatography. *Nature* **228,** 1327–1328 (1970).

194. Zucca, P., Fernandez-Lafuente, R. & Sanjust, E. Agarose and its derivatives as supports for enzyme immobilization. *Molecules* **21,** 1–25 (2016).

195. Hickson, T. G. & Polson, A. Some physical characteristics of the agarose molecule. *Biochimica et Biophysica Acta - Biomembranes* **165,** 43–58 (1968).

196. Buckley, C. T., Thorpe, S. D., O'Brien, F. J., Robinson, A. J. & Kelly, D. J. The effect of concentration, thermal history and cell seeding density on the initial mechanical properties of agarose hydrogels. *Journal of the Mechanical Behavior of Biomedical Materials* **2,** 512–521 (2009).

197. Aymard, P. *et al.* Influence of thermal history on the structural and mechanical properties of agarose gels. *Biopolymers* **59,** 131–144 (2001).

198. Rahni, S. & Kazakov, S. Hydrogel Micro-/Nanosphere Coated by a Lipid Bilayer: Preparation and Microscopic Probing. *Gels* **3,** 7 (2017).

199. Echeverria, C., López, D. & Mijangos, C. UCST responsive microgels of poly(acrylamide-acrylic acid) copolymers: Structure and viscoelastic properties. *Macromolecules* **42,** 9118–9123 (2009).

200. Schindelin, J. *et al.* Fiji: An open-source platform for biological-image analysis. *Nature Methods* **9,** 676–682 (2012).

201. Kültz, D. Cellular osmoregulation: Beyond ion transport and cell volume. *Zoology* **104,** 198–208 (2001).

202. Assani, A., Moundanga, S., Beney, L. & Gervais, P. Vesicle formation in the membrane of onion cells (Allium cepa) during rapid osmotic dehydration. *Annals of Botany* **104,** 1389–1395 (2009).

203. Lang-Pauluzzi, I. & Gunning, B. E. A plasmolytic cycle: The fate of cytoskeletal elements. *Protoplasma* **212,** 174–185 (2000).

204. Cheng, X., Lang, I., Adeniji, O. S. & Griffing, L. Plasmolysis-deplasmolysis causes changes in endoplasmic reticulum form, movement, flow, and cytoskeletal association. *Journal of Experimental Botany* **68,** 4075–4087 (2017).

205. Bhatia, T., Robinson, T. & Dimova, R. Membrane permeability to water measured by microfluidic trapping of giant vesicles. *Soft Matter* **16,** 7359–7369 (2020).

206. Alinaghi, A., Rouini, M. R., Johari Daha, F. & Moghimi, H. R. Hydrogel-embeded vesicles, as a novel approach for prolonged release and delivery of liposome, in vitro and in vivo. *Journal of Liposome Research* **23,** 235–243 (2013).

207. Koslov, M. M. & Markin, V. S. A theory of osmotic lysis of lipid vesicles. *Journal of Theoretical Biology* **109,** 17–39 (1984).

208. Thompson, B. R. *et al.* Liposomes Entrapped in Biopolymer Hydrogels Can Spontaneously Release into the External Solution. *Langmuir* **36,** 7268–7276 (2020).

209. Gracià, R. S., Bezlyepkina, N., Knorr, R. L., Lipowsky, R. & Dimova, R. Effect of cholesterol on the rigidity of saturated and unsaturated membranes: fluctuation and electrodeformation analysis of giant vesicles. *Soft Matter* **6,** 1472 (2010).

210. Rasouli, M. Basic concepts and practical equations on osmolality: Biochemical approach. *Clinical Biochemistry* **49,** 936–941 (2016).

211. Chabanon, M., Ho, J. C., Liedberg, B., Parikh, A. N. & Rangamani, P. Pulsatile Lipid Vesicles under Osmotic Stress. *Biophysical Journal* **112,** 1682–1691 (2017).

212. Boroske, E., Elwenspoek, M. & Helfrich, W. Osmotic shrinkage of giant egg-lecithin vesicles. *Biophysical Journal* **34,** 95–109 (1981).

213. De Gier, J. Osmotic behaviour and permeability properties of liposomes. *Chemistry and Physics of Lipids* **64,** 187–196 (1993).

214. Ohno, M., Hamada, T., Takiguchi, K. & Homma, M. Dynamic behavior of giant liposomes at desired osmotic pressures. *Langmuir* **25,** 11680–11685 (2009).

215. Pamplona, D. C., Greenwood, J. A. & Calladine, C. R. The buckling of spherical liposomes. *Journal of Biomechanical Engineering* **127,** 1062–1069 (2005).

216. Preston, S. P., Jensen, O. E. & Richardson, G. Buckling of an axisymmetric vesicle under compression: The effects of resistance to shear. *Quarterly Journal of Mechanics and Applied Mathematics* **61,** 1–24 (2008).

217. Lipowsky, R. Spontaneous tubulation of membranes and vesicles reveals membrane tension generated by spontaneous curvature. *Faraday Discussions* **161,** 305–331 (2012).

218. Bhatia, T., Christ, S., Steinkühler, J., Dimova, R. & Lipowsky, R. Simple sugars shape giant vesicles into multispheres with many membrane necks. *Soft Matter* **16,** 1246–1258 (2020).

219. Paula, S., Volkov, A. G., Van Hoek, A. N., Haines, T. H. & Deamer, D. W. Permeation of protons, potassium ions, and small polar molecules through phospholipid bilayers as a function of membrane thickness. *Biophysical Journal* **70,** 339–348 (1996).

220. Mathai, J. C., Tristram-Nagle, S., Nagle, J. F. & Zeidel, M. L. Structural Determinants of Water Permeability through the Lipid Membrane. *The Journal of General Physiology* **131,** 69–76 (2008).

221. Weng, L., Liang, S., Zhang, L., Zhang, X. & Xu, J. Transport of glucose and poly(ethylene glycol)s in agarose gels studied by the refractive index method. *Macromolecules* **38,** 5236–5242 (2005).

222. Arumugam, S., Petrov, E. P. & Schwille, P. Cytoskeletal pinning controls phase separation in multicomponent lipid membranes. *Biophysical Journal* **108,** 1104–1113 (2015).

223. Fujimoto, T. & Parmryd, I. Interleaflet coupling, pinning, and leaflet asymmetry-major players in plasma membrane nanodomain formation. *Frontiers in Cell and Developmental Biology* **4,** 1–12 (2017).

224. Jie, Y., Zhang, L., Chen, P., Mao, X. & Tang, S. Preparation of agarose sulfate and its antithrombogenicity. *Journal Wuhan University of Technology, Materials Science Edition* **27,** 110–114 (2012).

225. Stellwagen, J. & Stellwagen, N. C. Internal structure of the agarose gel matrix. *Journal of Physical Chemistry* **99,** 4247–4251 (1995).

226. Kusukawa, N., Ostrovsky, M. V. & Garner, M. M. Effect of gelation conditions on the gel structure and resolving power of agarose-based DNA sequencing gels. *Electrophoresis* **20,** 1455–1461 (1999).

227. Bittman, R. & Blau, L. The Phospholipid-Cholesterol Interaction. Kinetics of Water Permeability in Liposomes. *Biochemistry* **11,** 4831–4839 (1972).

228. Zhou, H., Gabilondo, B. B., Losert, W. & Van De Water, W. Stretching and relaxation of vesicles. *Physical Review E - Statistical, Nonlinear, and Soft Matter Physics* **83,** 1–8 (2011).

229. Solon, J. *et al.* Negative tension induced by lipid uptake. *Physical Review Letters* **97,** 3–6 (2006).

230. Käs, J. & Sackmann, E. Shape transitions and shape stability of giant phospholipid vesicles in pure water induced by area-to-volume changes. *Biophysical Journal* **60,** 825–844 (1991).

231. Mui, B. L., Cullis, P. R., Evans, E. A. & Madden, T. D. Osmotic properties of large unilamellar vesicles prepared by extrusion. *Biophysical Journal* **64,** 443–453 (1993).

232. Zhelev, D. V. & Needham, D. Tension-stabilized pores in giant vesicles: determination of pore size and pore line tension. *Biochimica et Biophysica Acta - Biomembranes* **1147,** 89–104 (1993).

233. Sandre, O., Moreaux, L. & Brochard-Wyart, F. Dynamics of transient pores in stretched vesicles. *Proceedings of the National Academy of Sciences of the United States of America* **96,** 10591–10596 (1999).

234. Gözen, I. *et al.* Fractal avalanche ruptures in biological membranes. *Nature Materials* **9,** 908–912 (2010).

235. Gözen, I. *et al.* Repair of large area pores in supported double bilayers. *Soft Matter* **9,** 2787–2792 (2013).

236. Taylor, M., Gözen, I., Patel, S., Jesorka, A. & Bertoldi, K. Peridynamic modeling of ruptures in biomembranes. *PLoS ONE* **11,** 1–14 (2016).

237. Helfrich, W. Steric Interaction of Fluid Membranes in Multilayer Systems. *Zeitschrift fur Naturforschung - Section A Journal of Physical Sciences* **33,** 305–315 (1978).

238. Pernodet, N., Maaloum, M. & Tinland, B. Pore size of agarose gels by atomic force microscopy. *Electrophoresis* **18,** 55–58 (1997).

239. Brochard, F & Lennon, J. Frequency spectrum of the flicker phenomenon in erythrocytes. *Journal de Physique* **36,** 1035–1047 (1975).

240. Kang, M., Andreani, M. & Kenworthy, A. K. Validation of normalizations, scaling, and photofading corrections for FRAP data analysis. *PLoS ONE* **10,** 1–28 (2015).

241. Scomparin, C., Lecuyer, S., Ferreira, M., Charitat, T. & Tinland, B. Diffusion in supported lipid bilayers: Influence of substrate and preparation technique on the internal dynamics. *European Physical Journal E* **28,** 211–220 (2009).

242. Seifert, U. & Lipowsky, R. Adhesion of vesicles. *Physical Review A* **42,** 4768–4771 (1990).

243. Staykova, M., Arroyo, M., Rahimi, M. & Stone, H. A. Confined bilayers passively regulate shape and stress. *Physical Review Letters* **110,** 028101 (Jan. 2013).

244. Rim, J. E., Purohit, P. K. & Klug, W. S. Mechanical collapse of confined fluid membrane vesicles. *Biomechanics and Modeling in Mechanobiology* **13,** 1277–1288 (2014).

245. Watase, M. & Nishinari, K. Rheological and thermal properties of agarose and kappa-carrageenan gels containing urea, guanidine hydrochloride or formamide. *Topics in Catalysis* **1,** 25–36 (1986).

246. Normand, V. *et al.* Effect of sucrose on agarose gels mechanical behaviour. *Carbohydrate Polymers* **54,** 83–95 (2003).

247. Vilgis, T. A. Gels: Model systems for soft matter food physics. *Current Opinion in Food Science* **3,** 71–84 (2015).

248. Russ, N., Zielbauer, B. I. & Vilgis, T. A. Impact of sucrose and trehalose on different agarose-hydrocolloid systems. *Food Hydrocolloids* **41,** 44–52 (2014).

249. Baumgart, T. & Offenhäusser, A. Polysaccharide-supported planar bilayer lipid model membranes. *Langmuir* **19,** 1730–1737 (2003).

250. Komis, G., Apostolakos, P. & Galatis, B. Hyperosmotic stress-induced actin filament reorganization in leaf cells of Chlorophyton comosum. *Journal of Experimental Botany* **53,** 1699–1710 (2002).

251. Lang, I., Sassmann, S., Schmidt, B. & Komis, G. Plasmolysis: Loss of turgor and beyond. *Plants* **3,** 583–593 (2014).

252. Lee-Stadelmann, O. Y. & Stadelmann, E. J. Plasmolysis and deplasmolysis. *Methods in Enzymology* **174,** 225–246 (1989).

253. Oparka, K. J. Tansley Review No. 67. Plasmolysis: New insights into an old process. *New Phytologist,* 571–591 (1994).

254. Lang, I., Barton, D. A. & Overall, R. L. Membrane-wall attachments in plasmolysed plant cells. *Protoplasma* **224,** 231–243 (2004).

255. Reisen, D., Marty, F. & Leborgne-Castel, N. New insights into the tonoplast architecture of plant vacuoles and vacuolar dynamics during osmotic stress. *BMC Plant Biology* **5,** 1–13 (2005).

256. Dupont, S., Beney, L., Ritt, J. F., Lherminier, J. & Gervais, P. Lateral reorganization of plasma membrane is involved in the yeast resistance to severe dehydration. *Biochimica et Biophysica Acta - Biomembranes* **1798,** 975–985 (2010).

257. Gervais, P, Marechal, P. A. & Molin, P. Effects of the Kinetics of Osmotic Pressure Variation on Yeast Viability. *Journal of the American Chemical Society* **40,** 1432–1439 (1992).

258. Simonin, H., Beney, L. & Gervais, P. Sequence of occurring damages in yeast plasma membrane during dehydration and rehydration: Mechanisms of cell death. *Biochimica et Biophysica Acta - Biomembranes* **1768,** 1600–1610 (2007).

259. Festucci-Buselli, R. A., Otoni, W. C. & Joshi, C. P. Structure, organization, and functions of cellulose synthase complexes in higher plants. *Brazilian Journal of Plant Physiology* **19,** 1–13 (2007).

260. Sethaphong, L. *et al.* Tertiary model of a plant cellulose synthase. *Proceedings of the National Academy of Sciences of the United States of America* **110,** 7512–7517 (2013).

261. Schneider, R., Hanak, T., Persson, S. & Voigt, C. A. Cellulose and callose synthesis and organization in focus, what's new? *Current Opinion in Plant Biology* **34,** 9–16 (2016).

262. Crowell, E. F. *et al.* Pausing of golgi bodies on microtubules regulates secretion of cellulose synthase complexes in Arabidopsis. *Plant Cell* **21,** 1141–1154 (2009).

263. Hill, A. E., Shachar-Hill, B. & Shachar-Hill, Y. What Are Aquaporins For? *Journal of Membrane Biology* **197,** 1–32 (2004).

264. Taylor, T. M., Davidson, P. M., Bruce, B. D. & Weiss, J. Liposomal nanocapsules in food science and agriculture. *Critical Reviews in Food Science and Nutrition* **45,** 587–605 (2005).

265. Burey, P., Bhandari, B., Rutgers, R., Halley, P. & Torley, P. Confectionery Gels: A Review on Formulation, Rheological and Structural Aspects. *International Journal of Food Properties* **12,** 176–210 (Jan. 2009).

266. Del Vigna de Almeida, P., Trindade Gregio, A. M., Naval Machado, M. A., Soares de Lima, A. A. & Reis Azevedo, L. Saliva Composition and Functions : *Journal of Contemporary Dental Practice* **9,** 72–80 (2008).

267. Nayebi, I., Rajabi, O., Chamani, J. & Izi, S. In vitro evaluation of biophysical properties of an artificial saliva produced from Aloe vera gel. *Journal of Herbal Medicine* **19,** 100307 (2020).

268. Melvin, J. E., Yule, D., Shuttleworth, T. & Begenisich, T. Regulation of fluid and electrolyte secretion in salivary gland acinar cells. *Annual Review of Physiology* **67,** 445–469 (2005).

269. Horger, K. S., Estes, D. J., Capone, R. & Mayer, M. Films of Agarose Enable Rapid Formation of Giant Liposomes in Solutions of Physiologic Ionic Strength. *Journal of the American Chemical Society* **131,** 1810–1819 (Feb. 2009).

270. Shinoda, W. Permeability across lipid membranes. *Biochimica et Biophysica Acta - Biomembranes* **1858,** 2254–2265 (2016).

271. Kummrow, M. & Helfrich, W. Deformation of giant lipid vesicles by electric fields. *Physical Review A* **44,** 8356–8360 (1991).

272. Solmaz, M. E. *et al.* Optical stretching as a tool to investigate the mechanical properties of lipid bilayers. *RSC Advances* **3,** 16632–16638 (2013).

273. Lipowsky, R. Coupling of bending and stretching deformations in vesicle membranes. *Advances in Colloid and Interface Science* **208,** 14–24 (2014).

274. Boulbitch, A., Guttenberg, Z. & Sackmann, E. Kinetics of membrane adhesion mediated by ligand-receptor interaction studied with a biomimetic system. *Biophysical Journal* **81,** 2743–2751 (2001).

275. Roberts, S. R., Knight, M. M., Lee, D. A. & Bader, D. L. Mechanical compression influences intracellular Ca2+ signaling in chondrocytes seeded in agarose constructs. *Journal of Applied Physiology* **90,** 1385–1391 (2001).

276. Toyoda, T. *et al.* Hydrostatic Pressure Modulates Proteoglycan Metabolism in Chondrocytes Seeded in Agarose. *Arthritis and Rheumatism* **48,** 2865–2872 (2003).

277. Knight, M. M., Toyoda, T., Lee, D. A. & Bader, D. L. Mechanical compression and hydrostatic pressure induce reversible changes in actin cytoskeletal organisation in chondrocytes in agarose. *Journal of Biomechanics* **39,** 1547–1551 (2006).

278. Hunt, N. C. & Grover, L. M. Cell encapsulation using biopolymer gels for regenerative medicine. *Biotechnology Letters* **32,** 733–742 (2010).

279. Roberts, J. J., Earnshaw, A., Ferguson, V. L. & Bryant, S. J. Comparative study of the viscoelastic mechanical behavior of agarose and poly(ethylene glycol) hydrogels. *Journal of Biomedical Materials Research - Part B Applied Biomaterials* **99 B,** 158–169 (2011).

280. Caccavo, D., Cascone, S., Poto, S., Lamberti, G. & Barba, A. A. Mechanics and transport phenomena in agarose-based hydrogels studied by compression-relaxation tests. *Carbohydrate Polymers* **167,** 136–144 (2017).

281. Narayanan, J., Xiong, J. Y. & Liu, X. Y. Determination of agarose gel pore size: Absorbance measurements vis a vis other techniques. *Journal of Physics: Conference Series* **28,** 83–86 (2006).

282. Shivanandan, A., Radenovic, A. & Sbalzarini, I. F. MosaicIA: An ImageJ/Fiji plugin for spatial pattern and interaction analysis. *BMC Bioinformatics* **14** (2013).

283. Beney, L., Perrier-Cornet, J. J. M., Hayert, M. & Gervais, P. Shape modification of phospholipid vesicles induced by high pressure: influence of bilayer compressibility. *Biophysical Journal* **72,** 1258–1263 (Mar. 1997).

284. Bagatolli, L. A. & Gratton, E. Two-photon fluorescence microscopy observation of shape changes at the phase transition in phospholipid giant unilamellar vesicles. *Biophysical Journal* **77,** 2090–2101 (1999).

285. Bagatolli, L. A. & Gratton, E. Two photon fluorescence microscopy of coexisting lipid domains in giant unilamellar vesicles of binary phospholipid mixtures. *Biophysical Journal* **78,** 290–305 (2000).

286. Patton, J. N. & Palmer, A. F. Photopolymerization of bovine hemoglobin entrapped nanoscale hydrogel particles within liposomal reactors for use as an artificial blood substitute. *Biomacromolecules* **6,** 414–424 (2005).

287. Costello, R. F., Peterson, I. R., Heptinstall, J., Byrne, N. G. & Miller, L. S. A robust gel-bilayer channel biosensor. *Advanced Materials for Optics and Electronics* **8,** 47–52 (1998).

288. Beddow, J. A., Peterson, I. R., Heptinstall, J. & Walton, D. J. Reconstitution of Nicotinic Acetylcholine Receptors into Gel-Protected Lipid Membranes. *Analytical Chemistry* **76,** 2261–2265 (2004).

289. Lira, R. B., Dimova, R. & Riske, K. A. Giant unilamellar vesicles formed by hybrid films of agarose and lipids display altered mechanical properties. *Biophysical Journal* **107,** 1609–1619 (2014).

290. Arnott, S. *et al.* The agarose double helix and its function in agarose gel structure. *Journal of Molecular Biology* **90,** 269–284 (1974).

291. Tako, M. & Nakamura, S. Gelation mechanism of Agarose. *Carbohydrate Research* **180,** 277–284 (1988).

292. Deszczynski, M., Kasapis, S., MacNaughton, W. & Mitchell, J. R. Effect of sugars on the mechanical and thermal properties of agarose gels. *Food Hydrocolloids* **17,** 793–799 (2003).

293. Deszczynski, M., Kasapis, S. & Mitchell, J. R. Rheological investigation of the structural properties and aging effects in the agarose/co-solute mixture. *Carbohydrate Polymers* **53,** 85–93 (2003).

294. Buschmann, M. D., Gluzband, Y. A., Grodzinsky, A. J. & Hunziker, E. B. Mechanical compression modulates matrix biosynthesis in chondrocyte/agarose culture. *Journal of Cell Science* **108,** 1497–1508 (1995).

295. Mu, Y., Lyddiatt, A. & Pacek, A. W. Manufacture by water/oil emulsification of porous agarose beads: Effect of processing conditions on mean particle size, size distribution and mechanical properties. *Chemical Engineering and Processing: Process Intensification* **44,** 1157–1166 (2005).

296. Gu, W. Y., Yao, H., Huang, C. Y. & Cheung, H. S. New insight into deformation-dependent hydraulic permeability of gels and cartilage, and dynamic behavior of agarose gels in confined compression. *Journal of Biomechanics* **36,** 593–598 (2003).

297. Liu, Q., Subhash, G. & Moore, D. F. Loading velocity dependent permeability in agarose gel under compression. *Journal of the Mechanical Behavior of Biomedical Materials* **4,** 974–982 (2011).

298. Ed-Daoui, A. & Snabre, P. Poroviscoelasticity and compression-softening of agarose hydrogels. *Rheologica Acta* **60,** 327–351 (2021).

299. Christianson, D. D., Casiraghi, E. M. & Bagley, E. B. Uniaxial Compression of Bonded and Lubricated Gels. *Journal of Rheology* **29,** 671–684 (1985).

300. Casiraghi, E., Bagley, E. & Christianson, D. Behaviour of Mozzarella, Cheddar and Processed Cheese Spread in Lubricated and Bonded Uniaxial Compression. *Journal of Texture Studies* **16,** 281–301 (Sept. 1985).

301. Bagley, E. B., Wolf, W. J. & Christianson, D. D. Effect of sample dimensions, lubrication and deformation rate on uniaxial compression of gelatin gels. *Rheologica Acta* **24,** 265–271 (1985).

302. Koç, H. *et al.* Emulsion filled polysaccharide gels: Filler particle effects on material properties, oral processing, and sensory texture. *Food Hydrocolloids* **94,** 311–325 (2019).

303. Khalesi, H., Lu, W., Nishinari, K. & Fang, Y. New insights into food hydrogels with reinforced mechanical properties: A review on innovative strategies. *Advances in Colloid and Interface Science* **285,** 102278 (2020).

304. El Kechai, N. *et al.* Effect of liposomes on rheological and syringeability properties of hyaluronic acid hydrogels intended for local injection of drugs. *International Journal of Pharmaceutics* **487,** 187–196 (2015).

305. Watase, M. & Arakawa, K. Rheological Properties of Hydrogels of Agar-agar. III. Stress Relaxation of Agarose Gels. *Bulletin of the Chemical Society of Japan* **41,** 1830–1834 (1968).

306. Ross-Murphy, S. B. Structure–property relationships in food biopolymer gels and solutions. *Journal of Rheology* **39,** 1451–1463 (1995).

307. Barrangou, L. M., Drake, M., Daubert, C. R. & Foegeding, E. A. Textural properties of agarose gels. II. Relationships between rheological properties and sensory texture. *Food Hydrocolloids* **20,** 196–203 (2006).

308. Ostry, D. J. & Flanagan, J. R. Human jaw movement in mastication and speech. *Archives of Oral Biology* **34,** 685–693 (1989).

309. Shama, F., Parkinson, C. & Sherman, P. Identification of Stimuli Controlling the Sensory Evaluation of Viscosity I. Non-Oral Methods. *Journal of Texture Studies* **4,** 102–110 (Apr. 1973).

310. DeMars, L. L. & Ziegler, G. R. Texture and structure of gelatin/pectin-based gummy confections. *Food Hydrocolloids* **15,** 643–653 (2001).

311. Imberty, A., Buléon, A., Tran, V. & Péerez, S. Recent Advances in Knowledge of Starch Structure. *Starch - Stärke* **43,** 375–384 (1991).

312. Mohnen, D. Pectin structure and biosynthesis. *Current Opinion in Plant Biology* **11,** 266–277 (2008).

313. Parker, N. G. & Povey, M. J. Ultrasonic study of the gelation of gelatin: Phase diagram, hysteresis and kinetics. *Food Hydrocolloids* **26,** 99–107 (2012).

314. Wright, J. *et al. Food Flavor Technology* Second Edi, 129–133 (2010).

315. Barenholz, Y. Relevancy of drug loading to liposomal formulation therapeutic efficacy. *Journal of Liposome Research* **13,** 1–8 (2003).

316. Mourtas, S. *et al.* Liposomal drugs dispersed in hydrogels. Effect of liposome, drug and gel properties on drug release kinetics. *Colloids and Surfaces B: Biointerfaces* **55,** 212–221 (2007).

317. Stubbington, L. Lipid bilayers on deformable elastic substrates, 1–194 (2018).

318. Faivre, M., Campillo, C. C., Viallat, A. & Pepin-Donat, B. in *Smart Colloidal Materials* 41–44 (Springer Berlin Heidelberg, 2008).

319. Sun, H., Chen, J., Han, X. & Liu, H. Multi-responsive hydrogels with UCST- and LCST-induced shrinking and controlled release behaviors of rhodamine B. *Materials Science and Engineering C* **82,** 284–290 (2018).

320. Wandera, D., Wickramasinghe, S. R. & Husson, S. M. Stimuli-responsive membranes. *Journal of Membrane Science* **357,** 6–35 (2010).

321. Theato, P., Sumerlin, B. S., O'Reilly, R. K. & Epps III, T. H. Stimuli responsive materials. *Chemical Society Reviews* **42,** 7055 (2013).

322. Cai, S. & Suo, Z. Mechanics and chemical thermodynamics of phase transition in temperature-sensitive hydrogels. *Journal of the Mechanics and Physics of Solids* **59,** 2259–2278 (2011).

323. Niskanen, J. & Tenhu, H. How to manipulate the upper critical solution temperature (UCST)? *Polymer Chemistry* **8,** 220–232 (2017).

324. Echeverria, C., Peppas, N. A. & Mijangos, C. Novel strategy for the determination of UCST-like microgels network structure: Effect on swelling behavior and rheology. *Soft Matter* **8,** 337–346 (2012).

325. Seuring, J. & Agarwal, S. Polymers with upper critical solution temperature in aqueous solution: Unexpected properties from known building blocks. *ACS Macro Letters* **2,** 597–600 (2013).

326. Hellweg, T., Dewhurst, C. D., Eimer, W. & Kratz, K. PNIPAM-co-polystyrene core-shell microgels: Structure, swelling behavior, and crystallization. *Langmuir* **20,** 4330–4335 (2004).

327. Costa, M. C., Silva, S. M. & Antunes, F. E. Adjusting the low critical solution temperature of poly(N-isopropyl acrylamide) solutions by salts, ionic surfactants and solvents: A rheological study. *Journal of Molecular Liquids* **210,** 113–118 (2015).

328. Katono, H. *et al.* Thermo-responsive swelling and drug release switching of interpenetrating polymer networks composed of poly(acrylamide-co-butyl methacrylate) and poly (acrylic acid). *Journal of Controlled Release* **16,** 215–227 (1991).

329. Xiao, X. C., Chu, L.-Y., Chen, W. M. & Zhu, J. H. Monodispersed thermoresponsive hydrogel microspheres with a volume phase transition driven by hydrogen bonding. *Polymer* **46,** 3199–3209 (2005).

330. Serrano-Ruiz, D. *et al.* Influence of the inter-chain hydrogen bonds on the thermoresponsive swelling behavior of UCST-like microgels. *Polymer* **54,** 4963–4971 (2013).

331. Rey, M., Hou, X., Tang, J. S. J. & Vogel, N. Interfacial arrangement and phase transitions of PNiPAm microgels with different crosslinking densities. *Soft Matter* **13,** 8717–8727 (2017).

332. Aguirre, G., Ramos, J. & Forcada, J. Synthesis of new enzymatically degradable thermo-responsive nanogels. *Soft Matter* **9,** 261–270 (2013).

333. Singh, B., Chauhan, G. S., Kumar, S. & Chauhan, N. Synthesis, characterization and swelling responses of pH sensitive psyllium and polyacrylamide based hydrogels for the use in drug delivery (I). *Carbohydrate Polymers* **67,** 190–200 (2007).

334. Lehmann, M., Krause, P., Miruchna, V. & von Klitzing, R. Tailoring PNIPAM hydrogels for large temperature-triggered changes in mechanical properties. *Colloid and Polymer Science* **297,** 633–640 (2019).

335. Bonina, F. *et al.* Flavonoids as potential protective agents against photo-oxidative skin damage. *International Journal of Pharmaceutics* **145,** 87–94 (1996).

336. Hamada, T. *et al.* Construction of asymmetric cell-sized lipid vesicles from lipid-coated water-in-oil microdroplets. *Journal of Physical Chemistry B* **112,** 14678–14681 (2008).

337. Shen, Y. *et al.* Effect of chemical composition on properties of pH-responsive poly(acrylamide-co-acrylic acid) microgels prepared by inverse microemulsion polymerization. *Colloids and Surfaces A: Physicochemical and Engineering Aspects* **350,** 87–90 (2009).

338. Ng, C. C., Cheng, Y.-L. & Pennefather, P. S. Properties of a Self-Assembled Phospholipid Membrane Supported on Lipobeads. *Biophysical Journal* **87,** 323–331 (2004).

339. Vleugels, L. F., Ricois, S., Voets, I. K. & Tuinier, R. Determination of the 'apparent pKa' of selected food hydrocolloids using ortho-toluidine blue. *Food Hydrocolloids* **81,** 273–283 (2018).

340. Stark, B., Pabst, G. & Prassl, R. Long-term stability of sterically stabilized liposomes by freezing and freeze-drying: Effects of cryoprotectants on structure. *European Journal of Pharmaceutical Sciences* **41,** 546–555 (2010).

341. Shoichet, M. S., Li, R. H., White, M. L. & Winn, S. R. Stability of hydrogels used in cell encapsulation: An in vitro comparison of alginate and agarose. *Biotechnology and Bioengineering* **50,** 374–381 (1996).

342. Knight, M. M., Ghori, S. A., Lee, D. A. & Bader, D. L. Measurement of the deformation of isolated chondrocytes in agarose subjected to cyclic compression. *Medical Engineering and Physics* **20,** 684–688 (1998).

343. Grossutti, M., Seenath, R., Noël, J. A. & Lipkowski, J. Infrared and fluorescence spectroscopic studies of a phospholipid bilayer supported by a soft cationic hydrogel scaffold. *Journal of Colloid and Interface Science* **473,** 162–171 (2016).

344. Schantz, B. & Rohm, H. Influence of lecithin-PGPR blends on the rheological properties of chocolate. *LWT - Food Science and Technology* **38,** 41–45 (2005).

345. Cevc, G. Isothermal lipid phase transitions. *Chemistry and Physics of Lipids* **57,** 293–307 (1991).